

Old Dominion University

ODU Digital Commons

Mechanical & Aerospace Engineering Theses & Dissertations

Mechanical & Aerospace Engineering


Fall 2020

Finite Element Analysis Investigation of Hybrid Thin-Ply Composites for Improved Performance of Aerospace Structures

Alana M. Zahn

Old Dominion University, alana.zahn@gmail.com

Follow this and additional works at: https://digitalcommons.odu.edu/mae_etds

 Part of the [Aerospace Engineering Commons](#), [Materials Science and Engineering Commons](#), and the [Mechanical Engineering Commons](#)

Recommended Citation

Zahn, Alana M.. "Finite Element Analysis Investigation of Hybrid Thin-Ply Composites for Improved Performance of Aerospace Structures" (2020). Master of Science (MS), Thesis, Mechanical & Aerospace Engineering, Old Dominion University, DOI: 10.25777/0w6g-ah98
https://digitalcommons.odu.edu/mae_etds/323

This Thesis is brought to you for free and open access by the Mechanical & Aerospace Engineering at ODU Digital Commons. It has been accepted for inclusion in Mechanical & Aerospace Engineering Theses & Dissertations by an authorized administrator of ODU Digital Commons. For more information, please contact digitalcommons@odu.edu.

**FINITE ELEMENT ANALYSIS INVESTIGATION OF HYBRID
THIN-PLY COMPOSITES FOR IMPROVED PERFORMANCE OF
AEROSPACE STRUCTURES**

by

Alana M. Zahn

B.S. December 2010, State University of New York College at Cortland

A Thesis Submitted to the Faculty of Old Dominion University in Partial
Fulfillment of the Requirements for the Degree of

MASTER OF SCIENCE

AEROSPACE ENGINEERING

OLD DOMINION UNIVERSITY
December 2020

Approved by:

Oleksandr Kravchenko (Director)

Gene Hou (Member)

Miltos Kotinis (Member)

Andrew E. Lovejoy (Member)

ABSTRACT

FINITE ELEMENT ANALYSIS INVESTIGATION OF HYBRID THIN-PLY COMPOSITES FOR IMPROVED PERFORMANCE OF AEROSPACE STRUCTURES

Alana M. Zahn
Old Dominion University, 2020
Director: Dr. Oleksandr Kravchenko

Commercial and private aircraft have a need for strong yet light materials in order to have the most ideal performance possible. This study looks at the use of thin-ply composite materials to improve the performance of aircraft structures by means of weight savings and/or strength increase when compared to laminates that are composed of exclusively standard-ply materials. In order to perform an investigation based solely on finite element analysis, validation efforts were performed using test data from open hole tension, open hole compression, notched tension, and notched compression specimens. Once the models were validated sufficiently, the same modeling practices were used to compare laminates with varying ply angle orientations and various laminate stacking sequences. Initial investigations showed that for a one-to-one comparison of standard-ply laminates to hybrid laminates, there can be up to a 10% tensile load advantage, as well as an over 40% compressive load advantage when considering the final failure load of a small notched specimen. Secondary investigations showed that changing the ply angle orientation away from a more typical 45° ply to angles at various increments of 10° and 15° can yield both tensile and compressive advantages simultaneously. A final investigation determined that by adding or removing certain plies from the laminate, the previously mentioned tension and compression advantages can be expanded upon for failure load advantages up to 65% higher than baseline specimens, as well as the ability to potentially change failure modes. All of these load and damage mechanism advantages also come with the added benefit of weight savings between 10-25% of the baseline specimen original weight. The study presented herein shows initial successes in determining laminates that will reduce weight while increasing strength under various loading conditions.

NOMENCLATURE

K	= interface stiffness due to traction
α	= adhesive factor parameter
E	= Young's modulus
t	= thickness
G_{12}	= In-plane shear modulus
τ_0	= Maximum interfacial strength
G_C	= Fracture energy release rate
N_e	= Number of elements in the cohesive crack area
l_e	= length of an element in the cohesive zone

TABLE OF CONTENTS

	Page
List of Tables	v
List of Figures	vi
Chapter	
I. Introduction	1
A. Previous Thin Ply Work.....	1
B. Current Stacking Sequence Practices	6
II. Analysis Validation	7
A. Model Specifications.....	7
B. Open Hole Tension and Open Hole Compression Characterization Specimens	11
C. Unstiffened Standard-Ply Specimens	17
D. Unstiffened Hybrid-Ply Specimens.....	27
III. Design Parameters and Design of Experiments	34
A. Varying Ply Angles and Stiffness Ratios	34
i. Small Unstiffened Tension Specimens	39
ii. Small Unstiffened Compression Specimens	47
B. Varying Stacking Sequence and Stiffness Ratios.....	54
i. Initial Stacking Sequence Changes.....	55
ii. Secondary Stacking Sequence Changes	57
IV. Discussion and Results	61
A. Ply Angle Variation Highs and Lows	61
B. Stacking Sequence Variation Highs and Lows.....	61
V. Conclusions and Future Work.....	64
References.....	66
Appendices.....	68

List of Tables

Table	Page
1. Cohesive properties used for Abaqus analyses	10
2. Open hole tension and open hole compression specimen stacking sequences and average thicknesses	11
3. Material properties from the open hole characterization tests	12
4. Material properties from the unnotched characterization tests	13
5. Failure load and displacement for the unstiffened test specimens	36
6. Stiffness ratios and effective Young's moduli for investigated ply angle changes	38
7. Small tension percent differences between simple model and advanced model.....	47
8. Stacking sequence initial laminate changes	55
9. Weight and strength comparison for standard modified laminate specimens.....	63
10. Weight and strength comparison for hybrid modified laminate specimens.....	64

List of Figures

Figure	Page
1. The Groupama catamaran which contains thin-ply composites	2
2. Damage initiation and ultimate strength for various quasi-isotropic materials	3
3. An automated lamination machine created by the Mitsuya Company.....	4
4. Notched test specimens after failure	5
5. Mesh convergence study element size versus failure load results	9
6. Mesh convergence comparison between 2D and 3D elements	9
7. Mesh size example used for unstiffened small tension specimens	9
8. American Society for Testing and Materials standards for open hole tension and open hole compression testing.....	14
9. Images of model dimensions and mesh pattern at notch.....	14
10. Load-displacement comparison for open hole tension and open hole compression specimens	15
11. Load-strain comparison for open hole tension and open hole compression specimens.....	16
12. Load-displacement comparison for 70 gsm open hole tension and open hole compression specimens.....	16
13. Load-strain comparison for 70 gsm open hole tension and open hole compression specimens	17
14. Test specimens within the test stand vs. analysis boundary conditions	18
15. Test data vs. analysis load-displacement curves.....	19
16. Strain gage locations for unstiffened test specimens	20
17. Load-strain plots for small standard tension specimens	21
18. Small standard tension failed test specimens and Abaqus failure prediction	21
19. Advanced small standard tension model.....	22
20. Load-strain plots for small standard compression specimens.....	24
21. Small standard compression failed test specimens and Abaqus failure prediction.....	24
22. Load-strain plots for intermediate standard tension specimens	26
23. Intermediate standard tension failed test specimens and Abaqus failure prediction.....	26
24. Test data vs. analysis load-displacement curves.....	28
25. Load-strain plots for small hybrid tension specimens.....	29
26. Small hybrid tension failed test specimens and Abaqus failure prediction.....	29
27. Advanced small hybrid tension model.....	30
28. Load-strain plots for small hybrid compression specimens	31
29. Small hybrid compression failed test specimens and Abaqus failure prediction.....	32
30. Load-strain plots for intermediate hybrid tension specimens	33
31. Intermediate hybrid tension failed test specimens and Abaqus failure prediction.....	33
32. Standard laminate vs. hybrid laminate load conditions	35
33. Standard laminate vs. hybrid laminate Abaqus load-displacement predictions	37
34. Initiation and failure loads for small tension angle study	40
35. Initiation of failure in the Standard-15T model	41
36. Hashin damage propagation within various plies of the Standard-45T model	42
37. Hashin damage propagation within various plies of the Hybrid-45T model	43
38. Hashin damage propagation within various plies of the Standard-15T model	44
39. Hashin damage propagation within various plies of the Hybrid-15T model	44
40. Hashin damage propagation within various plies of the Standard-75T model	45
41. Hashin damage propagation within various plies of the Hybrid-75T model	45
42. Failure load vs. axial displacement for the tension laminates.....	46
43. Initiation and failure loads for small compression angle study.....	48
44. Initiation of failure in the Standard-45C model	49
45. Hashin damage propagation within various plies of the Standard-45C model	50
46. Hashin damage propagation within various plies of the Hybrid-45C model.....	51
47. Hashin damage propagation within various plies of the Standard-15C model	51

48. Hashin damage propagation within various plies of the Hybrid-15C model	52
49. Hashin damage propagation within various plies of the Standard-75C model	53
50. Hashin damage propagation within various plies of the Hybrid-75C model	53
51. Load vs. displacement curves for tensile 45° laminate changes	56
52. Load vs. displacement curves for compressive 45° laminate changes.....	57
53. Load-displacement curves for standard 15° laminate changes and 45° baseline.....	58
54. Load-displacement curves for standard 75° laminate changes and 45° baseline.....	59
55. Load-displacement curves for hybrid 15° laminate changes and standard 45° baseline	60
56. Load-displacement curves for hybrid 75° laminate changes and standard 45° baseline	60

I. Introduction

There is a need for stronger and simultaneously lighter composite specimens to be used within flight applications. However, a thorough design of experiments (DOE) requires a large number of coupons to be built and tested to determine the most ideal laminates, which increases cost and development time significantly. To reduce the cost, finite element analysis can be used to determine the feasibility and benefits or detriments to a large percentage of the DOE, and then only a small subset of the most promising coupons can be built and tested. This study takes a look at previous thin ply work to determine what lessons were learned and how it can be built upon. Additionally, in order to ensure confidence in an investigation based significantly on finite element analysis, validated modeling efforts are required. Abaqus finite element models were analyzed and validated against test data from multiple types of specimens and loading scenarios. Those models were then used to examine various new laminate designs under tension and compression loading. This document begins with the review of previous work available in the open literature, followed by the analysis validation process, the design parameters and DOE investigation, the results of the laminate design study, and finishes with conclusions and recommendations for future work.

A. Previous Thin-Ply Work

Thin-ply materials have been used in various industries for decades, but further investigation is still necessary to ensure their full benefits are taken advantage of properly. The most common use for thin-ply composites is in aerospace applications, but they have been used in naval, automotive, and even golf industries as well. An example of a naval use of thin-ply materials is in ocean racing yachts, most famously in the hulls of the award-winning catamaran called Groupama [1] shown in Figure 1. Ocean racing yachts are most commonly made of carbon/epoxy laminates, but since they are often not cured in autoclaves, the hulls become very porous [2]. There is also the need for the hulls to be as light as possible so that the yachts are able to skim over the water and perform well in races. The desire for less porosity and lighter structures points to the need for thin-ply laminates. Baley et. al. [2] state that thicker laminates are more likely to contain more defects than those with thinner plies, and the thicker laminates also fail at significantly lower stresses. This decrease in defects, and thus decrease in porosity, as well as the increase in failure stress make thin-ply laminates appealing in the racing yacht industry.



Figure 1. The Groupama catamaran that contains thin-ply composites. [1]

The aerospace industry has had many independent and collaborative studies to determine the most appropriate uses of thin-ply materials. In most cases, the studies originate with fully thin-ply laminates, and some of them continue onto more hybrid designs, combining thin and standard or thick plies. Fuller and Wisnom state that the usage of composite materials is often limited by the brittle failure of said composites [3]. They suggest that the way to counteract this disadvantage is to use thin plies that are better able to suppress the damage mechanisms that create this brittle failure. Using computed tomography (CT) scans, Fuller and Wisnom observed that when using plies that were a quarter of the standard ply thickness, the delaminations were suppressed within the carbon-fiber reinforced polymer (CFRP). The CT and microscopy also showed that there was a kind of “pseudo-ductility” in the CFRP that enabled higher strengths than thicker laminates while still maintaining the initial stiffness of the test samples.

Cugnoni et. al. also were able to show that thin-ply composites suppress delamination, as well as delay matrix cracks that lead to failure [4]. Their research involved three different composite materials, M40JB, T800, and AS4, and for each of these three fibers, two epoxy resins were used, TP80ep and TP120ep, to create six different matrix formulations to their study. All six of these were tested at varying ply thicknesses between 30 and 300 microns, or roughly 0.0012 in. to 0.012 in. equivalent thicknesses. Another way to notate 30 micron material is 30 g/m² or 30 gsm, and this is considered a very thin ply, with standard ply thicknesses typically in the 190 gsm, equivalent to 0.0072 in. thickness, range. Figure 2 contains the plots from the Cugnoni study, including all three materials tested. In these graphs, it is apparent that ultimate strengths are higher at lower ply thicknesses for the unnotched tension (UNT) tests of all three materials. The study also shows that there is much less through-thickness cracking in both the longitudinal and transverse thin-ply microscope images than those with intermediate and thick laminates during compression after impact (CAI) testing. This study showed that thin-ply laminates are able to reach up to 92% of the

material's ultimate strain, while thick-ply laminates can only reach up to 66% of the thick fiber's ultimate strain.

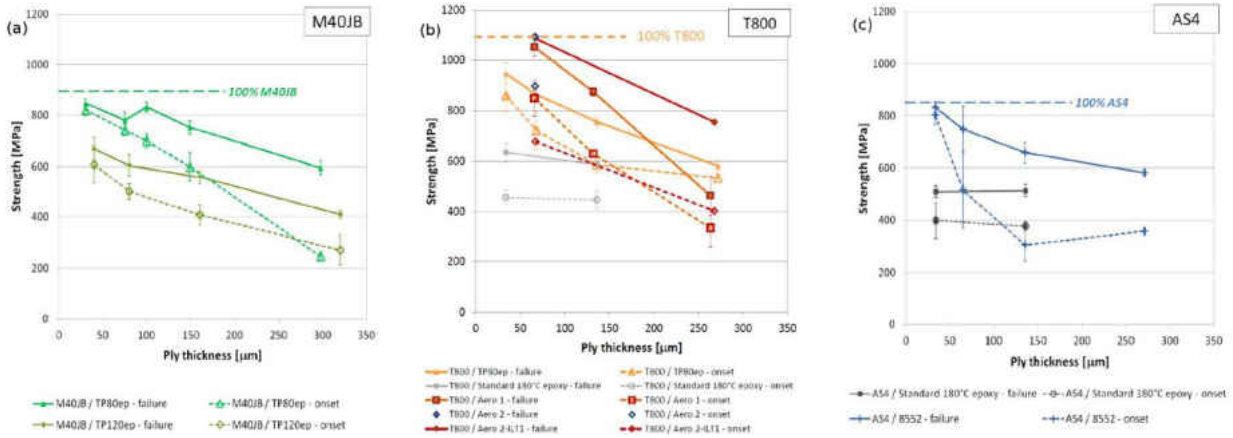


Figure 2. Damage initiation and ultimate strength for various quasi-isotropic materials. [4]

There have also been studies done with spread-tow fabrics (STF) that look at the effect of thin composite materials. Arteiro et. al. looked at 160 gsm and 240 gsm laminates, which are both on the thicker scale, but can be used for comparison between themselves at a minimum [5]. They, too, found that the thin STF specimen had enhanced unnotched tensile strength when compared to the thick STF, as well as increased damage suppression. They also note that the compression loading cases for both notched and unnotched specimens showed a noteworthy advantage in the thinner laminates. The unnotched compression strength of the thinner STF was 16.2% higher than that of the thick STF, and the unnotched tensile strength of the thin STF was 13.9% higher than its thicker counterpart. They also note that although the thick STF material had a higher longitudinal strength than the thin STF composite, that advantage did not create an increase in laminate strength within the thick STF.

An additional study that shows the benefits of size-effects within thin-ply laminates is by Amacher et. al. from 2014 [6]. They also studied carbon/epoxy plies between 30-300 gsm, but they limited themselves to M40JB fibers in TP80ep matrix only. They did, however, run additional loading cases, examining uniaxial tension, open hole tension (OHT), and open hole compression (OHC) on multiple quasi-isotropic stacking sequences. Their investigation showed delayed damage initiation and ultimate strength improvements as ply thickness decreased. Once again, delamination growth and transverse cracks were either delayed or suppressed almost completely when using thin-ply laminates. Instead of delamination growth, the thin-ply specimens had damage paths that were perpendicular to loading, rather than following

axial or off-axis plies the way the thicker ply specimens failed. This perpendicular failure also occurred at much higher loads than the delamination failure, and this is likely due to dissipated energy within the thin-ply laminates.

Not only has it been shown that delaminations can be suppressed with thin-ply laminates, but Tsai, Shin, and Kim show in their paper, titled simply “Thin Ply Composites”, that thin laminates are also able to resist micro-cracks and splitting. [7] They propose the use of hybrid laminates consisting of both thick and thin plies in order to reduce the weight while increasing the strength and damage tolerance. The dilemma of creating hybrid, however, is the increased time and cost of alternating materials. To mitigate this issue, they discuss an “automated lamination machine”. The machine mentioned, created by the Mitsuya Company, is currently only available in Japan and is shown in Figure 3. This machine can create a multidirectional laminate with thick and thin plies in a reduced timeframe. It is also able to simplify any ply drops or layup issues during design or assembly.



Figure 3. An automated lamination machine created by the Mitsuya Company. [7]

Moon et. al. also worked with hybrid composites to improve performance when dealing with low Earth orbit (LEO) conditions [8]. Their study focused on adding multi-wall carbon nanotube (MWNT) and thin plies to CFRP in four different configurations for simulated ground tests including high vacuum, ultraviolet light, and thermal cycling as an aging process. They found that the configurations that added thin ply materials and MWNT fillers had improvements in tensile strength, and the greatest increase in strength was when the thin-ply and MWNT were both added to the CFRP. This greatest increase scenario was found to be the case for both LEO aged and non-aged ground conditions. However, it is not always reasonable to add both MWNT and thin-ply materials, and doing so actually decreased the tensile stiffness due to the

decrease of fiber volume fractions and excess resin during the build process. It is important to note the conclusion that solely adding thin-ply to CFRP laminates allowed delamination to delay again until there was evidence of fiber breakage.

Perhaps one of the most comprehensive study of hybrid laminates so far is that done in Portugal by Furtatdo, Arteiro, Catalanotti, Xavier, and Camanho in 2016 [9]. Their experiments focused on the effects within tensile notched and unnotched tests of composite laminates, also with ply thicknesses between 30 and 300 gsm. From their first investigation, representative samples of the test specimens after failure are shown in Figure 4. As seen in Figure 4a, the thin laminates, made up of only 30 gsm (0.0012 in. thick) plies, show brittle failure without any evidence of delamination or transverse cracks. There is also no evidence of failure along the 45° outer plies, but instead only failure perpendicular to the load path. The intermediate laminates, shown in Figure 4b and composed of only 100 gsm (0.004 in. thick) plies, have mostly fiber pull-out failure with some evidence of failure along the outer 45° plies and some matrix cracking. The thick laminates in Figure 4c are made of 300 gsm (0.012 in. thick) plies and show failure of the $\pm 45^\circ$ plies and 90° plies before the 0° ply fails, so the rest of the laminate separates from the 0° plies, and then the whole specimen fails. Finally the thick-ply level laminate was built to effectively be the same as the thick laminate, but it was built with 10 thin, 30 gsm, plies stacked together to determine the effect of “blocking” ply duplicates together rather than using less plies with a larger thickness. This investigation will be explored more in the next section.

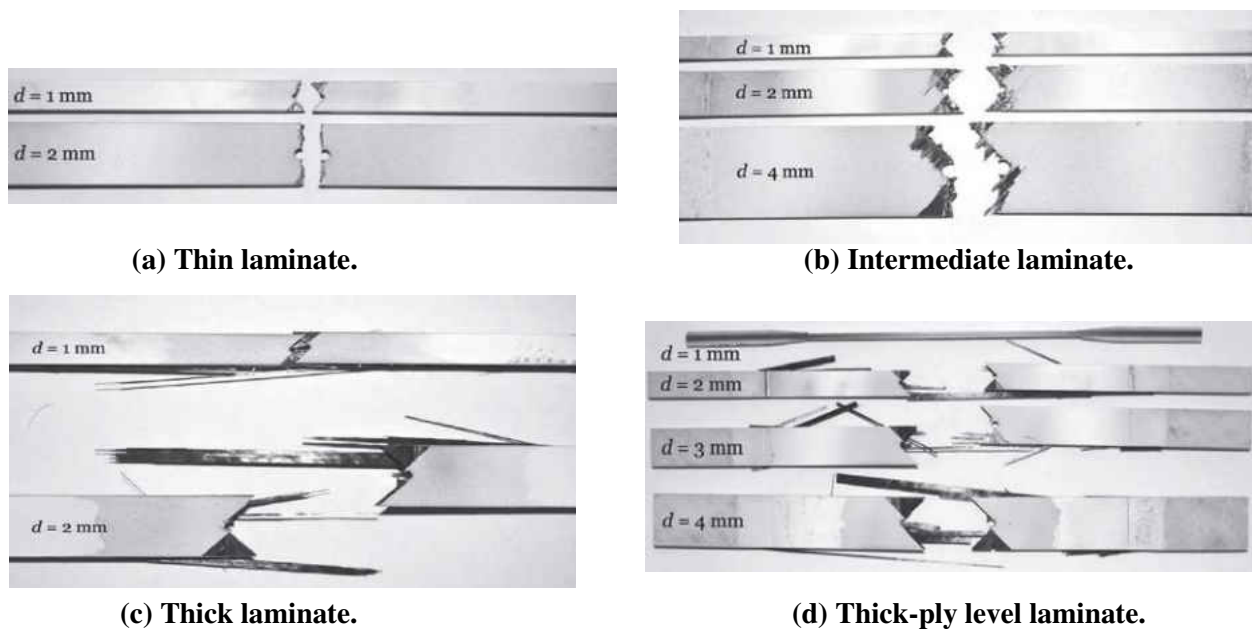


Figure 4. Notched test specimens after failure. [9]

Another study reported in the Furtado paper involved using non-crimp fabrics (NCF) to create NCF-thin, NCF-intermediate, and NCF-hybrid laminates.[9] The NCF-thin laminate consisted a “disperse stacking sequence” with plies of each various angle orientation scattered throughout the laminate, the NCF-intermediate consisted of “blocking” as many orientation plies together as possible, and the NCF-hybrid laminate consisted of dispersed off-axis plies and blocked 0° plies where possible. These specimens were tested in OHT tests with notch sizes of 2, 5, and 8 mm (0.079, 0.197, and 0.315 in.) to determine their notched tensile strength. At all notch sizes, the lowest notched strength is the NCF-thin laminate, then the NCF-intermediate laminate, and finally the NCF-hybrid has the highest notched tensile strength among the three laminate styles. The highest notched tensile strength also occurs at the smallest hole diameter for each configuration, with decreasing strengths at increasing hole diameter. The need to investigate hybrid laminate advantages further is apparent, and many aspects of this in-depth study is presented in the subsequent sections of this document.

B. Current Stacking Sequence Practices

There aren't many written rules for stacking sequences within certain laminate types, but each company and industry has “best practices” that they like to follow. According to a 2020 study from the Fraunhofer Institute for High-Speed Dynamics, it is “aerospace standard to design composite laminates using a zero [B]-matrix” [10]. A zero [B]-matrix indicates a symmetric laminate, which is one unwritten rule that is common within NASA and many of its industry partners. Another best practice is what is called a “balanced” laminate. In a balanced laminate, each 45° ply has an equivalent -45° ply, or if they were any other angle between 1° and 89° , the negative of that angle would also be in the stacking sequence [11]. Shi and Zhao also propose that every ply ratio, for example the number of 0° plies divided by the total number of plies, must fall between 6-80%, non-inclusive. Other aerospace industry companies try to keep their ratios above 10% at a minimum. It is also proposed in Shi and Zhao's study that there should not be four, or more, consecutive plies with the same angle orientation. This is also different than some industry policies to not stack more than two, or more than three, depending on the company with whom you speak.

Another issue with composite laminates is delaminate due to free edge effects, particularly with notched specimens. Since the origin of this investigation started with determining notched failure strengths within aircraft, replicating some kind of fuselage strike mid-air, this is particularly important to address. Fotouhi et. al. were able to successfully suppress free edge delaminations within both unnotched and notched specimens by using what they called “orientation-blocked hybrids” [12]. They were also able to achieve some measure of notch-insensitivity, thus the ability to suppress edge effects within unnotched and small-notched specimens as well. This is another example of blocked laminates performing better than those laminates with more evenly distributed ply angle orientations. Furtado et. al. also found a different way to

try to address damage suppression near the hole free edge [9]. Their study was able to determine that fiber damage initiations wherever the fiber direction is tangent to the notch's free edge. To prevent this damage, the use of what they refer to as "ultra-thin" plies at 0.03 mm. (0.00118 in.) thickness along with 0.10 mm. (0.00394 in.) thick plies, they are able to change from a brittle failure to a pull-out failure mode. The change in failure mode can be taken advantage of within certain applications, and therefore the hybridization of laminates can be a benefit for laminate strengths as well as failure mode.

The written and unwritten rules for thin-ply or hybrid-ply laminates are even fewer. As mentioned in the prior section, Furtado et. al. have studied the effects of blocking thin plies, but very minimally [9]. They were also able to discover that when thin-ply off-axis material is laid up with 0° standard plies, the unnotched response will be very similar to that of a solely thin-ply laminate, and it will be superior to that of a notched laminate with blocked plies. It must be ensured, however, that the 0° section thickness is sufficiently small to avoid the delamination that the thin plies are placed in the laminate to suppress. It was also shown that with respect to notched hybrid laminates, the notched tensile strength can also be increased because the off-axis thin plies will still suppress the longitudinal splitting in a thicker 0° block, and the hybrid laminate will perform better than a fully blocked laminate. This study points to the need to intelligently block plies for the most efficient hybridization in order to improve the reduced tensile strength of thin-ply laminates and improve the unnotched and fatigue behaviors of standard-ply laminates, making it a "best of both worlds" scenario. This investigation into blocking is discussed fully in the "Varying Stacking Sequence and Stiffness Ratios Section" of this paper.

II. Analysis Validation

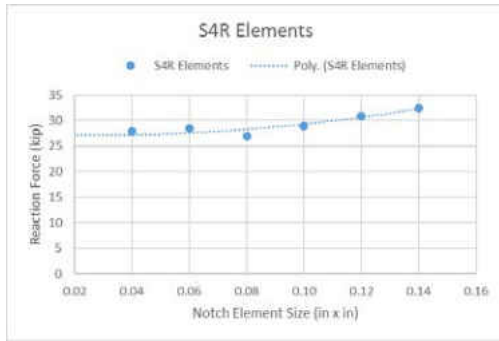
A. Model Specifications

In order to investigate a variety of different stacking sequences without incurring significant costs, finite element analysis (FEA) can be used to determine the most favorable laminates that can then be built and tested. Three types of laminate models were built for this investigation, thin ply laminate, standard ply laminate, and hybrid laminates that contain both thin and standard ply material. All laminate models had a center notch that is representative of discrete damage in order to track damage progression and final failure load within each of the various laminates. The validity of the modeling practices must also be determined, and the comparisons to various test data are presented in later sections of the Analysis Validation topic.

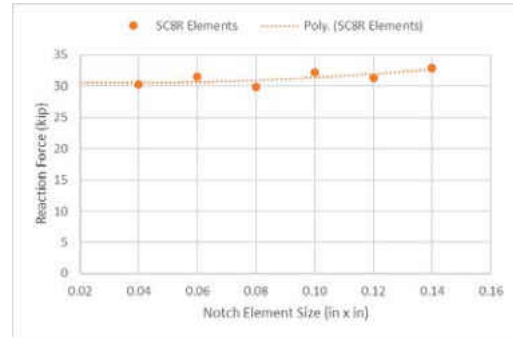
All models for this investigation were created using MSC Software's Patran modeling software, and they were built to be run with the Abaqus analysis code created by Dassault Systeme [13, 14]. The models were built with solid geometry and meshed with SC8R elements. The SC8R elements are 8-noded continuum shell elements that behave similarly to two-dimensional (2D) shell elements, but they are three-dimensional (3D) and only have 3 degrees of freedom at each node rather than traditional shell elements' 6

degrees of freedom. According to the Abaqus online reference manual, it is critical that continuum shells are oriented correctly because the through-thickness behavior is different than the in-plane behavior [14]. The element normal is oriented from what is defined as the “bottom” of the element up through the “top” of the element, and this defines the through-thickness direction. The element is also defined by nodal connectivity, with the first four nodes on the bottom face, and nodes 5-8 on the top face, in accordance with the normal.

When comparing damage progression using progressive failure analyses, SC8R elements were shown to produce results that are most comparable to known test data in three different sets of tests. Some of the tests that were looked at with both S4R and SC8R elements are from proprietary contractor reports, however the unstiffened small standard-ply tension specimens that will be discussed within Section IIC were also used for this mesh study. A full mesh convergence study was run with both S4R two-dimensional shell elements and SC8R three-dimensional continuum shell elements. The two-dimensional results of the mesh convergence study, as compared to test data for two sets of tests done under axial tension, are shown in Figure 5a. The results of the mesh convergence study with three-dimensional elements are shown in Figure 5b, and the comparison between two- and three-dimensional elements is shown in Figure 6. The labels on the x-axis of the graph correspond to the element size at the notch tip and along the transverse path leading from the notch tip. Mesh with a label of 0.06 in. would correspond to elements within the notch region that are 0.06 in. x 0.06 in. An example of the 0.08-in. mesh is shown in Figure 7, with (a) showing the notch region and transverse path and (b) showing the far-field mesh which is coarser than that at the notch region. All models contain only one element through the thickness to reduce computation size and cost. The 2D element study shows that there is convergence at smaller element sizes, and the 3D element study shows even better convergence at smaller element sizes. For both element types, the number of computational degrees of freedom is larger in models with smaller element sizes. Smaller elements meshed over the same surface area leads to the need for more elements and, thus, more nodes. This larger number of nodes and degrees of freedom will cause the analysis to take longer and cost more. In order to again reduce computation size and cost, it was determined that the largest reasonable converged element size should be used for all models, and since the 0.08 in. mesh is the most conservative of the converged elements, this was chosen for all models moving forward. Thus, the SC8R elements with 0.08 in. x 0.08 in. element size within the notch region, and maintaining an aspect ratio of no more than 1:5 for notch mesh to far-field mesh, was deemed to be sufficient for the entire finite element modeling effort.



(a) Two-dimensional elements.



(b) Three-dimensional elements.

Figure 5. Mesh convergence study element size versus failure load results.

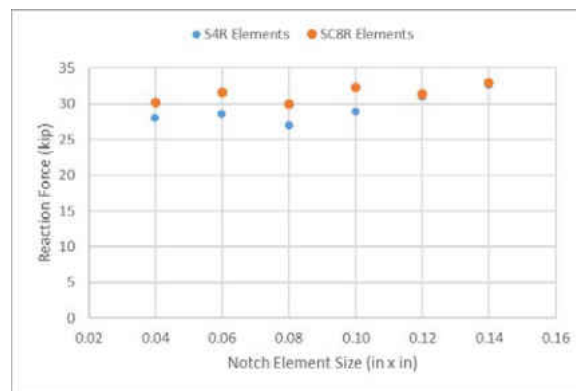
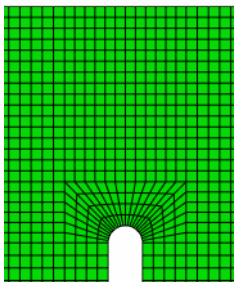
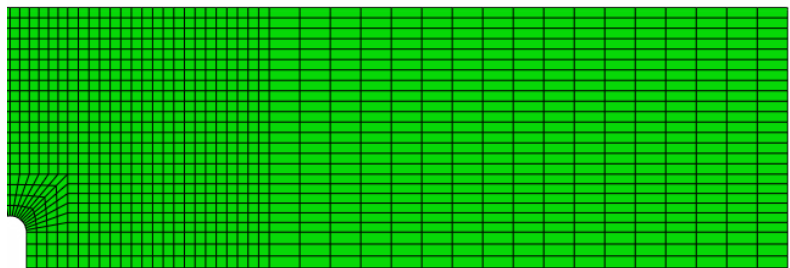


Figure 6. Mesh convergence comparison between 2D and 3D elements.



(a) Notch and transverse path mesh.



(b) Far-field mesh.

Figure 7. Mesh size example used for unstiffened small tension specimens.

All models were run with Abaqus explicit progressive failure analysis (PFA), including the Hashin damage initiation criterion and an energy-based softening damage evolution [14]. A select few models were also expanded to contain cohesive elements between each ply in order to predict and track interlaminar

delamination between plies. These cohesive-containing models also used an energy-based damage evolution with elastic traction and damage initiation based on Turon calculations using the equations below [15]. The cohesive traction properties are shown in Table 1, although they are only used for a select few “advanced” tension models within the study. The damage initiation strength properties can be found in Table 3 within the next section, as well a full example of the materials cards within an Abaqus input deck within Appendix A. There is also a table in Appendix B that contains all necessary properties that are used within the analyses for ease of comparison between ply types. The models designated throughout the document as “simple” are one SC8R element through the thickness, with all plies contained within one SHELL SECTION card of the input deck. Appendix C also contains two examples of how the laminate properties for various stacking sequences, including those with hybrid layups, were included within the Abaqus input deck. Within these laminates, each ply is assigned a material property based on its ply type (30, 70, or 190 gsm), as well as its orientation angle. The named material properties are those shown in the examples in Appendix A. The models that are referred to as “advanced” are the ones that contain the cohesive layers, created as COH3D8 elements also with one element through the thickness. These cohesive elements are layered between each SC8R layer, and each SC8R surface representing a ply is assigned its own material and thickness as appropriate for standard and thin ply layers within the laminate.

$$K_1 = \frac{\alpha E_3}{t} \quad \text{and} \quad K_2 = K_3 = \frac{\alpha G_{12}}{t}$$

(where t = adjacent sublaminates thickness)

$$\tau_0 = \sqrt{\frac{9\pi E G_C}{32 N_e l_e}}$$

Table 1. Cohesive properties used for advanced Abaqus analyses.

Elastic Properties, Interface Stiffness	Damage Initiation, Interface Strength	Damage Evolution, Energy Release
$K_1 = 501.5 \text{ ksi}$	$\tau_{01} = 3703.9 \text{ psi}$	$G_{IC} = 1.37 \text{ in-lb/in}^2$
$K_2 = K_3 = 262.0 \text{ ksi}$	$\tau_{02} = \tau_{03} = 5121.3 \text{ psi}$	$G_{IIC} = G_{IIIC} = 4.2 \text{ in-lb/in}^2$

The validation of each type of laminate analysis was done using various sets of test data from tests done at both the National Aeronautics and Space Administration (NASA) Langley Research Center (LaRC) in Hampton, VA, and the National Institute for Aviation Research (NIAR) in Wichita, KS under contract to LaRC. Analyses were done to compare to open-hole tension (OHT) and open-hole compression (OHC) tests done at NIAR, unstiffened standard- and hybrid ply specimen tests done at NASA LaRC, and stiffened standard specimen tests also tested at NASA LaRC. The description of each test and analysis comparison follows.

B. Open Hole Tension and Open Hole Compression Characterization Specimens

A wide variety of characterization tests were run to help determine material properties of both 30gsm and 70 gsm thin-ply laminates [16]. Among these tests were open-hole tension (OHT) and open-hole compression (OHC) that were performed at NIAR's laboratory according to the American Society for Testing and Materials (ASTM) standards 5766 and 6484, respectively, as well as unnotched tension (UNT) and unnotched compression (UNC) according to ASTM standards 3039 and 6641, respectively [17-20]. The loading cases were performed for multiple laminate layups, including unidirectional, cross-ply, quasi-isotropic, and hybrid laminates. The current analysis validation exclusively focused on the quasi-isotropic laminates for OHT and OHC testing from this list. The stacking sequence and average specimen thickness for each of the four laminate types are shown in the reference document, with the validation within this section only using the laminates shown in Table 2.

Table 2. Characterization testing specimen stacking sequences and average thicknesses [16].

	Stacking Sequence	Total Number of Plies	Total Thickness (in.)
30gsm-OHT/OHC – Quasi-Isotropic	[45/0/-45/90] ₈	32	0.0384
70gsm-OHT/OHC – Quasi-Isotropic	[45/0/-45/90] ₄	16	0.0448

The characterization tests yielded the material properties shown within Tables 3 and 4. The open hole tension and open hole compression properties resulting from these characterization tests are shown in Figure 3a and Figure 3b, respectively. The two types of laminates created for the tests, quasi-isotropic and hybrid, both have results shown within the table, however only the quasi-isotropic laminates were used for the model validation effort described in the following pages.

Table 3. Material properties from the open hole characterization tests [16].**(a) Open hole tension results. Blank cells indicate no data.**

Lay-up Type	Specimen Type	# Plies*	t_{lam} (in.)	t_{ply} (in.)	E^{**} (Msi)	ν	Failure Strength (ksi)	Failure Strain ($\mu\text{in/in}$)
Quasi-isotropic	D-30 gsm-OHT-0°	64	0.0792	0.0012	8.44	0.3490	58.67	
	D-70 gsm-OHT-0°	32	0.0912	0.0028	8.43	0.0263	58.82	
	NCAMP-0°	16	0.1150	0.0072	8.39		59.00	
Hybrid	F-30 gsm-hybrid-OHT-0°	[72/16/12]	0.1225			0.0227	202.65	
	F-70 gsm-hybrid-OHT-0°	[60/30/10]	0.1490			0.3160	131.03	
	NCAMP-0°	[50/40/10]	0.1440		13.15		86.59	

*For hybrid type, ply percentages given by [0/±45/90] are shown

E calculated using strains in the range 1000-3000 $\mu\text{in/in}$ **(b) Open hole compression results. Blank cells indicate no data.

Lay-up Type	Specimen Type	# Plies*	t_{lam} (in.)	t_{ply} (in.)	E^{**} (Msi)	ν	Failure Strength (ksi)
Quasi-isotropic	D-30 gsm-OHC-0°	64	0.080	0.0012	8.40		52.85
	D-70 gsm-OHC-0°	32	0.092	0.0029	7.76		48.55
	NCAMP-0°	16	0.173	0.0072			49.08
Hybrid	F-30 gsm-hybrid-OHC-0°	[72/16/12]	0.123		17.44		71.12
	F-70 gsm-hybrid-OHC-0°	[60/30/10]	0.149		14.23		71.94
	NCAMP-0°	[50/40/10]	0.144	0.0072			63.24

*For hybrid type, ply percentages given by [0/±45/90] are shown

**E calculated using strains in the range 1000-3000 $\mu\text{in/in}$

In addition to the open hole characterization tests, the paper also looked at the material characterization of unnotched specimens as well. The results from these unnotched tension and unnotched compression tests are shown in Figures 4a and 4b, respectively. Though there were multiple laminate types tested, the uni-directional properties are the only ones used within this study, and are therefore the only ones included here. The other laminate unnotched results can be found within the reference material. The

material properties for each specimen type were then applied to each individual ply within specific laminates, as shown in the stacking sequence cards within Appendix B.

Table 4. Material properties from the unnotched characterization tests [16].

(a) Unnotched tension results. Blank cells indicate no data.

Lay-up Type	Specimen Type	# Plies*	t_{lam} (in.)	t_{ply} (in.)	E^{**} (Msi)	ν	Failure Strength (ksi)	Failure Strain ($\mu\text{in/in}$)
Uni-directional	A-30 gsm-UNT-0°	64	0.078	0.0012	21.29	0.349	386.1	16,436
	A-70 gsm-UNT-0°	32	0.092	0.0029	21.22	0.347	362.0	15,499
	NCAMP-0°	6	0.043	0.0072	22.99	0.316	362.7	
	A-30 gsm-UNT-90°	64	0.077	0.0012	1.49	0.0263	10.22	7185
	A-70 gsm-UNT-90°	32	0.09	0.0028	1.42	0.0227	11.58	8654
	NCAMP-90°	11	0.079	0.0072	1.3		9.29	

*For hybrid type, ply percentages given by [0/±45/90] are shown

**E calculated using strains in the range 1000-3000 $\mu\text{ in/in}$

(b) Unnotched compression results. Blank cells indicate no data.

Lay-up Type	Specimen Type	# Plies*	t_{lam} (in.)	t_{ply} (in.)	E^{**} (Msi)	ν	Failure Strength (ksi)	Failure Strain ($\mu\text{in/in}$)
Uni-directional	A-30 gsm-UNC-0°§	64	0.078	0.0012	19.70	0.368	244.1	7840
	A-70 gsm-UNC-0°§	32	0.091	0.0028	19.50	0.367	240.2	7765
	NCAMP-0°§	14	0.101	0.0072	20.04	0.356	248.9	
	A-30 gsm-UNC-90°	64	0.078	0.0012	1.39	0.027	38.22	
	A-70 gsm-UNC-90°	32	0.091	0.0028	1.40	0.028	41.84	
	NCAMP-90°	14	0.101		1.41	0.024	41.44	

*For hybrid type, ply percentages given by [0/±45/90] are shown

**E calculated using strains in the range 1000-3000 $\mu\text{ in/in}$

§Failure strength calculated using cross-ply data and backout factor method presented in Ref. [16]

The ASTM standard open hole tension test specimen specification is shown in Figure 8a, and the ASTM standard open hole compression test fixture specifications are shown in Figure 8b. All analysis models for

the open hole characterization tests discussed herein were 1.5 in. x 11.0 in. with a 0.25-in. diameter hole in the center of the flat plate, as shown in Figure 9. The open-hole tension analyses were run with an applied displacement of 0.125 in. and the progressive failure of the specimen was tracked until catastrophic failure for both thin-ply and both hybrid-ply laminate types. The open-hole compression analyses were run with an applied displacement of -0.125 in. and the progressive failure was again tracked until catastrophic failure for each of the different laminates. Once the analysis predicted catastrophic failure, the total reaction force at the fixed end of each specimen was calculated to determine the final failure load that was associated with the corresponding axial displacement at that time step.

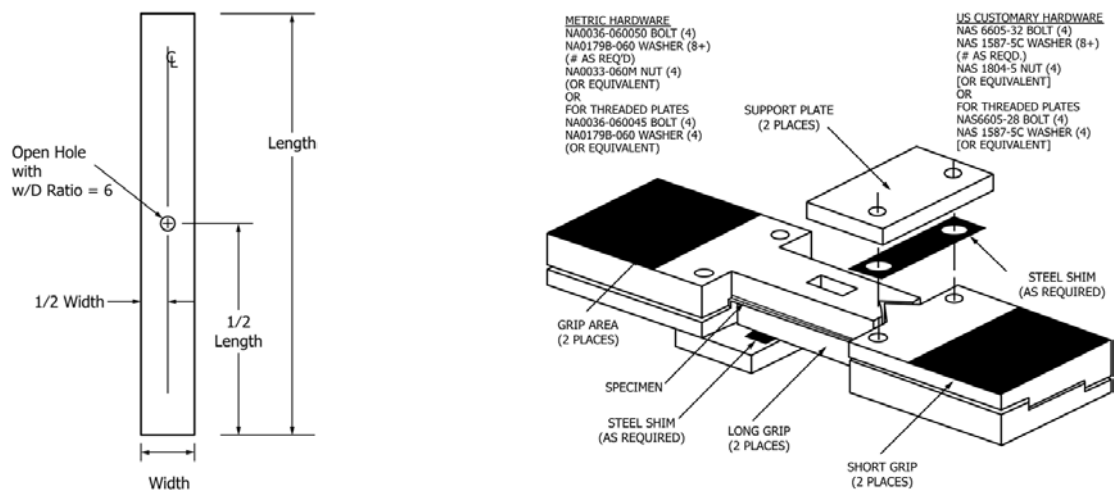


Figure 8. ASTM standards for OHT and OHC testing. (a) Schematic of OHT test specimen [17]. (b) Support fixture assembly for OHC testing [18].

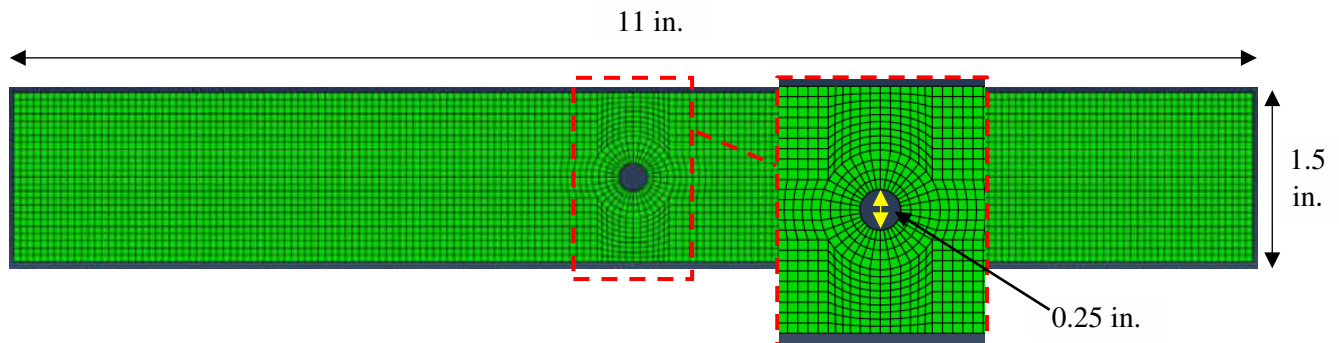


Figure 9. Images of model dimensions and mesh pattern at notch.

The Abaqus analysis was run for the 30 gsm and 70 gsm quasi-isotropic open hole tension and open hole compression laminates, yielding a total of four validation comparisons. Figure 10 shows the 30 gsm cases under OHT and OHC. As seen in the left image, the analysis stiffness matched the OHT test data well, and predicted a failure load of 7.736 kip which is 11.31% higher than the average test failure load of 6.950 kip. The right image of Figure 10 shows stiffness match with two of the tests, but the failure load is much higher than the test average. The OHC compression model predicted a failure load of 7.479 kip compared to the test average of 6.331, which is an 18.11% higher prediction. The far-field strains were only recorded for the first two replicates of the test specimens, for example 30gsm-OHT-1 and 30gsm-OHT-2 as open hole tension replicates one and two for the 30gsm specimens, respectively, and they are shown in Figure 11 along with the corresponding analysis predictions. There is less than 5% strain difference at failure, so this is a good indication of a model that is properly replicating the testing boundary conditions and specimen stiffness.

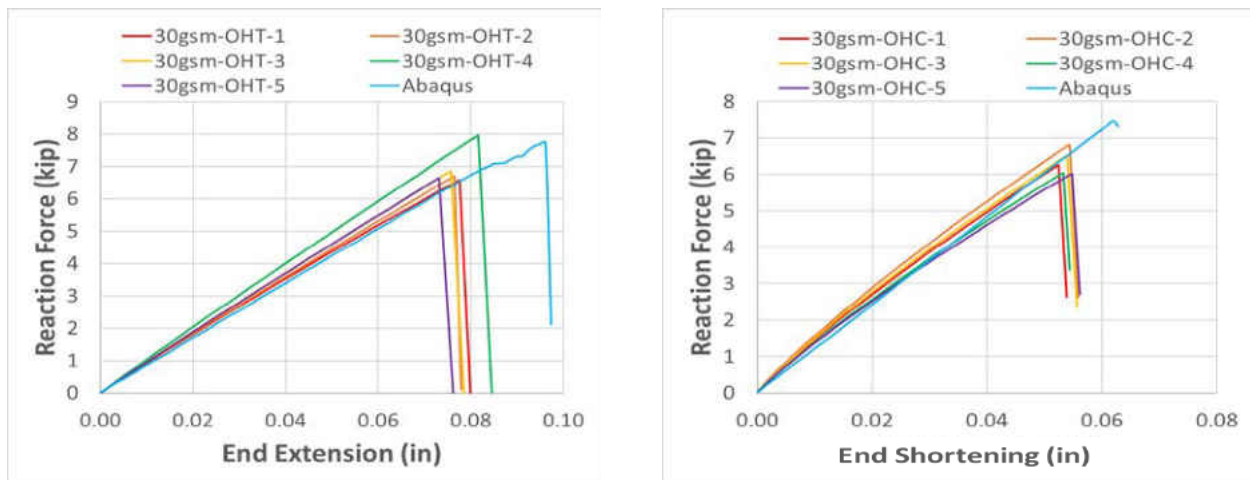


Figure 10. Load-displacement comparison for 30 gsm OHT (left) and OHC (right) specimens.

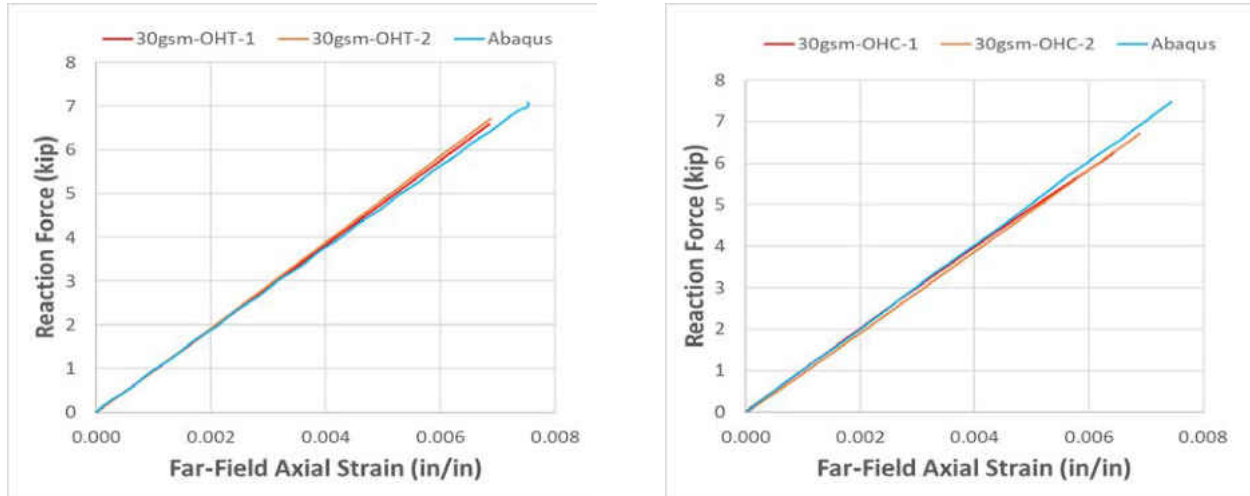


Figure 11. Load-strain comparison for 30 gsm OHT (left) and OHC (right) specimens.

The 70 gsm OHT and OHC load-displacement curves are seen in Figure 12. The OHT prediction on the left shows a failure load of 8.401 kip which is 4.18% higher than the average test failure load of 8.064 kip. The OHC failure load prediction is again much higher than the test average, with a 16.65% higher predicted failure load of 7.833 kip compared to the test average of 6.715 kip. The far-field strains were only recorded for the first two replicates of the test specimens, and they are shown in Figure 13 along with the corresponding analysis predictions. There is again less than 5% strain difference at failure, so the model is performing as expected.

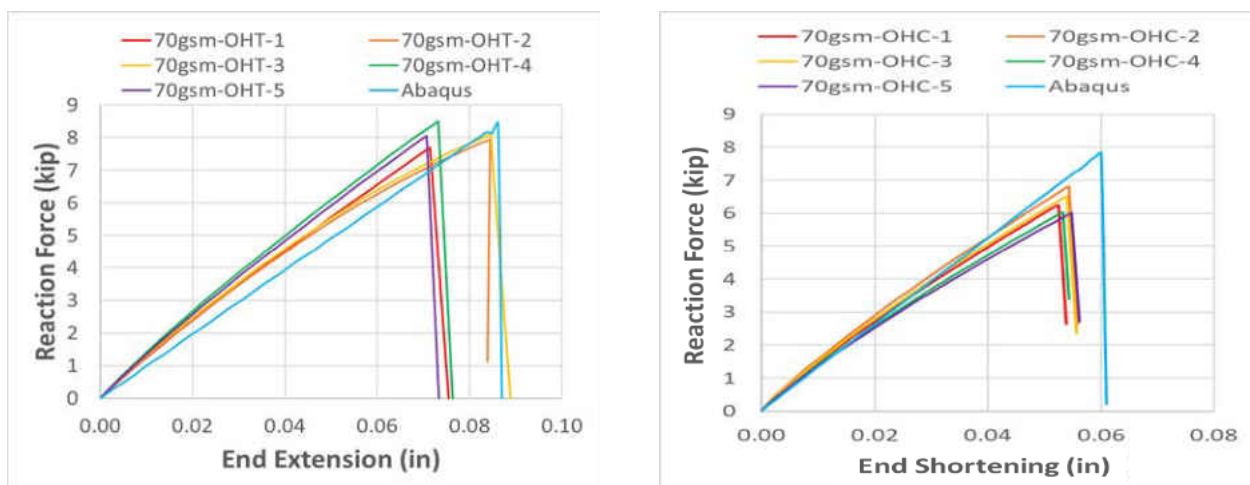


Figure 12. Load-displacement comparison for 70 gsm OHT (left) and OHC (right) specimens.

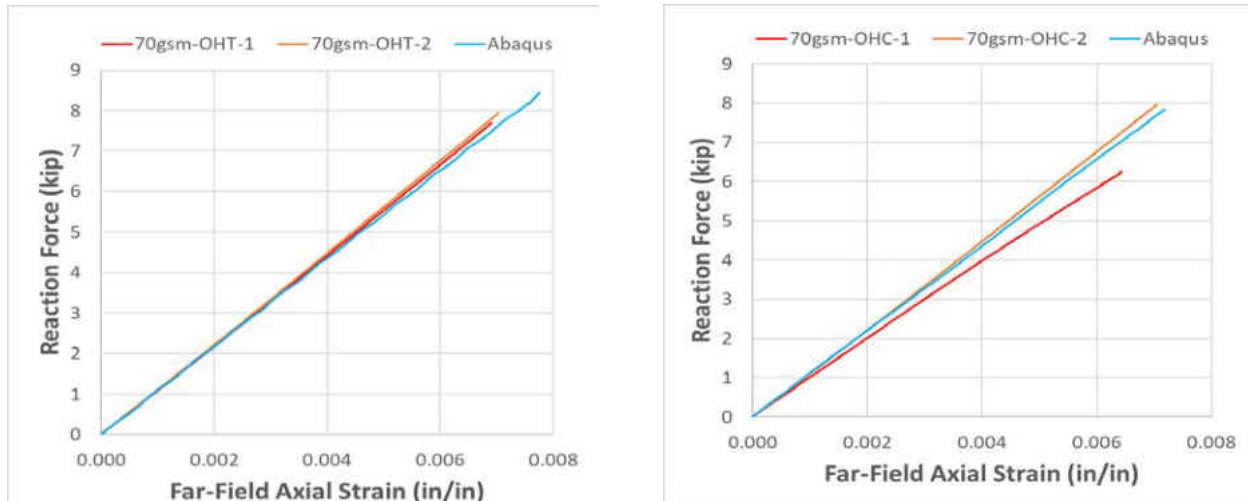


Figure 13. Load-strain comparison for 70 gsm OHT (left) and OHC (right) specimens.

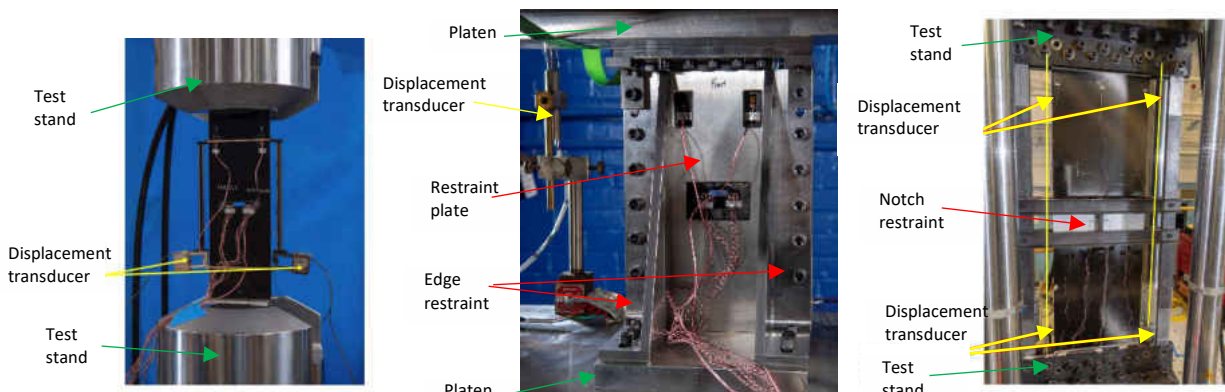
These OHT and OHC validation models are imitating the test boundary conditions and stiffnesses well, but it should be noted that the compression failure load is up to 20% too high when compared to the test data. Any compression models that are run using the material properties mentioned previously will need to be given a possible reduction factor of some kind to better predict the actual failure load. The tension predictions were better attuned, and can thus be used as-is without a significant concern of over- or under-prediction.

C. Unstiffened Standard-Ply Specimens

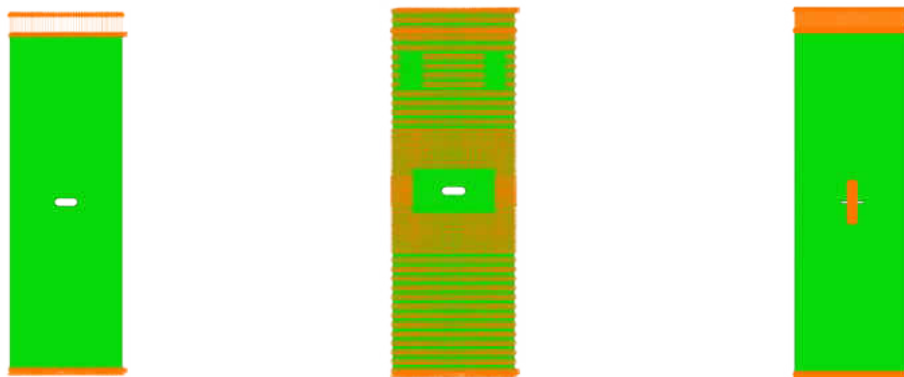
The next set of analyses that were performed to help ensure model validation was for “small” and “intermediate” unstiffened standard-ply specimens [21]. The specimens that will be referred to as “small” were 4 in. x 12 in. flat specimens with a center notch that was 0.8 in. long and had a 0.125-in. radius at both notch ends. The “intermediate” unstiffened specimens were 20 in. x 60 in. and contained a 4-in. long center notch with a 0.125-in. radius at the notch ends and a tapered design to a total notch width at the middle of 0.375 in. The reason for the tapered notch within the intermediate specimens was to ensure there was not complete closure and interference when the specimens were tested under compression. However, this analysis validation only discusses the small specimens under tensile and compressive loading, and the intermediate specimens under tensile loading because the compression tests were conducted by industry partners and the results have not been published.

The three types of unstiffened standard-ply specimens were all tested at the NASA Langley Research Center Structures and Materials Laboratory, and all test specimens had 190gsm standard-ply material, with a stacking sequence of $[45/90/-45/0_2/45/90/-45/0]_s$, which yielded a specimen thickness of 0.1296 in. The

comparison between the test specimens within the test stands and the analysis models with corresponding test fixture boundary conditions is shown in Figure 14a and 14b, respectively. The small standard tension specimen analysis was run to a displacement of 0.125 in., the small standard compression specimen analysis was run to a displacement of -0.125 in., and the intermediate standard tension specimen analysis was run to a displacement of 0.4 in. The final failure load of each specimen was again calculated by finding the total reaction force within the fixed end of the specimens. The load-displacement curve of the each test specimen compared to the Abaqus SC8R element analysis is shown in Figures 15a-c. Each test specimen also contained strain gages at the notch region as well as far-field on the specimen, and the location of all strain gages are shown in Figure 16 for the small tension, small compression, and intermediate tension specimens, for both standard-ply and hybrid-ply laminates. There were three small standard tension and compression specimens for each test, each with two displacement transducers measuring end extension or end shortening. The intermediate standard tests only had two replicates, each also with two displacement transducers measuring end extension.

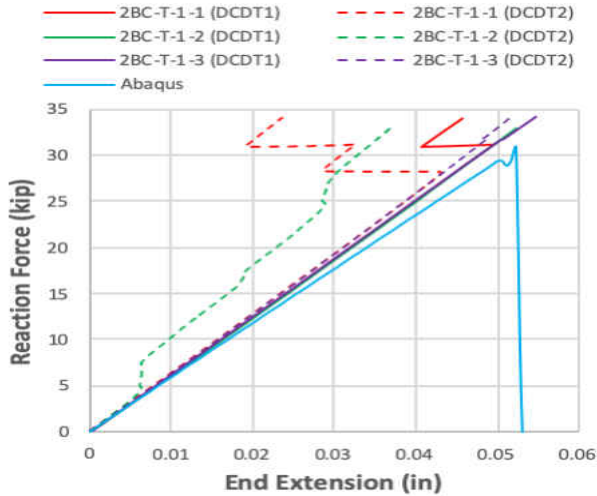


(a) Test Images. Left to right: Small tension, small compression, and intermediate tension.

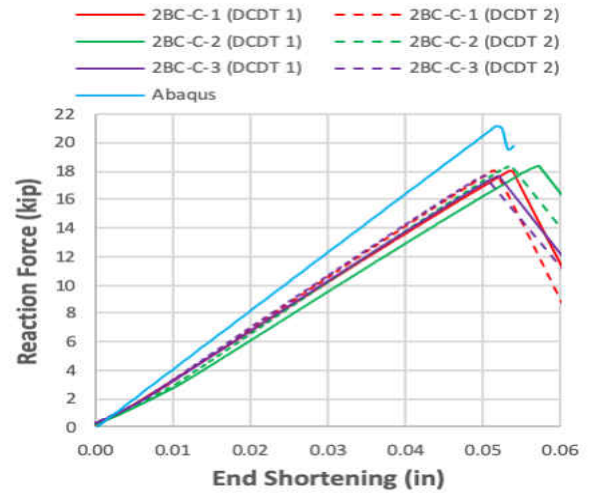


(b) Analysis Images. Left to right: Small tension, small compression, and intermediate tension.

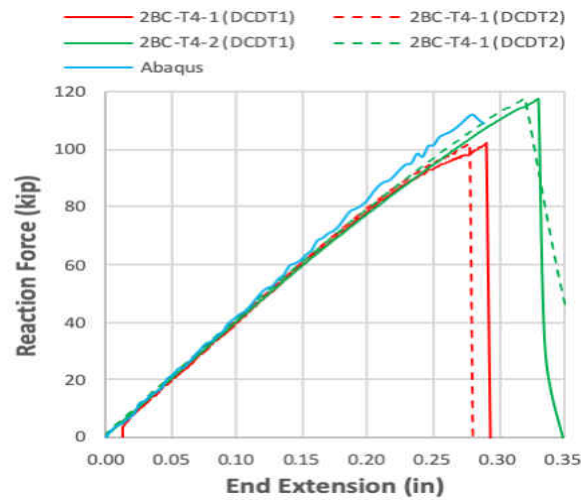
Figure 14. Test specimens within the test stand vs. analysis boundary conditions. Not to scale.



(a) Small standard tension specimens.



(b) Small standard compression specimens.



(c) Intermediate standard tension specimens.

Figure 15. Test data vs. analysis load-displacement curves.

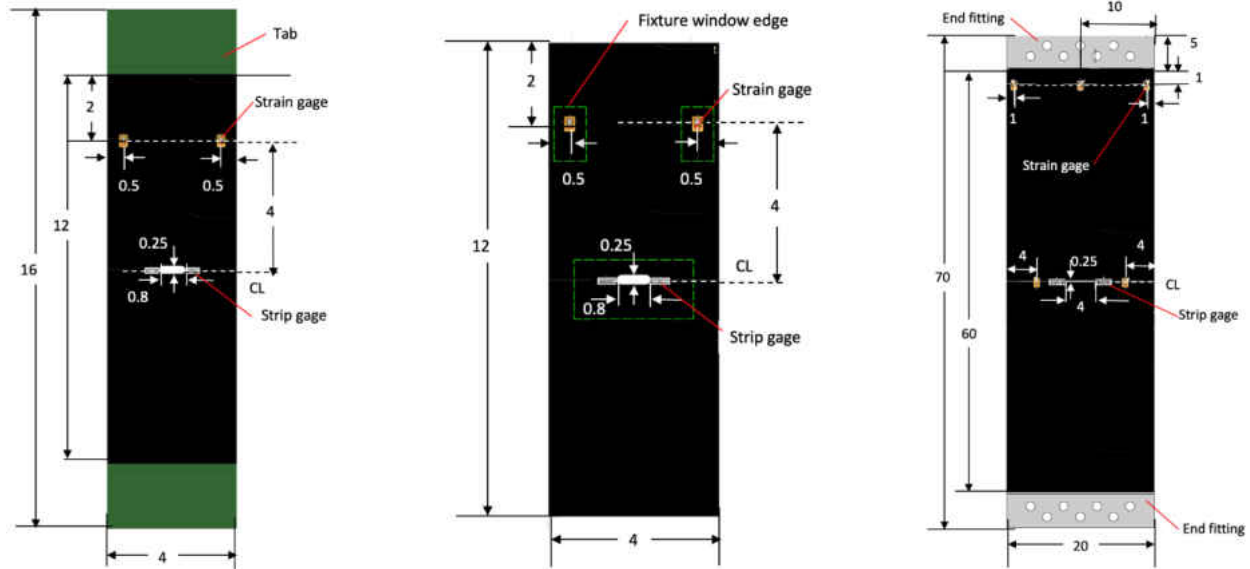


Figure 16. Strain gage locations for unstiffened test specimens. From left to right: small tension, small compression, and intermediate tension. Not to scale, dimensions are in inches.

The small standard tension analysis compared fairly well with the test data, with the difference of the final failure load of the analysis 8.74% higher than that of the average test failure load. As shown in Figure 17, the far-field strains for the analysis correspond very closely with those from the test data. The notch strain gages also correspond as well as can be expected for such a damage-heavy area. The strain gages that are referenced in each graph are circled in red. The load-displacement curve for the small standard tension specimen in Figure 15a shows a slightly different slope for the analysis than for the tests, so this could be due to strength differences from the modeling practices. The failed specimens, shown in Figure 18, show a failure path perpendicular to the direction of loading, originating at the notch tips. There is also evidence of delamination or peeling of the outer 45° plies. When compared to the test images, the Abaqus model shown on the right side of the same figure shows clear Hashin tensile matrix damage from the notch tips as well. The contour legend shows numbers that represent the percentage of failure within each element, with 1.000e+00 equivalent to 100% failure within those red elements. The gaps between the red sections are where there is actual separation or element deletion due to total failure within those individual elements. The bright green contours in this plot represent a minimum of 51% of the element having failed, and these diagonal paths of partial failure within the top ply, LAYER_18 in the legend, are likely representative of the same delamination failures we see within the test specimens on the left.

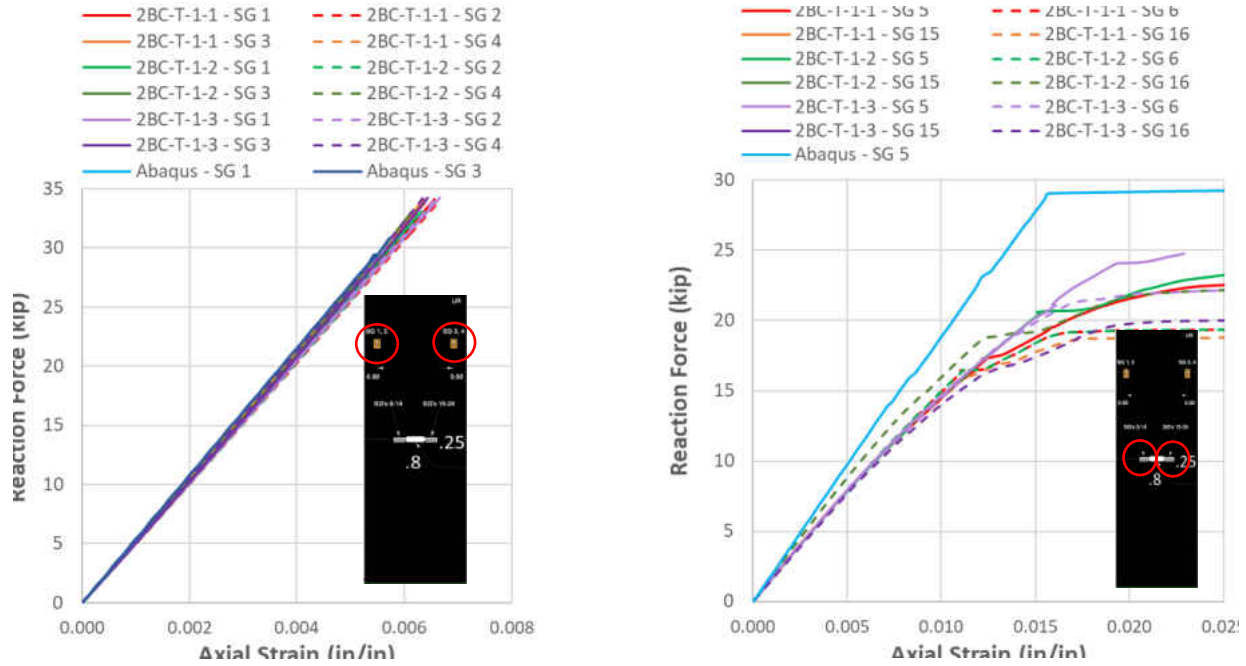


Figure 17. Load-strain plots for small standard tension specimens at far-field locations (left) and notch-tip locations (right).

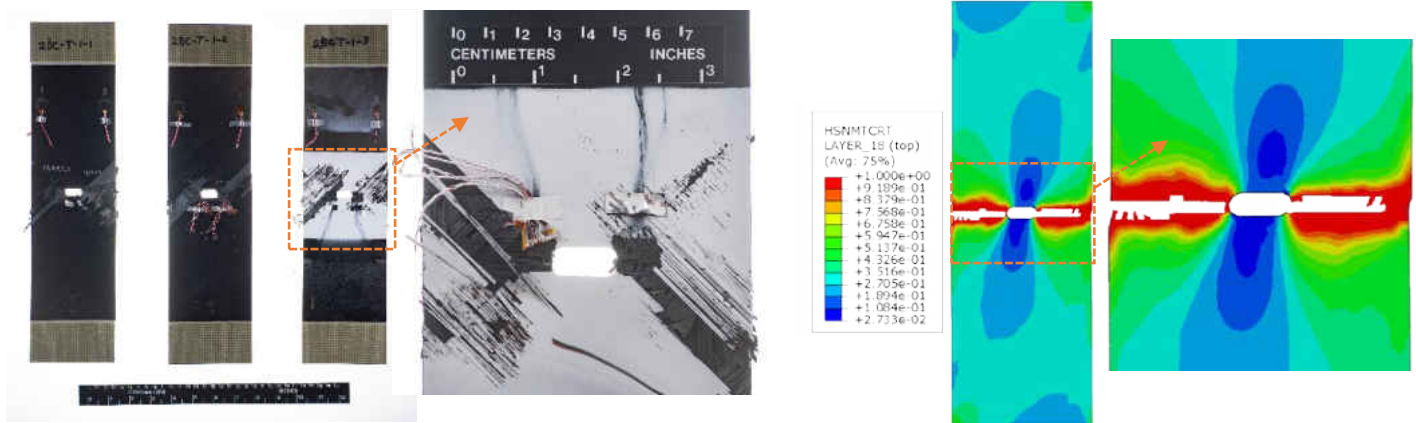
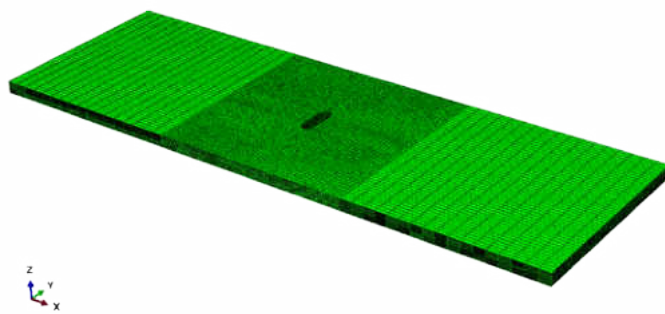


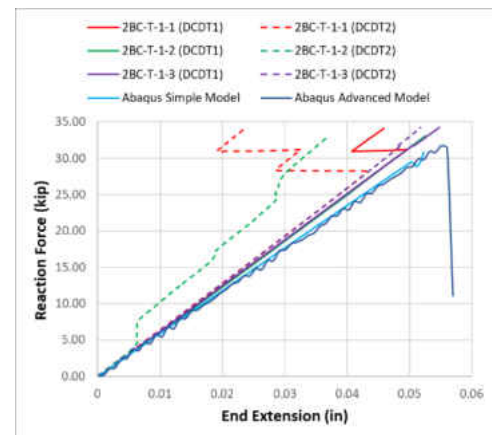
Figure 18. Small standard tension failed test specimens (left) and Abaqus failure prediction (right).

The analysis model is only one element through the thickness, and does not accommodate for any interactions that may happen between plies. There was also significant peeling of the outer plies during failure progression within the tests, but this simplified model does not accommodate those responses. Therefore, another model was created that had individual elements through the thickness for each ply, as well as the COH3D8 cohesive elements previously mentioned that are between each ply. This advanced

model was able to better track the damage progression in between plies as well as some small instances of surface ply delamination at failure. This type of model is very complex and expensive to run, so it is not ideal for all cases. However, it is a good example of more detailed models matching test data better, and also helping to decide that the less complex models are good enough for the large amount of analyses that need to be run for the design study investigations that are presented later in this document. A side-view of the advanced model is shown in Figure 19a, and the load-displacement comparison between the advanced model and the test data is shown in Figure 19b. Figure 19c shows the comparison between the advanced model and one of the test specimens, and the Hashin tensile matrix failure within the top ply element shows much better correlation of the delamination failure than the simple model comparison. The contour plot in that figure, labeled SDEG in the legend, shows the cohesive degradation that occurred between the top ply and the one immediately below it, showing the delamination of the outer plies that is seen in the photograph on the right of Figure 19C. However, when comparing the blue load-displacement curves within Figure 19b, there is little change between the simple model and advanced model, so the simple model was deemed appropriate enough for the future modeling investigation, with the caveat that any delamination investigations may be more appropriate within advanced modeling efforts due to the lack of small-scale fidelity shown within the bright green damage contour in Figure 18.

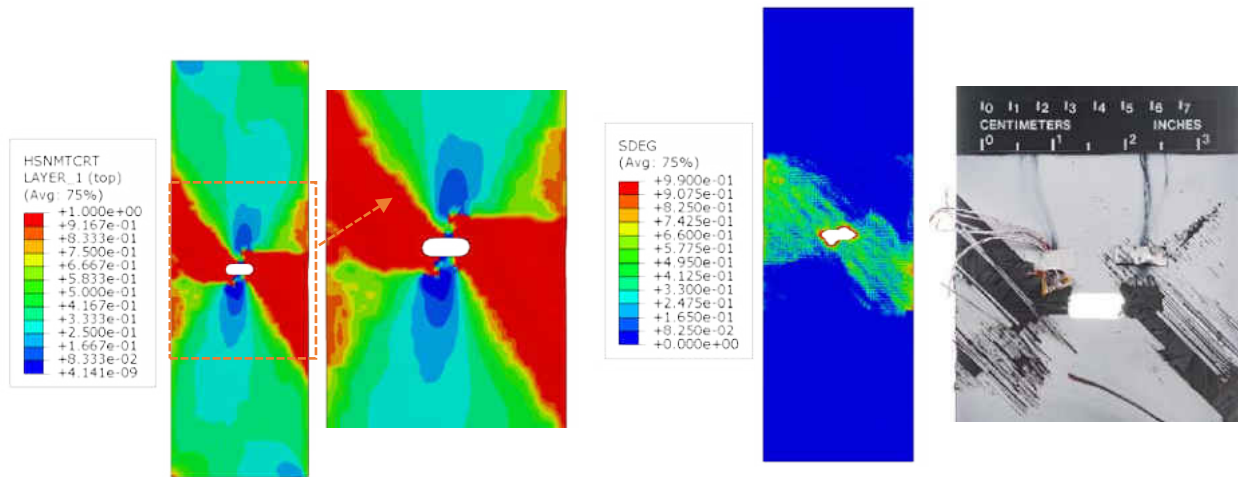


(a) Isometric view of advanced model.



(b) Load-displacement model comparison.

Figure 19. Advanced small standard tension model.



(c) Hashin matrix failure prediction (left) and cohesive degradation (center) compared to test specimen failure (right).

Figure 19. Advanced small standard tension model (concluded).

The small standard compression analysis did not predict the failure load as well as the small standard tension analysis, which is consistent with what was observed with the OHT and OHC comparisons. The small standard compression analysis failure load was 16.56% higher than the average test results, and the slopes of the analysis and test data, shown in Figure 15b, are significantly different. Again, the slope difference could be due to the simplicity of the modeling or interactions between plies that are not known but can be exacerbated under compressive loading. To continue with compressive predictions using this modeling approach, it must be acknowledged that the failure load will be significantly over-predicted, and either a knockdown factor should be applied as a kind of factor of safety for future design, or the damage progression energy would need to be corrected for each different laminate. The far-field strains match well between the analysis and test, as shown in Figure 20, and the analysis notch-tip strains also follow the trend of the test notch-tip strains. The failed specimens shown in Figure 21 show the specimens failed straight across along the path from the notch tips. There is minimal evidence of damage to the outer 45° plies, but one side of the zoomed-in specimen does show a diagonal path as the crack propagates across the rest of the way, outlined with the yellow box. Only one of the three tested specimens failed in this manner. The Abaqus model shown on the right shows Hashin compressive matrix damage perpendicular to the load application starting from the notch tips as well, as indicated by the 100% failed red elements again. The left side of the model contour shows more damage predicted than the right side, but in general the bright green contours show only a transverse failure path. This aligns well with 2BC-C-2 and 2BC-C-3, the middle and right test specimens on the left set of images within Figure 21, but 2BC-C-1 had the diagonal failure path

that was not predicted by the simple model. An advanced model used in this scenario may be able to capture this diagonal path, but due to time and cost constraints it was not included in this study.

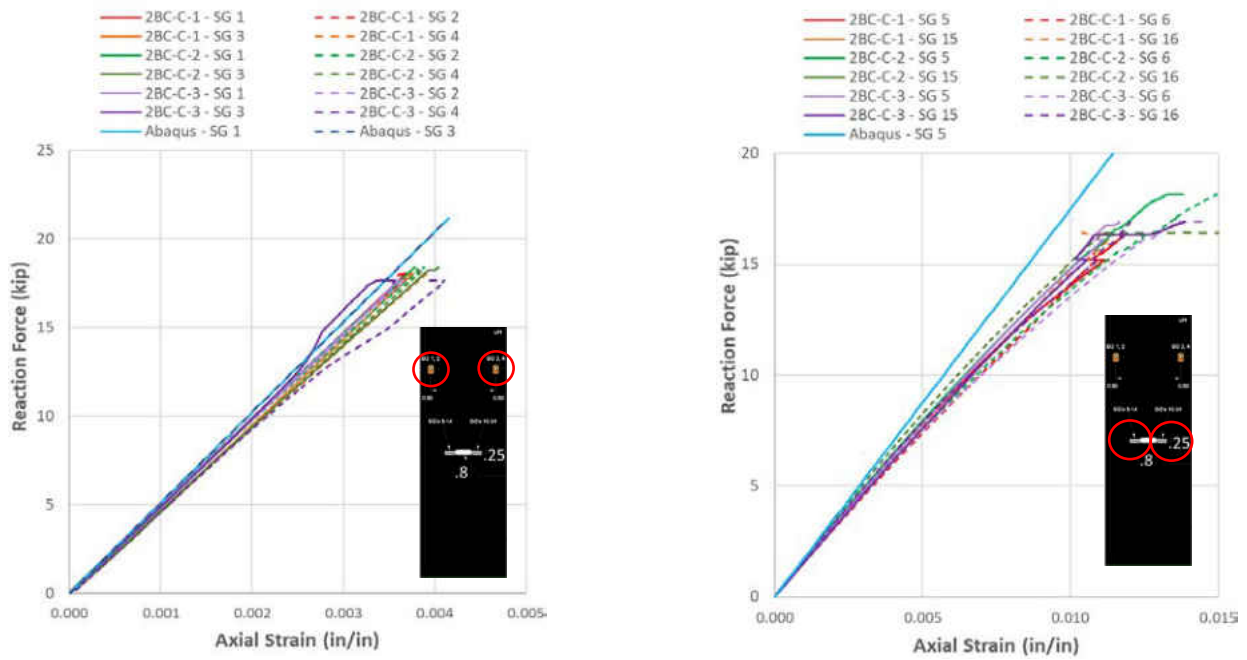


Figure 20. Load-strain plots for small standard compression specimens at far-field locations (left) and notch-tip locations (right).

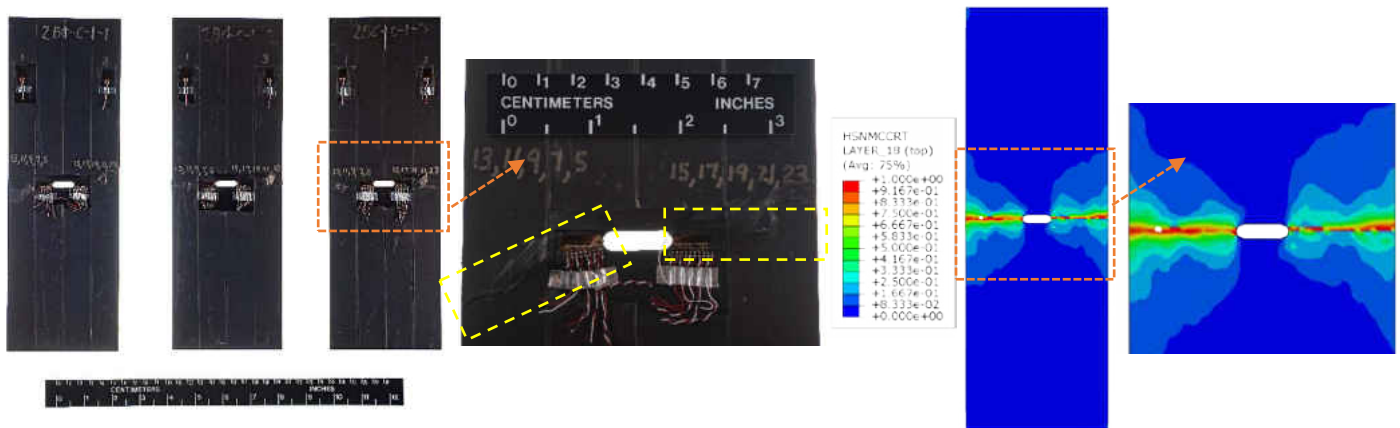


Figure 21. Small standard compression failed test specimens (left) and Abaqus failure prediction (right).

The intermediate standard tension analysis matched the best out of this set of analyses, with the failure load prediction only 2.25% lower than the test average failure load. The two tests had about a 15% spread between their failure loads, as seen in Figure 15c, but the analysis prediction fell between the two tests, thus matching the average failure load well. The slope of the analysis also matches the slopes of the load-displacement test curves up until the two tests start experiencing nonlinear behavior. The far-field strain plots show a small amount of deviation from linear within the second-tested specimen, 2BC-T-4-2 in Figure 22, but the analysis follows the far-field linear behavior of the first specimen tested, 2BC-T-4-1, fairly well. The notch-tip behavior is very consistent among both tests and the analysis, which shows damage initiation for the tests and analysis are occurring at roughly the same load value. The test specimens are shown after failure, but still in the test stands, on the left side of Figure 23. These specimen images show significant peeling of the outside 45° plies, as well as a fairly transverse crack path with a few diagonal sections as the damage worked its way away from the notch tips. The predicted Hashin tensile matrix contours on the right show an almost completely straight crack path from the notch tips along the red 100% failed elements. The bright green contours do have a wide range at the edges of the specimens, so even though the completely failed elements are along a solely transverse path, there is some variation within the top color ranges that could indicate the delaminations shown in the test images, or a more diagonal crack path than the fully failed elements would lead one to believe. Again, an advanced model would be beneficial in this case to better predict the failure paths, but the simple model is so large that a more advanced model would be computationally very expensive and lengthy to run. For this reason, the decision was made to exclusively model the predictive investigations with the small 4 in. x 12 in. models.

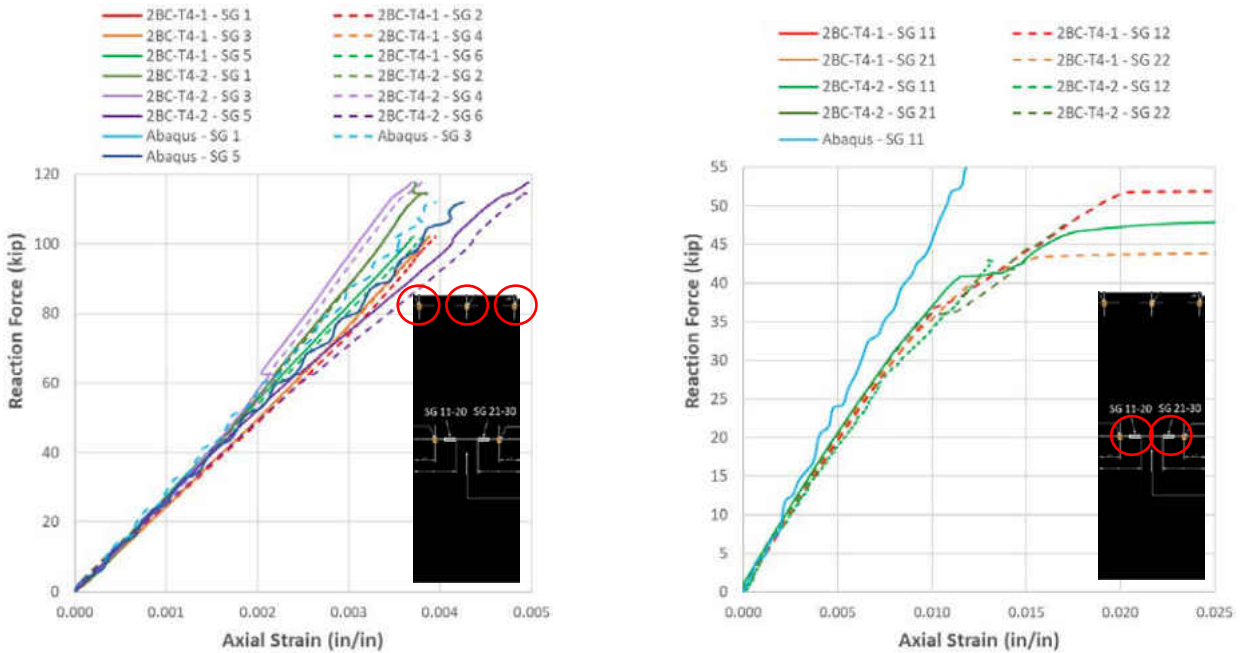


Figure 22. Load-strain plots for intermediate standard tension specimens at far-field locations (left) and notch-tip locations (right).

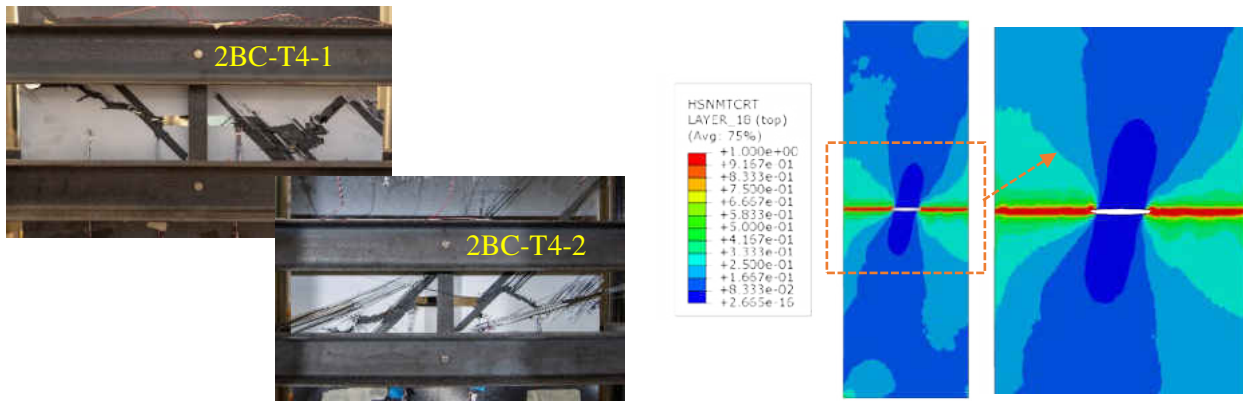


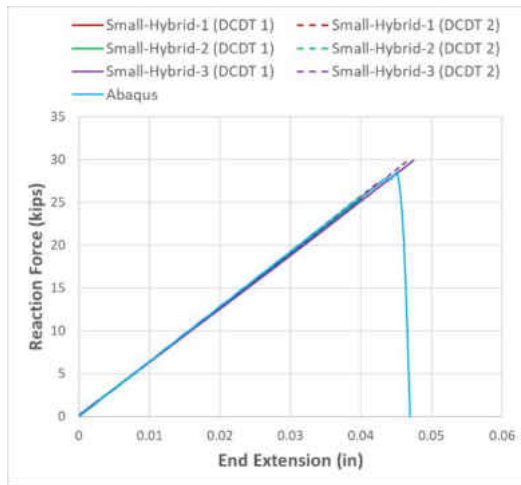
Figure 23. Intermediate standard tension failed test specimens (left) and Abaqus failure prediction (right).

The unstiffened standard-ply analyses were performed as part of the model validation to ensure future modeling will be accurate enough to predict trends that can be expected. The trends taken from these models show that tension analyses are more accurate at this time than compression analyses, and that the compression models will predict higher failure loads than the real test specimens.

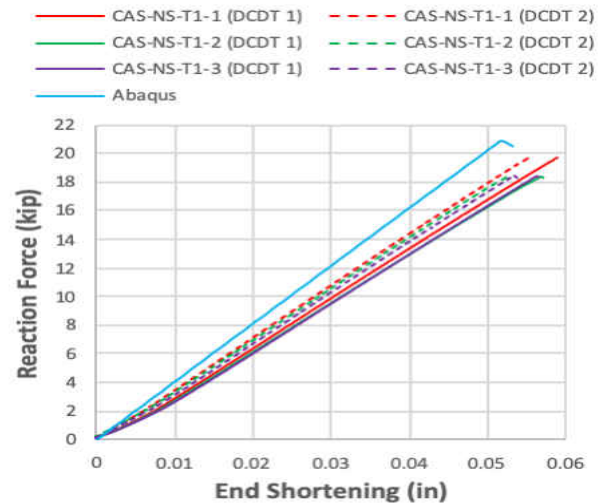
D. Unstiffened Hybrid-Ply Specimens

Another set of analyses that were performed to help ensure model validation was for “small” and “intermediate” unstiffened hybrid-ply specimens [22]. The hybrid-ply specimens were designed to be the same dimensions as the standard-ply specimens previously mentioned, with the only difference being the stacking sequence in order to also replicate the specimen thickness of 0.1296 in. The small specimens were 4 in. x 12 in. with a 0.8 in. long center notch and the intermediate specimens were again 20 in. x 60 in. with a 4-in. long tapered center notch. The small and intermediate hybrid laminate tests were run similarly to the equivalent standard laminate tests, and the test setup and model images for the hybrid-ply specimens are the same as those in Figure 14.

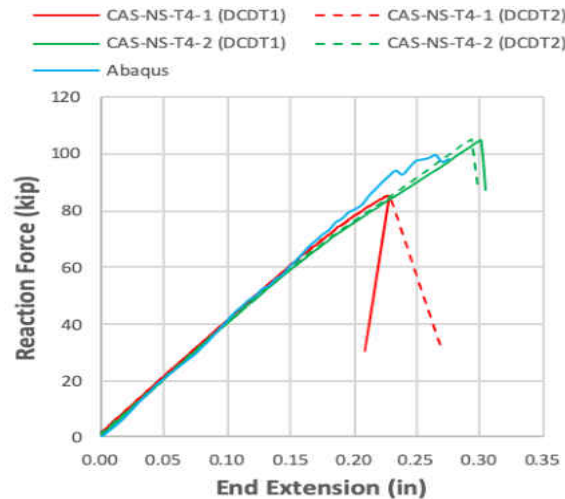
The three types of unstiffened hybrid-ply specimens were also tested at the NASA Langley Research Center Structures and Materials Laboratory, and each test specimen had a hybrid mix of standard- and thin-ply materials. The stacking sequence of all hybrid specimens was $[\pm 45/90/\mp 45/0/\pm 45/0/\pm 45/90/\mp 45/0/\pm 45_{(t30)}]_s$, with all 45 degree plies, both positive and negative, being 70 gsm thin-ply material except where designated with “(t30)” that was the 30 gsm thin-ply material. All 0 and 90 degree plies were laid down in the 190 gsm standard-ply material. The small hybrid tension analysis was run with an applied displacement of 0.125 in., the small hybrid compression analysis was run with an applied displacement of -0.125 in., and the intermediate hybrid tension analysis was run with an applied displacement of 0.4 in, just as their corresponding standard laminate specimens. The final failure load of each specimen was still calculated by finding the total reaction force on the fixed specimen edge. The load-displacement curves for each test specimen and its analysis comparison are shown in Figure 24. All test specimens contained strain gages at the same locations as on their respective standard-ply test specimens, shown previously in Figure 16. There were again three small hybrid tension and compression replicates with two displacement transducers on each. The intermediate hybrid tests only had two replicates with two displacement transducers as well.



(a) Small hybrid tension specimens.



(b) Small hybrid compression specimens.



(c) Intermediate hybrid tension specimens.

Figure 24. Test data vs. analysis load-displacement curves.

The small hybrid tension analysis compared very well with the test data, with the final failure load of the analysis only 2.35% lower than the average failure load of the tests, which is an improvement on performance compared with the small standard tension analysis. The far-field strains for the analysis correspond well with the test data strains at the same location, as shown in Figure 25. The notch strain gages also correspond well among the test and analysis data. The load versus displacement curves for the small hybrid specimen show almost an exact correlation between the analysis and the tests, showing that the behavior of the specimen was modeled well in this case. This analysis may match better than the small standard tension specimen because there was less outer-ply delamination that can't be tracked as well by the simple models. Thus, the more exclusively self-similar failure of the small hybrid specimens was

predicted well with the analysis. The failure path in Figure 26 initiates at the notch tips and runs mainly transversely. There is also minimal evidence of delamination of the outer 45° plies in two of the specimens. There is also a small triangular piece that separated completely from the specimen furthest to the right of the three test specimens. The Abaqus model on the right side of the Figure 26 shows clear Hashin tensile matrix damage from the notch tips, and the bright green damage shows a slight tendency for minimal additional damage alongside the crack path.

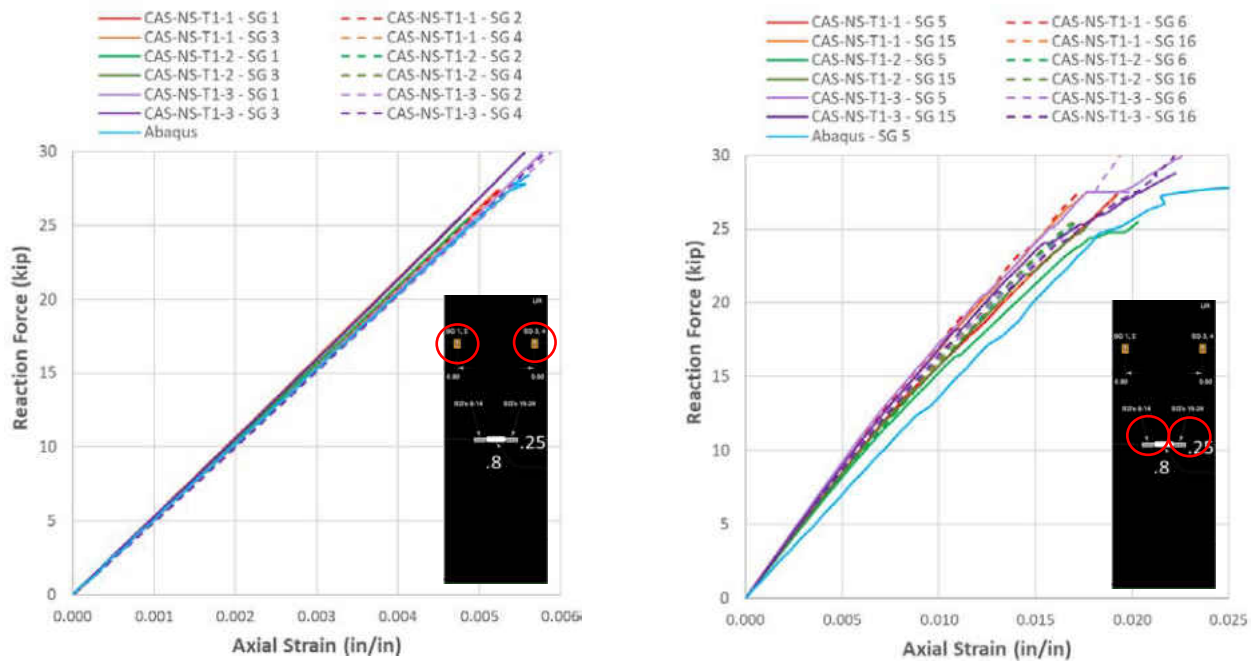


Figure 25. Load-strain plots for small hybrid tension specimens at far-field locations (left) and notch-tip locations (right).

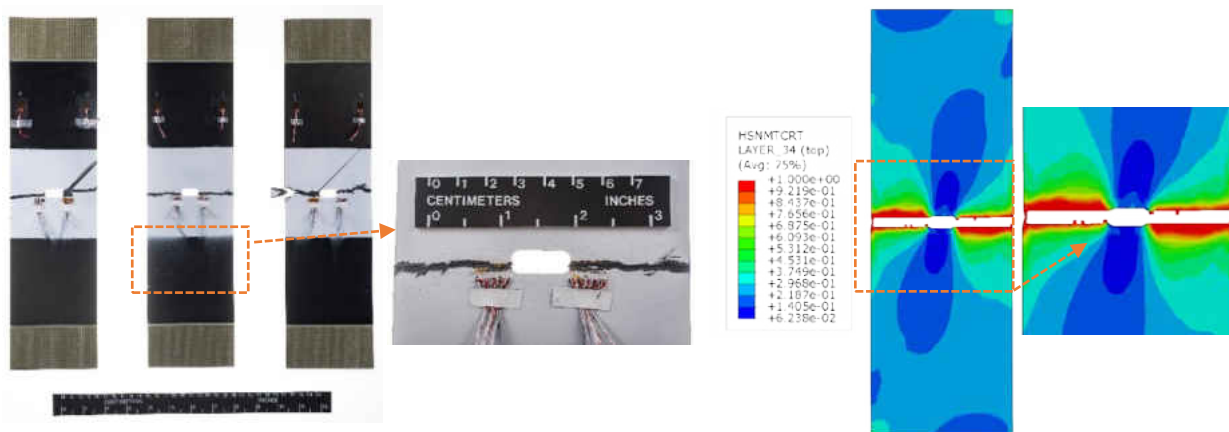


Figure 26. Small hybrid tension failed test specimens (left) and Abaqus failure prediction (right).

An advanced model with cohesive elements between each ply was also created for this specimen to predict a triangular failure at the end of the self-similar growth of the small hybrid tension specimen, as shown in Figure 27. This model was able to predict the failure load well, with under 10% difference from the test average. The model was also able to show evidence of the triangular damage section, indicated by the green section “trapped” within the red crack path along the bottom of the analysis specimen on the left of figure 27c. This ability to predict the full failure modes, including any non-typical failures, would be good to use for situations where a detailed analysis is needed and cost minimization is not as critical.

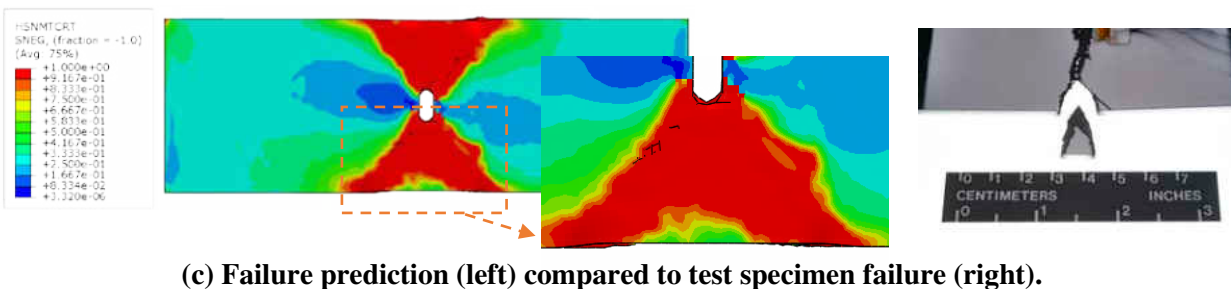
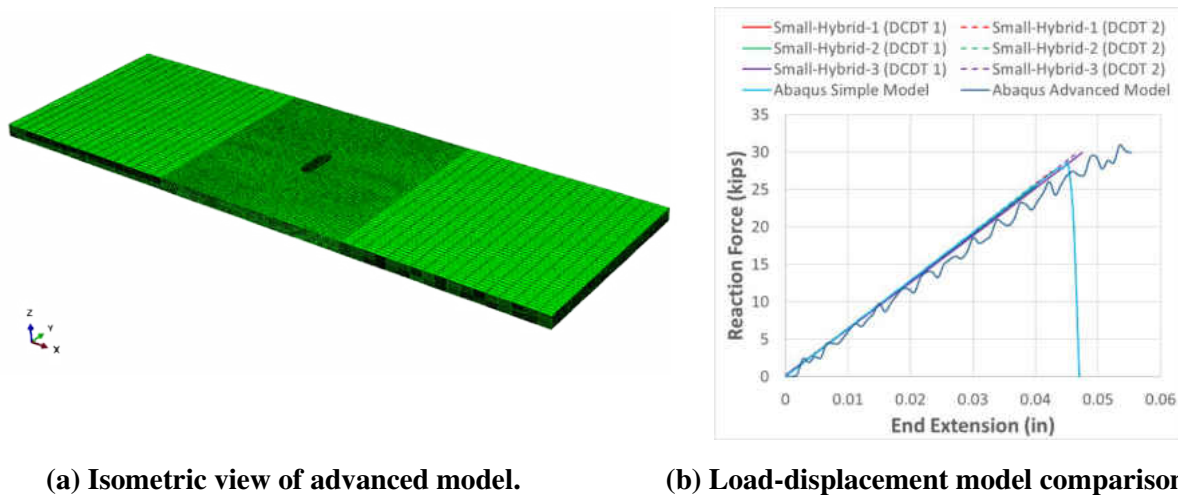


Figure 27. Advanced small hybrid tension model.

The small hybrid compression analysis predicted the failure load as well as the small hybrid tension analysis predicted its corresponding test data, and it predicted failure much better than the equivalent small standard compression comparison. The small hybrid compression analysis failure load was only 2.45% higher than the average test results, but the slopes of the analysis and test data in Figure 24b are significantly different again, just as in the small standard compression analysis. It is clear again there are issues with the

simple models that are more extreme in models with compressive loading. However, the hybrid models perform better than the standard laminate models. The far-field strains of the small hybrid compression analysis match the test data despite some spread within the test data, as shown in Figure 28, and the analysis notch-tip strains also agree with the notch-tip strains fairly accurately. The only thing the simple model was seemingly not able to predict is the evidence of bending in the far-field strain gages of CAS-NS-C-2 and CAS-NS-C-3, indicated by the solid and dotted lines diverging from each other above around 12 kip. In Figure 29, the predicted failure path is similar to that of the small standard compression analysis. The red damage, Hashin compressive matrix damage runs straight across the specimen from the notch tips, and the bright green 50% damage is close to the transverse crack path as well, without much spread like in the small hybrid tension analysis. The test specimens on the left show completely perpendicular failure, although still slightly hard to see due to the Teflon tape placed on the faces to allow sliding along the test fixture. The analysis matches this failure well, and neither the test specimens nor the model show signs of external delamination.

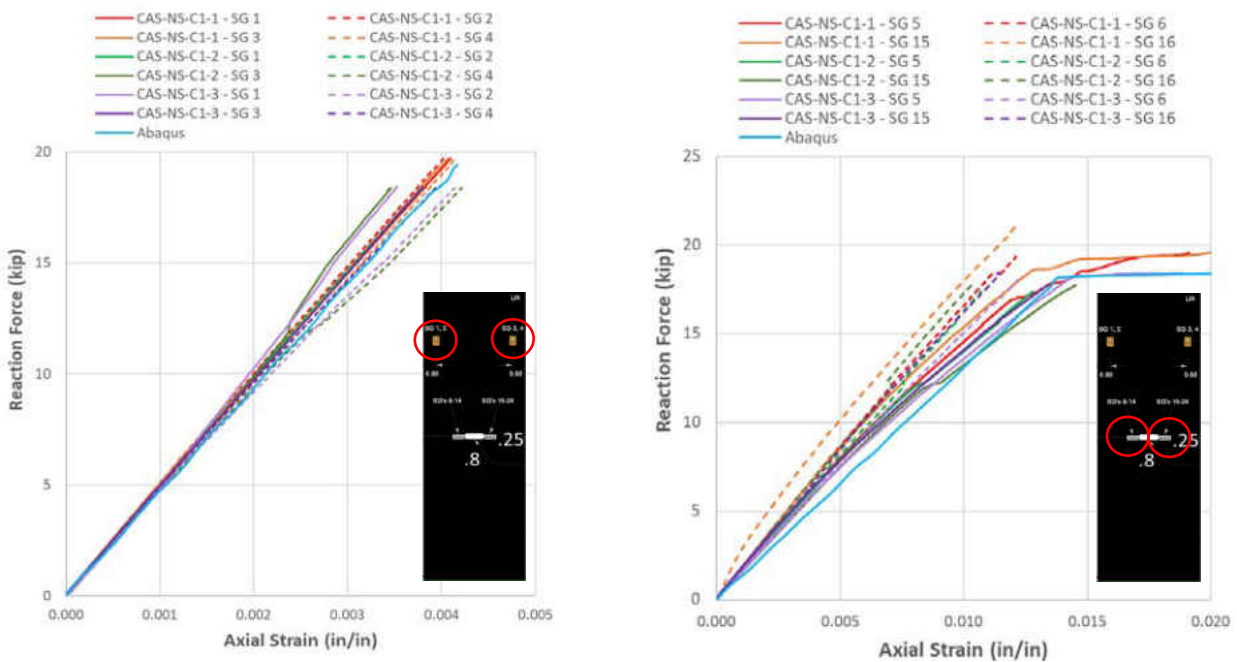


Figure 28. Load-strain plots for small hybrid compression specimens at far-field locations (left) and notch-tip locations (right).

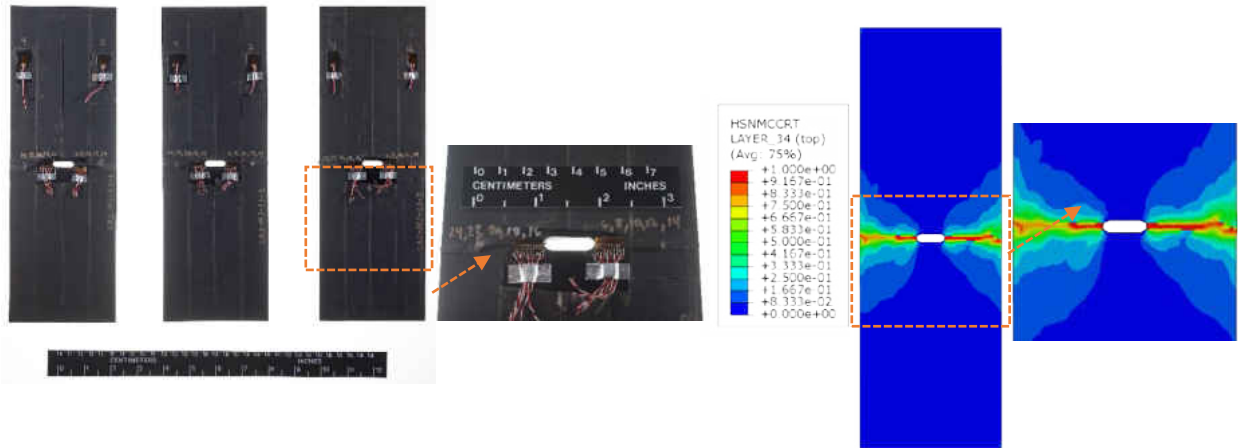


Figure 29. Small hybrid compression failed test specimens (left) and Abaqus failure prediction (right).

The intermediate hybrid tension analysis predicted a failure load 3.35% higher than the test average failure load. There was some slippage during one of the two tests, but after adjusting the final failure load based on the load-strain curve, the two tests also had about a 15% spread between their failure loads just like the intermediate standard tests. As shown in Figure 24c, however, the analysis prediction once again fell between the two tests and was even able to capture some of the nonlinear behavior of the tests as the model started to fail. An additional advanced model was not done for this analysis since the initial analysis displayed some of the nonlinear loading behavior. The far-field strain plots show the slippage within the first specimen, CAS-NS-T4-1 in Figure 30, and the analysis tends to follow the slope trends of the second-tested specimen, despite the plots not overlaying each other perfectly. The notch-tip strains align very well between both tests and the analysis, which shows that the model is predicting damage initiation among the hybrid laminate models accurately. Both failed test specimens, shown in Figure 31, show failure paths originating at the notch tips and maintaining a mostly transverse path on at least one side. CAS-NS-T4-1 had the left side run in a series of diagonal and transverse paths towards the end, while CAS-NS-T4-2 had cracks perpendicular to loading on both sides. Both specimens also exhibited the triangular disconnected piece on one side, just like one of the small hybrid tension specimens. The Abaqus prediction shows transverse Hashin tensile matrix damage from the notch tips, and the bright green damage is more severe on the right side of the specimen. This could be an indication of an analytic tendency towards the triangular failure for this model, but the simple model may not be able to capture the full behavior like an advanced model would, as shown for the small hybrid tension specimen in Figure 27 above. The intermediate specimens were so large that an advanced model would be very expensive in terms of modeling and analysis

time, so it was not performed in this case. However, there is at least some indication within the simple model that there is non-symmetric failure on either side of the notch as seen in the actual test specimens.

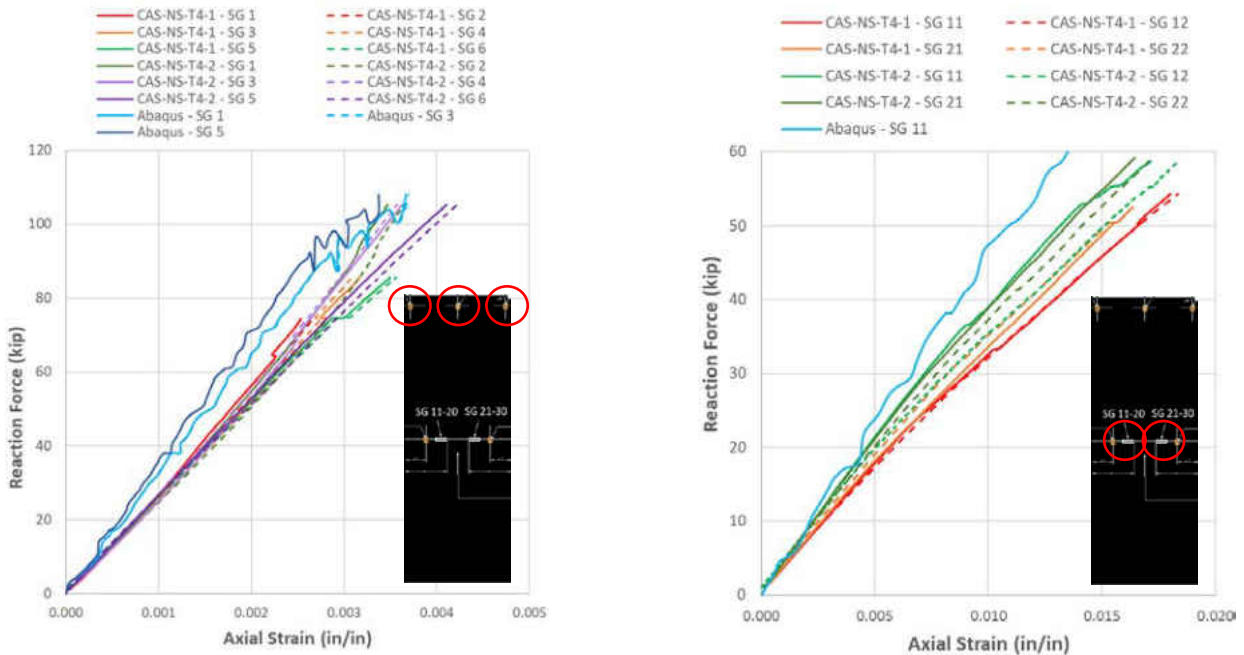


Figure 30. Load-strain plots for intermediate hybrid tension specimens at far-field locations (left) and notch-tip locations (right).

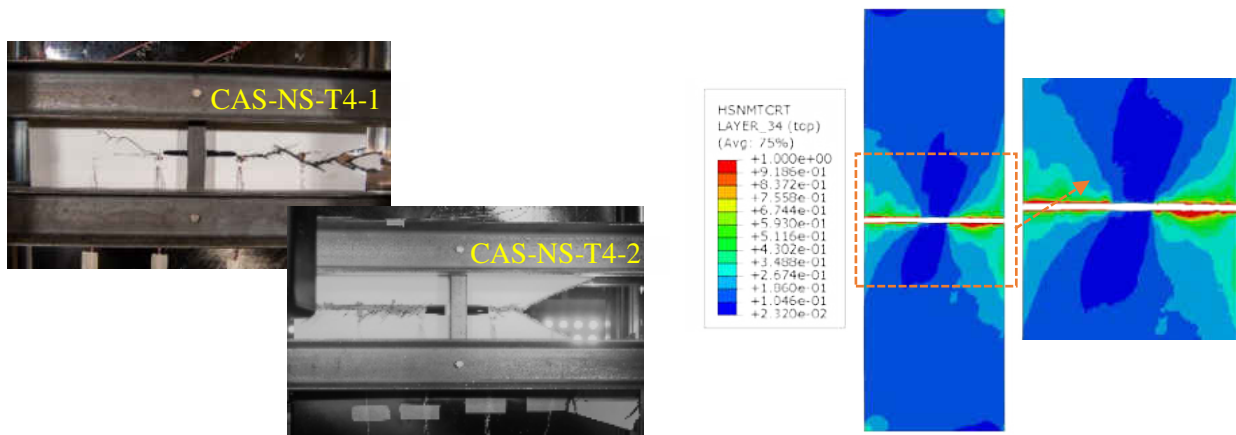


Figure 31. Intermediate hybrid tension failed test specimens (left) and Abaqus failure prediction (right).

A series of unstiffened hybrid-ply analyses were performed as another part of model validation so that finite element analysis can be used exclusively to investigate future laminate changes. The trends taken from the hybrid laminate models show that all analyses are statistically comparable to test data within 5%, and that all of the hybrid models investigated herein predicted slightly higher than the recorded test data. There was also another advanced model prediction to determine if the greater fidelity would be able to better predict the test failure. The small hybrid tension advanced model did predict all failure modes better than the corresponding simple model, and it would be ideal to use in cases where time and cost are not as important as model prediction reliability. In any other case, the simple models were deemed sufficient for their comparisons with the test data, with the reminder that the standard-ply laminate compression predictions are 10-20% higher than the test failure and a knockdown may need to be applied for future predictions.

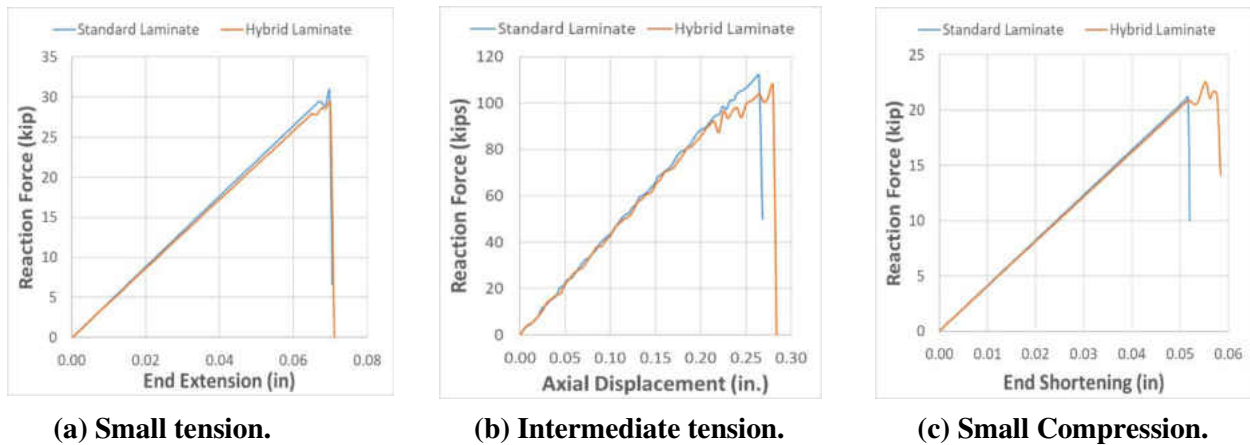
III. Design Parameters and Design of Experiments

A. Varying Ply Angles and Stiffness Ratios

The primary goal of this study was to determine the advantage of hybrid laminate specimens when compared to standard-ply laminate specimens. The hybrid specimens were built to have the same specimen thickness as the standard specimens, with a thickness of 0.1296 in., as well as to match stiffnesses. However, to accomplish that, extra plies had to be added to the hybrid laminates, which also added weight and changed the possible stiffness advantages between the specimen comparisons. The originally tested small unstiffened standard laminates were 18 plies with a total specimen weight of approximately 0.353 lbs., while the hybrid laminates were 34 plies with a total specimen weight of 0.376 lbs. This is a 6.28% weight penalty by using the hybrid laminate with 16 extra plies for the small unstiffened specimens. The originally tested intermediate unstiffened standard laminates were also 18 plies, but weighed approximately 8.834 lbs. due to the larger specimen design, and the intermediate unstiffened hybrid laminates weighed 9.388 lbs. for their 34-ply stacking sequence. This yields the same 6.28% weight penalty by using the hybrid laminates for the intermediate unstiffened specimens.

The small unstiffened standard tension specimens had an average final failure load of 33.795 kip, while the small unstiffened hybrid tension specimens had an average failure load of 27.591 kip, as shown in the load displacement curves in Figure 32, as well as within Table 5. Figure 32d contains a bar graph that shows the normalized failure load comparisons for both laminate types between the test data and the Abaqus predictions. All data is normalized with respect to the standard test specimen failure load for each corresponding test type and loading condition. For example, the small standard tension model prediction, the small hybrid tension test data, and the small hybrid tension model prediction are all normalized with respect to the small standard tension test data. The hybrid small tension specimen failed at an 18.36% lower

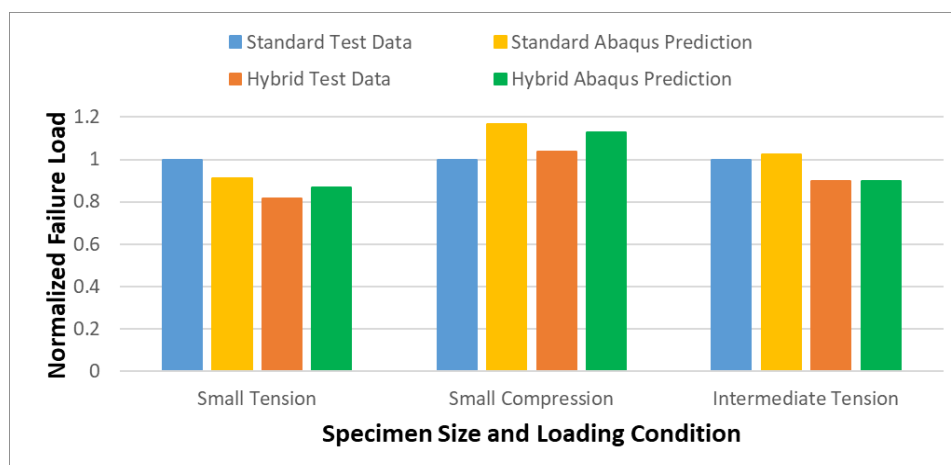
load than the standard small tension specimen. The intermediate unstiffened standard tension specimens failed at an average load of 109.591 kip, and the intermediate hybrid tension specimens failed at an average load of 98.363 kip, which is a 10.25% failure load decrease from its standard laminate equivalent. Finally, the average failure load for the small standard compression specimens was 18.158 kip, with the average small hybrid compression specimens failing at 18.839 kip. The small hybrid compression specimens yielded a 3.75% failure load advantage. Even though the tension specimens did not show a load advantage in this case, the manipulation of the specimen stacking sequences to match specimen thickness does not provide an accurate one-to-one comparison. Additionally, the study by Lovejoy and Scotti [16] showed that the laminate changes resulted in a 20.2% stiffness ratio reduction among the small unstiffened tension specimens, so more appropriate laminate comparisons needed to be completed.



(a) Small tension.

(b) Intermediate tension.

(c) Small Compression.



(d) Normalized failure load comparisons for all loading conditions.

Figure 32. Standard laminate vs. hybrid laminate load comparisons.

Table 5. Failure load and displacement for the unstiffened test specimens. (a) Standard laminates. (b) Hybrid laminates.

(a)	Failure Load (kip)	Failure Displacement (in)
2BC-T-1-1	34.099	0.046
2BC-T-1-2	33.047	0.053
2BC-T-1-3	34.240	0.055
Average Small Tension	33.795	0.051
2BC-C-1	18.404	0.053
2BC-C-2	18.388	0.055
2BC-C-3	17.681	0.051
Average Small Compression	18.158	0.053
2BC-T4-1	102.160	0.284
2BC-T4-2	117.022	0.295
Average Intermediate Tension	109.591	0.290
(b)	Failure Load (kip)	Failure Displacement (in)
CAS-NS-T1-1	27.372	0.043
CAS-NS-T1-2	25.472	0.040
CAS-NS-T1-3	29.929	0.047
Average Small Tension	27.591	0.043
CAS-NS-C1-1	19.706	0.055
CAS-NS-C1-2	18.385	0.053
CAS-NS-C1-3	18.425	0.053
Average Small Compression	18.839	0.054
CAS-NS-T4-1	91.485*	0.246
CAS-NS-T4-2	105.240	0.297
Average Intermediate Tension	98.363	0.272

* Corrected from 85.524 to account for slippage on one side of the test article as described in Ref. [23]

The first investigation to determine a more accurate standard-hybrid comparison was removing all additional plies within the 34 ply hybrid laminates that were originally there to ensure the hybrid specimen thicknesses matched the 18 ply standard specimens. The comparison between only 18-ply laminates, with the same stacking sequence of $[45/90/-45/0_2/45/90/-45/0]_s$, that was used for the original standard laminates, would then provide a more accurate strength and weight comparison, rather than comparing with respect to total specimen thickness. The 18-ply hybrid laminate reduced the small specimen weight down to 0.263

lbs., which is a 25.50% weight savings over the 18-ply standard laminate. Abaqus PFA was used to predict the performance of the 18-ply hybrid laminates, as well as compare them to the predictions for the standard laminates. The load-displacement curves for the small tension and small compression Abaqus comparisons are shown in Figure 33, and it is apparent that the specimen stiffness is no longer a match between laminate types. It is also apparent in the load-displacement curves, that the updated 18-ply hybrid laminates are not only able to take more load than their 34-ply counterparts, they are also able to take more load than the standard 18-ply laminates. In the case of the compression analyses, the small standard specimen fails catastrophically as soon as there is a load drop. However, the small hybrid specimen has a load drop and then stabilizes again to carry an additional 27.51% of the initial load drop. This is promising because the tension-loaded specimens see fiber damage grow more slowly while the original compression specimens were more likely to experience immediate catastrophic failure. A scenario that allows for slower damage progression or load redistribution within compressive loading as well is ideal. The 18-ply hybrid laminate under tensile loading was predicted to fail at 33.185 kip, which is a 7.60% advantage over the standard laminate prediction of 30.840 kip. The 18-ply hybrid compression laminate initially had a load drop at 23.996 kip, and then had a final failure at 30.597 kip, which is a 44.56% failure load advantage over the standard laminate failure at 21.165 kip. The initial hybrid load drop occurred 13.38% higher than the standard final failure, so even if the specimen didn't stabilize and hold additional load, there is a clear compressive advantage when using hybrid laminates over standard laminates with the same stacking sequence.

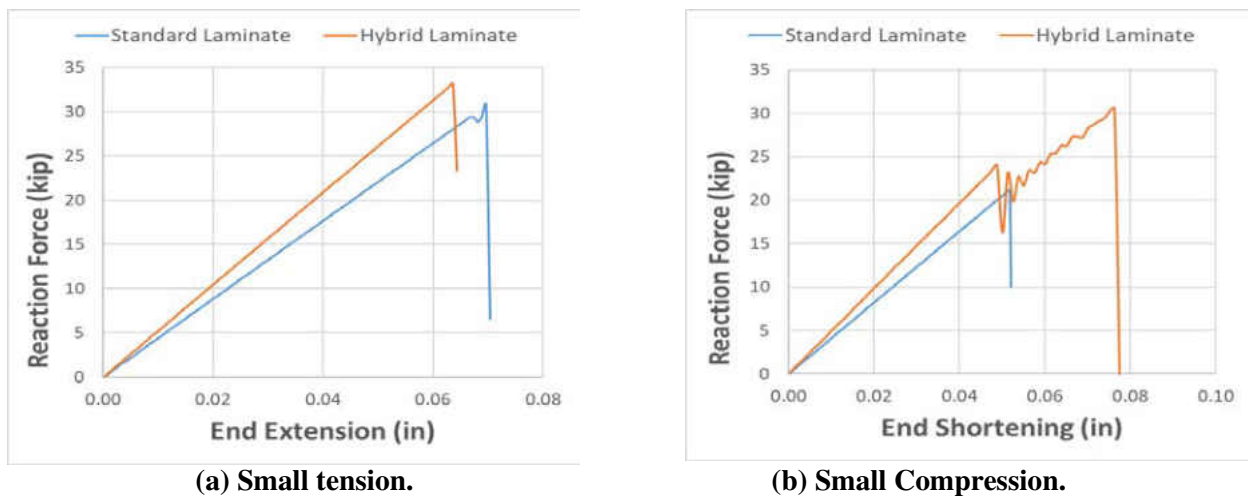


Figure 33. Standard laminate vs. hybrid laminate Abaqus load-displacement predictions.

The second investigation done was to compare the standard and hybrid 18-ply laminates, but with varying degree angles replacing the 45° plies. All 45° plies within each laminate were replaced in increments of both 10° and 15°, for both tension and compression loading. The angles explored, as well as their corresponding specimen stiffness and bending ratios, and the effective Young's moduli of the specimens, are shown in Table 6. The most promising of these laminates were then built into the advanced models to fully understand the damage progression as well as failure load benefits and deficiencies.

Table 6. Stiffness ratios and effective Young's moduli for investigated ply angle changes.

(a) Tension laminates

(a)	A_{11}/A_{22}	D_{11}/D_{22}	Effective E_x (Msi)	Effective E_y (Msi)
Standard – 10°	2.877	2.424	18.024	6.265
Hybrid – 10°	1.963	1.424	15.980	8.142
Standard – 15°	2.757	2.290	17.258	6.282
Hybrid – 15°	1.917	1.378	15.633	8.154
Standard – 20°	2.564	2.103	16.232	6.331
Hybrid – 20°	1.854	1.315	15.177	8.187
Standard – 30°	2.068	1.616	13.720	6.633
Hybrid – 30°	1.680	1.149	14.074	8.377
Standard – 40°	1.521	1.108	11.353	7.462
Hybrid – 40°	1.469	0.959	12.988	8.841
Standard – 45°	1.280	0.894	10.457	8.168
Hybrid – 45°	1.363	0.869	12.542	9.204
Standard – 50°	1.077	0.722	9.791	9.088
Hybrid – 50°	1.263	0.788	12.187	9.652
Standard – 60°	0.792	0.493	9.045	11.421
Hybrid – 60°	1.096	0.660	11.748	10.722
Standard – 70°	0.635	0.379	8.792	13.834
Hybrid – 70°	0.981	0.580	11.579	11.799
Standard – 75°	0.591	0.348	8.754	14.822
Hybrid – 75°	0.943	0.555	11.552	12.244
Standard – 80°	0.562	0.330	8.742	15.564
Hybrid – 80°	0.917	0.538	11.543	12.585

Table 6. Stiffness ratios and effective Young's moduli (concluded). (b) Compression laminates.

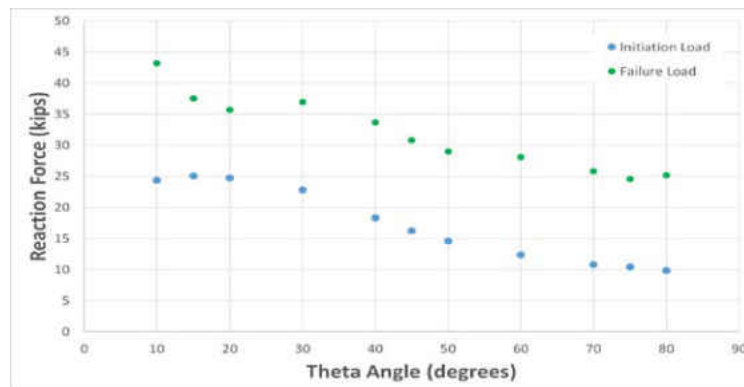
(b)	A_{11}/A_{22}	D_{11}/D_{22}	Effective E_x (Msi)	Effective E_y (Msi)
Standard – 10°	2.778	2.357	15.762	5.673
Hybrid – 10°	1.961	1.448	14.238	7.261
Standard – 15°	2.656	2.229	15.095	5.684
Hybrid – 15°	1.914	1.400	13.917	7.271
Standard – 20°	2.483	2.052	14.205	5.721
Hybrid – 20°	1.849	1.335	13.496	7.300
Standard – 30°	2.016	1.590	12.039	5.971
Hybrid – 30°	1.671	1.162	12.480	7.469
Standard – 40°	1.499	1.104	10.007	6.674
Hybrid – 40°	1.456	0.967	11.484	7.889
Standard – 45°	1.269	0.898	9.238	7.278
Hybrid – 45°	1.348	0.874	11.077	8.220
Standard – 50°	1.075	0.731	8.669	8.067
Hybrid – 50°	1.246	0.790	10.754	8.629
Standard – 60°	0.798	0.506	8.038	10.072
Hybrid – 60°	1.078	0.659	10.359	9.611
Standard – 70°	0.644	0.392	7.833	12.155
Hybrid – 70°	0.963	0.577	10.211	10.601
Standard – 75°	0.600	0.351	7.806	13.010
Hybrid – 75°	0.925	0.552	10.189	11.012
Standard – 80°	0.571	0.342	7.801	13.655
Hybrid – 80°	0.899	0.535	10.182	11.325

The final investigation done was to use the same models that were determined to be most promising and to explore new stacking sequence rules, since thin plies do not seem to have the same requirements within stacking sequences. Some of the new rules investigated were stacking duplicates of the same ply on top of each other, and changing the balance of the laminate by removing 0° and 90° plies from the original sequence. These second and final investigations are discussed completely within the following sections.

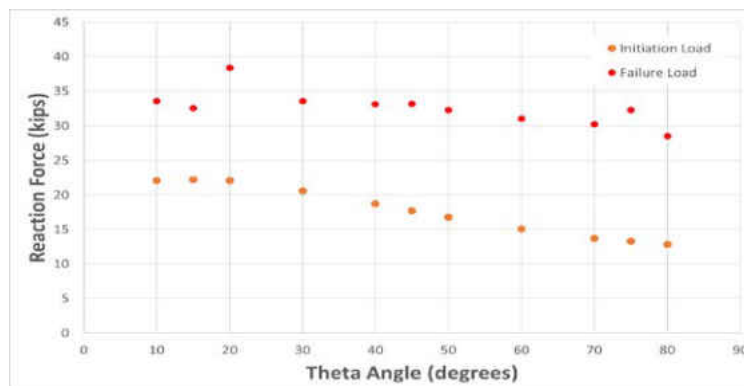
i. Small Unstiffened Tension Specimens

The angle investigation was done to determine which degree values, when replacing the 45° plies within the $[45/90/-45/0_2/45/90/-45/0]_s$ stacking sequences, would provide the best load advantage under both

tension and compression for the standard and hybrid laminates. The Abaqus finite element models were the same 4 in. x 12 in. small unstiffened specimens previously described, with the same 18 plies and 0.8 in. center notch. They were run with the same boundary conditions shown in Figure 14 and described in the Analysis Validation Section. The initiation loads and failure loads for all explored small tension laminates are shown in Figure 34, with the standard laminates, hybrid laminates, and comparison between them shown in 34a, b, and c, respectively. These will be referred to as the tension laminates, standard tension and hybrid tension, from this point forward. The initiation load was determined by looking at each time step of the analyses, and determining the load at which there is the first instance of either tensile fiber damage, or tensile matrix damage, again based on the Hashin failure and built-in Abaqus damage values. An example of the first instance of failure is shown in Figure 35 for the standard tension model with 15° plies, referred to as Standard-15T. As seen in the images, Standard-15T has no damage within the model at step 46, but the next step shows tensile matrix damage at an initiation load of 22.643 kip.

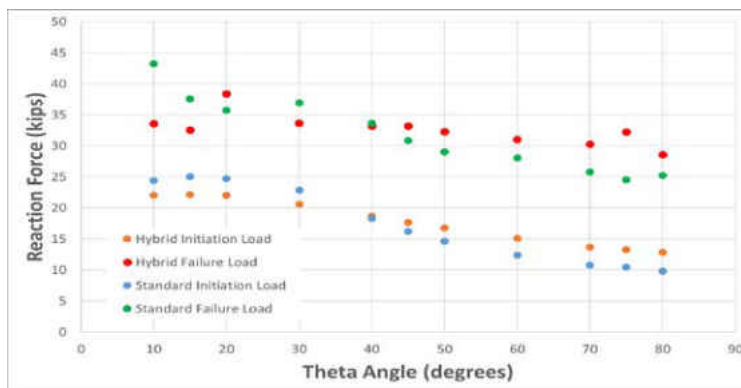


(a) Standard tension laminates.



(b) Hybrid tension laminates.

Figure 34. Initiation and failure loads for small tension angle study.

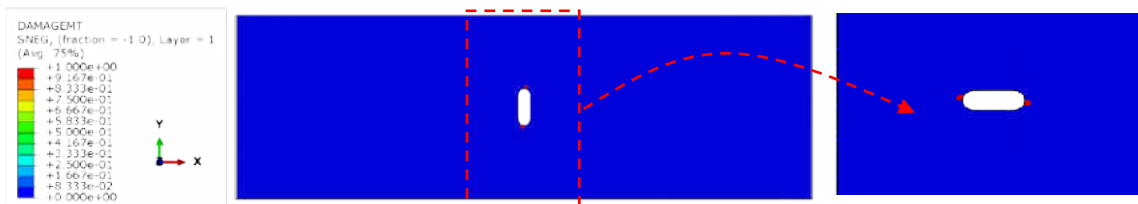


(c) Comparison between standard and hybrid tension laminates.

Figure 34. Initiation and failure loads for small tension angle study (concluded).



(a) Prior to damage initiation.



(b) First time step showing tensile matrix damage.

Figure 35. Initiation of failure in the Standard-15T model.

The failure load of the simple standard tension test prediction was 30.840 kip, and all replacement-angles investigated below 45° had a higher failure load, as shown in Figure 34a. Not only did all replacement-angle hybrid models below 45° also have a higher failure load than the original 30.840 kip simple standard test prediction, but almost all hybrid laminates examined had a higher failure load, as seen in Figure 34b. The only two hybrid tension laminates to fail below 30.840 kip was the Hybrid-70T which failed at 30.252 kip, or a 1.91% lower load, and the Hybrid-80T which failed at 28.518 kip, or a 7.5% lower load than the Standard-45 laminate. This shows that even without significant scrutinizing, there is an apparent hybrid unidirectional load advantage when the laminates have the same stacking sequence as a standard laminate.

When determining an angle to move forward with, the standard tension plot shows advantages when using Standard-15T, 21.75% load advantage, and Standard-30T, 19.81% load advantage. When looking for

angles that have significant shortcomings, Standard-75T, 20.49% load disadvantage, and Standard-80T, 18.32% load disadvantage, are ones that should be monitored. When analyzing the hybrid laminates for the same benefits and deficiencies, it is a little more challenging because of the uniform nature of the failure loads, with the exception of Hybrid-20T which may be an outlier. This challenge encourages the comparison plot shown in Figure 34c. The tension advantage comparison between Standard-15T vs. Hybrid-15T and Standard-30T vs. Hybrid-30T is close, but the 15 degree angle may provide a more interesting comparison with the larger delta between the standard and hybrid laminates at failure. Looking at the tension disadvantage angles with the same scope shows that Standard-75T vs Hybrid-75T will likely provide a more remarkable comparison.

The matrix and fiber failure plots shown in Figure 36 are for the Standard-45T damage, while those shown in Figure 37 are the damage within the Hybrid-45T laminate. The tensile matrix failure in Figure 36a is from a 0° ply just before final failure. The Hashin matrix damage is mostly in the transverse direction, with a slight indication of some possible diagonal failure for the unidirectional tension loading. The tensile matrix failure in Figure 36b shows more of the diagonal failure indication within the bright green 50% damage, which is expected in a 45° ply. The Hashin tensile fiber failure within Figure 36c shows that the majority of the damage is in the transverse direction from the notch tips in the 0° ply, but there is also evidence of some damage suppression in the dark blue region branching out. The transverse and slightly diagonal failure is still the main fiber fracture, however, and this is also shown within the outer 45° contour plot in Figure 36d. The 45° fiber failure plot shows localized damage near the notch on the outer surface of the panel just before failure. A laminate that suppresses damage would show more damage growth prior to failure, rather than the catastrophic failure that is alluded to just one step before failure in the contour plots in Figure 36.

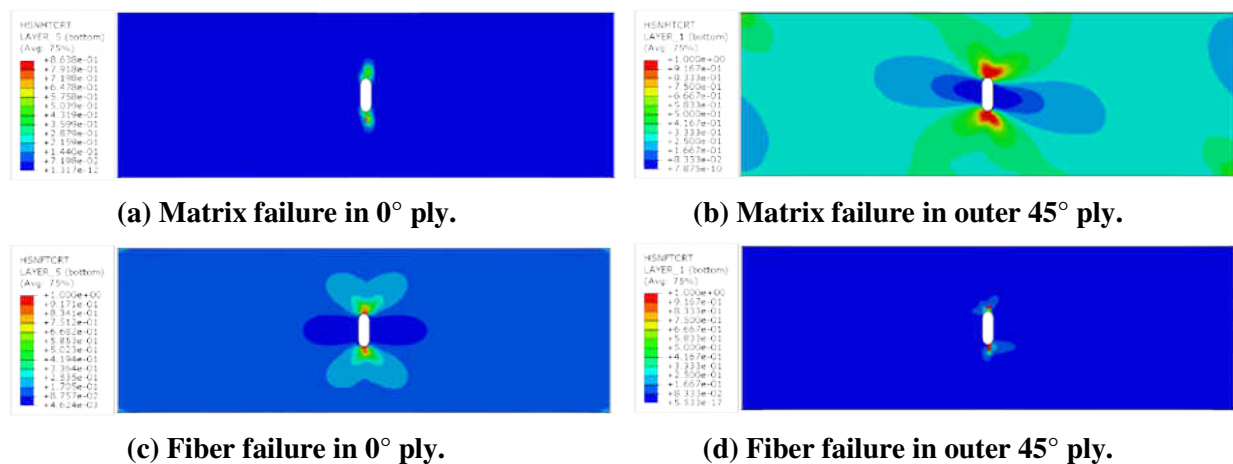


Figure 36. Hashin damage propagation within various plies of the Standard-45T model.

The Hashin matrix failure for the hybrid tension laminate within a 0° ply just before final failure is shown in Figure 37a. There is tensile matrix damage in the transverse direction as well as minor crack turning failure on either side of the notch. This is promising because that shows that the hybrid laminate is showing signs of changing failure modes, even without additional modifications to the baseline stacking sequence. The matrix failure in Figure 37b again shows more of the expected diagonal failure, but there is also less damage the last step before failure than in the equivalent Standard-45T model. This is an indication of minimal load distribution in the outer plies, leading towards a more catastrophic failure again. The Hashin tensile fiber failure in Figure 37c indicates that there is minimal transverse damage, and the 0° ply is again trying to dissipate some of the fracture energy, slightly more successfully in this laminate than the one shown in Figure 36c. The final contour plot for the Hybrid-45T laminate shows minimal crack progression in the transverse direction, and also indicates the initiation of crack turning, shown as the light blue contours. Damage suppression and crack turning in this unidirectional loading case would be ideal in the event of a catastrophic puncture within an aircraft, so the hybrid model has the advantage for the 45° laminates based on these contour plots.

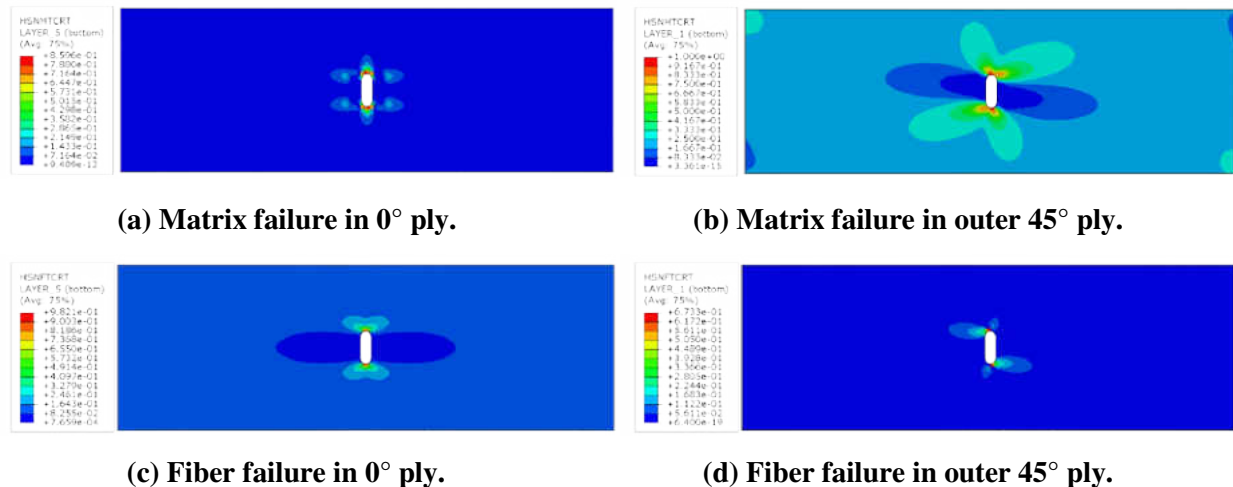


Figure 37. Hashin damage propagation within various plies of the Hybrid-45T model.

The Hashin tensile matrix and fiber failure plots for the 15° and 75° laminates are also shown for unidirectional tension loading. The Standard-15T and Hybrid-15T damage propagation images are shown in Figures 38 and 39, respectively, while the Standard-75T and Hybrid-75T contours are shown in Figures 40 and 41, respectively. The comparison between the Standard-15T matrix failure in Figure 38a and the Hybrid-15T matrix failure in Figure 39a shows that the standard laminate begins to change to crack turning

failure, also seen in Figure 38b in the 45° surface ply, but the hybrid laminate actually fully changes to failure in the load direction rather than transverse failure. When an aircraft is struck and the skin is pierced, a transverse failure can cause fracture that is unstoppable. A successfully turned crack, like within the Hybrid-15T laminate, can arrest crack propagation and allow the aircraft to safely return to the ground. All images in Figure 39 show evidence of successful mode changing and crack turning within the Hybrid-15T laminate, and this will be critical information for the later study. The evidence of crack turning within the Standard-15T is also promising, so this will also be important to track with other laminate changes in the secondary investigation.

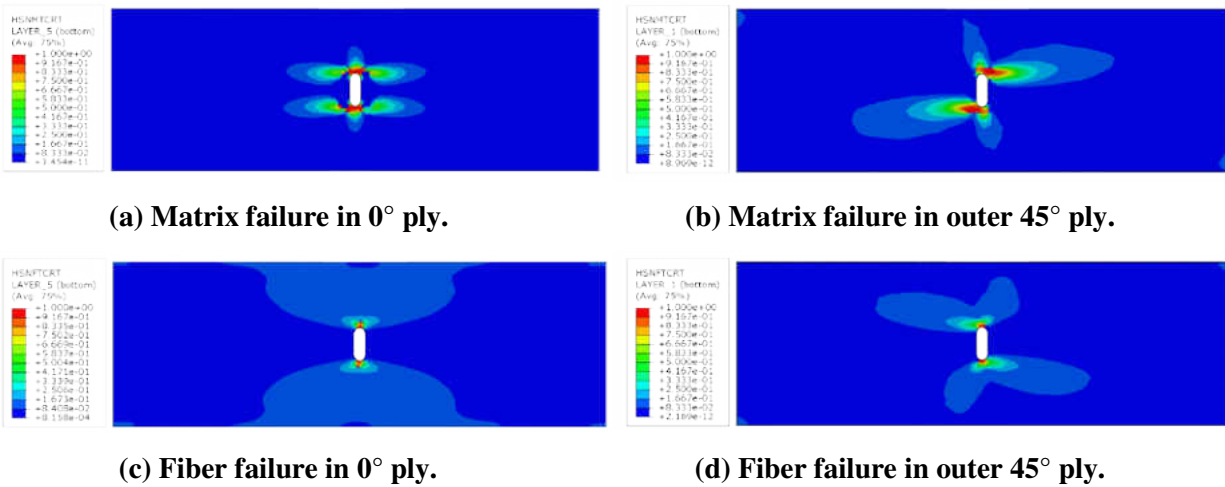


Figure 38. Hashin damage propagation within various plies of the Standard-15T model.

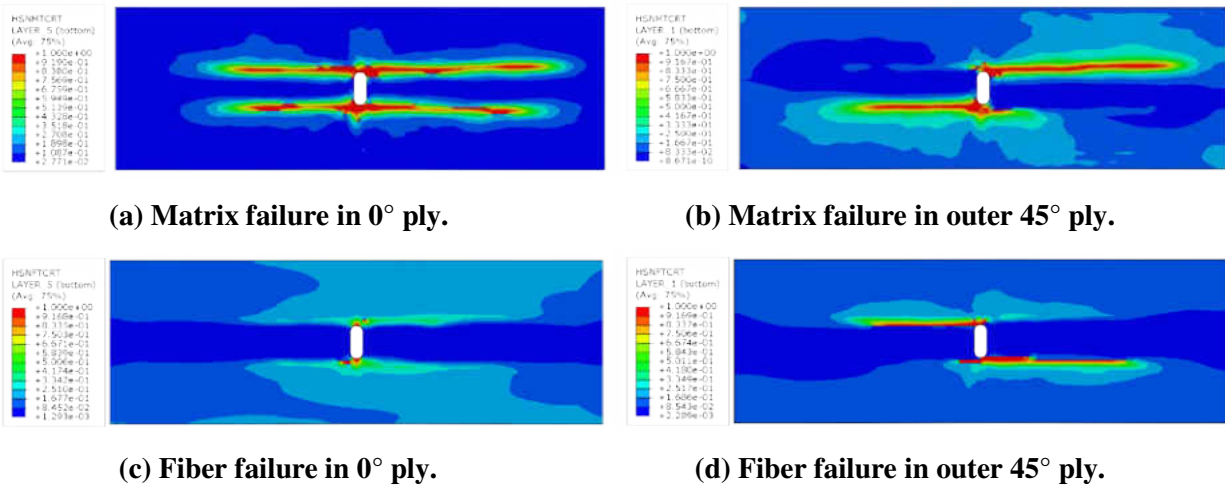


Figure 39. Hashin damage propagation within various plies of the Hybrid-15T model.

The comparison between the Standard-75T matrix failure in Figure 40a and the Hybrid-75T matrix failure in Figure 41a shows that again the hybrid laminate is better able to arrest the damage propagation and turn the crack towards the unidirectional loading direction. However, as seen in the Hashin 0° ply fiber contours for Figures 40c and Figures 41c, the laminates both still exhibit transverse failure. Those same figures also show that there is significant damage growth from the notch tip just before failure, so this slow progression is more indicative of load redistribution within the laminates rather than the more catastrophic failures shown within the Standard-45T and Hybrid-45T laminates. This is significant because there are also scenarios when load redistribution and damage suppression are more important design qualities than crack turning, so the 75° tensile laminates are critical to track within the next investigation as well.

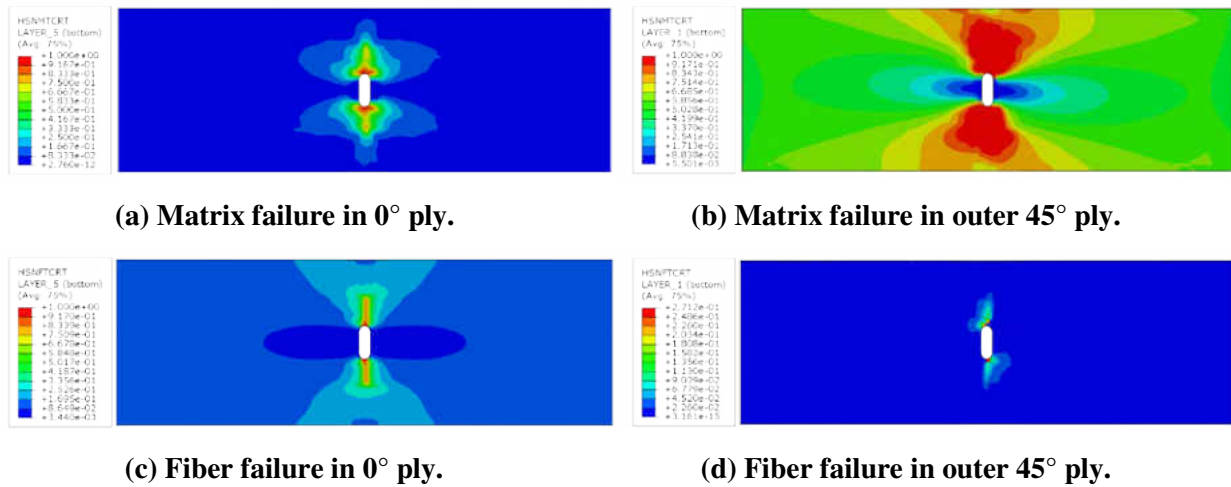


Figure 40. Hashin damage propagation within various plies of the Standard-75T model.

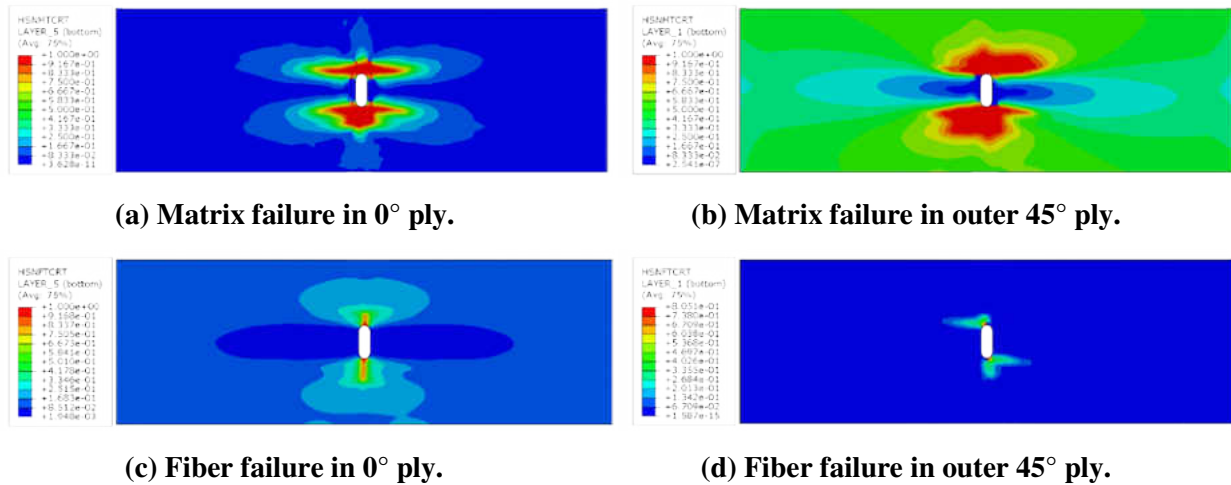


Figure 41. Hashin damage propagation within various plies of the Hybrid-75T model.

After the comparisons previously mentioned, the tension angle investigation was continued with the advanced models for 15° , 45° , and 75° for both standard and hybrid laminates. The advanced models were created to better determine the failure mode of each laminate, and if there are any internal advantages or disadvantages to each angle. The failure load versus displacement for each laminate is shown in Figure 42, as well as its comparison to the corresponding simple model in Table 7. The failure load for the Standard-15T was 35.325 kip and the Hybrid-15T failed at 34.991 kip, which is 0.95% lower than the Standard-15T and the least promising of the advanced tension models. The Hybrid-45T failed at 33.326 kips which was 6.29% higher than the Standard-45T failure load of 31.355 kip, which is more promising than the 15T hybrid-standard advantage. Finally, the Hybrid-75T failure load was 33.376 kips compared to the Standard-75T failure of 30.550 kip, which is a hybrid advantage of 9.25% and is the most promising advanced tension hybrid advantage. When comparing the advanced models among their laminate types, even though the Hybrid-15T has a minimally lower failure load than the Standard-15T, it had an advantage over the Hybrid-45T and should still be considered within the secondary investigation.

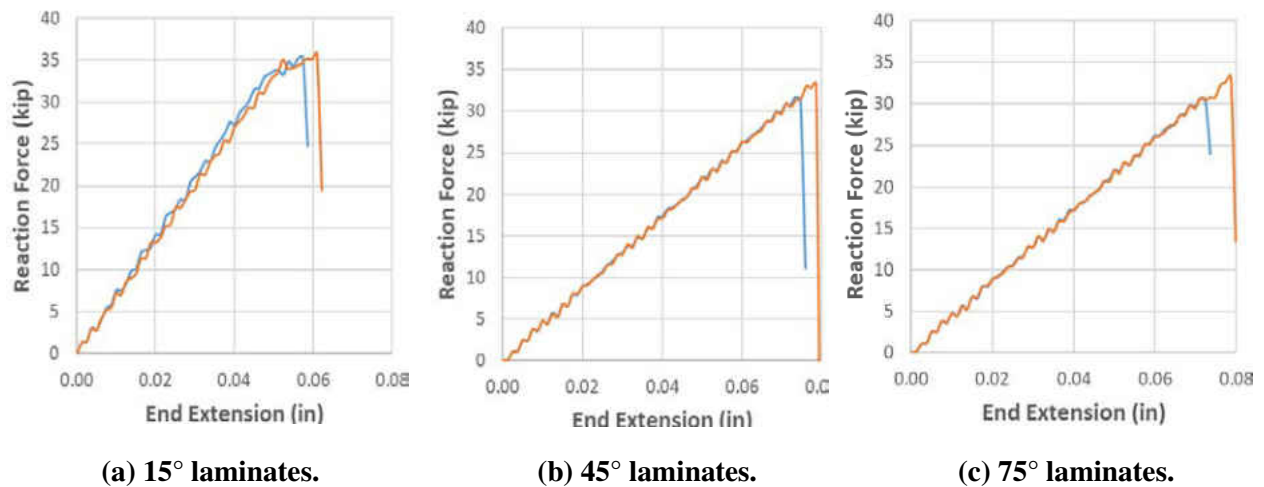


Figure 42. Failure load vs. axial displacement for the tension laminates.

Table 7. Small tension percent differences between simple model and advanced model.

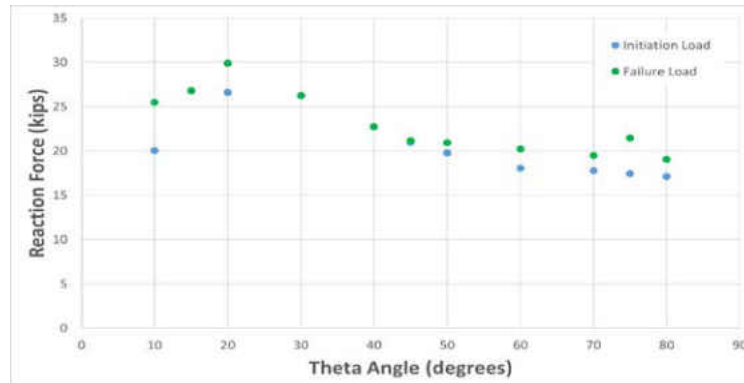
	Simple Model Failure Load (kip)	Advanced Model Failure Load (kip)	Percent Difference (%)
Standard-15T	37.547	35.325	6.10
Hybrid-15T	32.537	34.991	7.27
Standard-45T	30.840	31.354	1.65
Hybrid-45T	33.185	33.326	0.42
Standard-75T	24.523	30.550	21.89
Hybrid-75T	32.254	33.376	3.42

The tension angle investigation yielded interesting results for each of the angle comparisons between the two laminate types, as well as the hybrid-standard comparisons between for each examined angle. The 15°, 45°, and 75° laminates will also be carried further into the stacking sequence investigation to try to determine additional rules and advantages for various laminate lay-ups. All models investigated in this section are subjected solely to unidirectional tension loading, rather than the more complex biaxial loading or shear loading cases. A thorough design would have to investigate other loading scenarios as well before claiming that these laminates are superior in all aspects. This would also include modeling all laminates with the advanced models, rather than just the few discussed here, because they will be able to capture more advanced failure modes and delaminations than the simple models are able to portray. However, for this initial stage investigation, the trends are promising enough to continue working with the simple laminates.

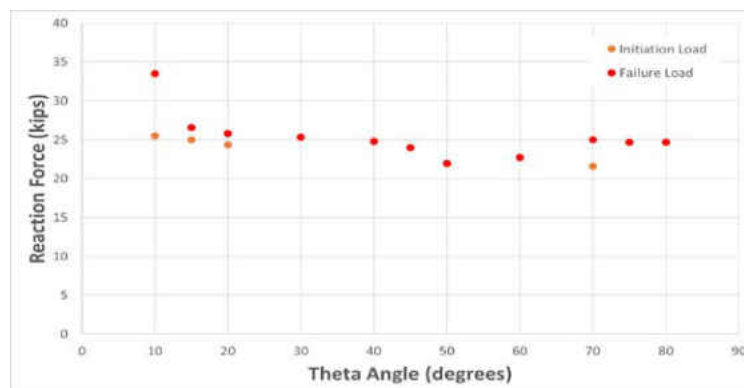
ii. Small Unstiffened Compression Specimens

The initiation loads and failure loads for all small compression laminates, run using the simple models, are shown below, with the standard laminates, hybrid laminates, and comparison between them shown in Figures 43a, b, and c, respectively. These will be referred to as the compression laminates, standard compression and hybrid compression, just like the tension laminates in the previous section. The initiation load was determined by looking at each time step of the analyses, and finding the load with the first instance of either compressive fiber or matrix damage, also based on the Hashin failure and built-in Abaqus damage values. The first instance of compressive matrix failure is shown in for the standard compression model with 45° plies, referred to as Standard-45C in the compressive laminate case, in Figure 44. As seen in the images, Standard-45C has no damage within the model at step 69, but the next step shows compressive matrix damage at an initiation load of 20.993 kip. The immediate failure across most of the specimen is a

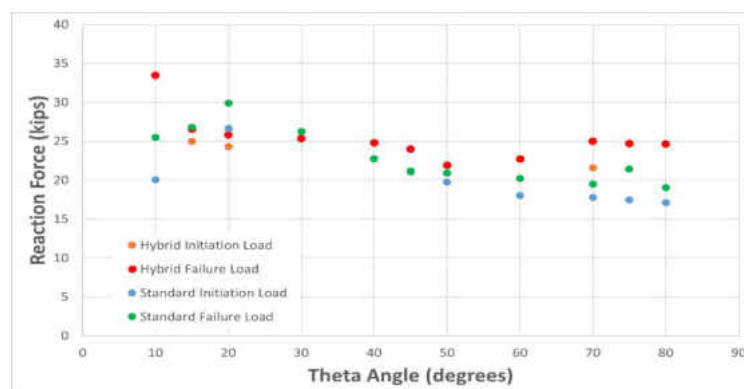
known problem with compression loading, and is something that would be ideal to mediate using a different ply angle or a hybrid laminate if possible.



(a) Standard compression laminates.



(b) Hybrid compression laminates.

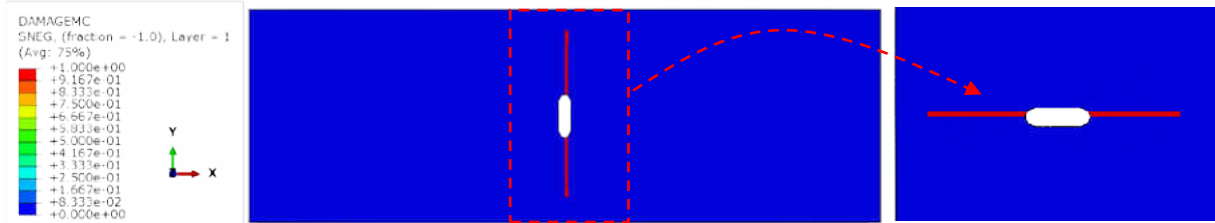


(c) Comparison between standard and hybrid compression laminates.

Figure 43. Initiation and failure loads for small compression angle study.



(a) Prior to damage initiation.



(b) First time step showing compressive matrix damage.

Figure 44. Initiation of failure in the Standard-45C model.

The failure load of the standard compression analysis prediction was 21.165 kip, and all replacement-angles below 45° had a higher failure load, as shown in Figure 43a, as well as Standard-75C also fails at a higher load and Standard-50C only 1% lower. Again, all hybrid models below 45° also have a higher failure load than the Standard-45C prediction, but in fact all hybrid laminates examined had a higher failure load than 21.165 kip, as seen in Figure 43b. The lowest hybrid failure load was for the Hybrid-80C, which at 24.660 kip it still had a 16.51% load advantage over the Standard-45 laminate, and the average hybrid failure load of 28.406 kip was a 34.21% load improvement. This shows there is an even better hybrid load advantage for compressive loading, which was shown as well even when the 34-ply hybrid specimen was used as a comparison.

The matrix and fiber failure plots shown in Figure 45 are for damage within the Standard-45C model, while those shown in Figure 46 are the damage in the Hybrid-45C laminate. The compressive matrix failure in Figure 45a is from a 90° ply just before final failure. The Hashin matrix damage is solely in the transverse direction, with only a few indications of minimal damage outside the crack path in red. The compressive matrix failure in Figure 45b shows more of the diagonal failure indication within the bright blue damage, as expected in the outer surface 45° ply. The Hashin compressive contour plot within Figure 45c shows that although there is significant matrix failure right before failure, the fiber failure is minimal. There is a greater indication of fiber damage in the surface in Figure 45d, but the crack path is still mainly transverse despite the fibers running in a 45° angle within that ply. These damage progression plots for the unidirectional

compression loading have a significant amount of panel damage just before failure, so this is a good indication that there was load redistribution and damage suppression within this laminate.

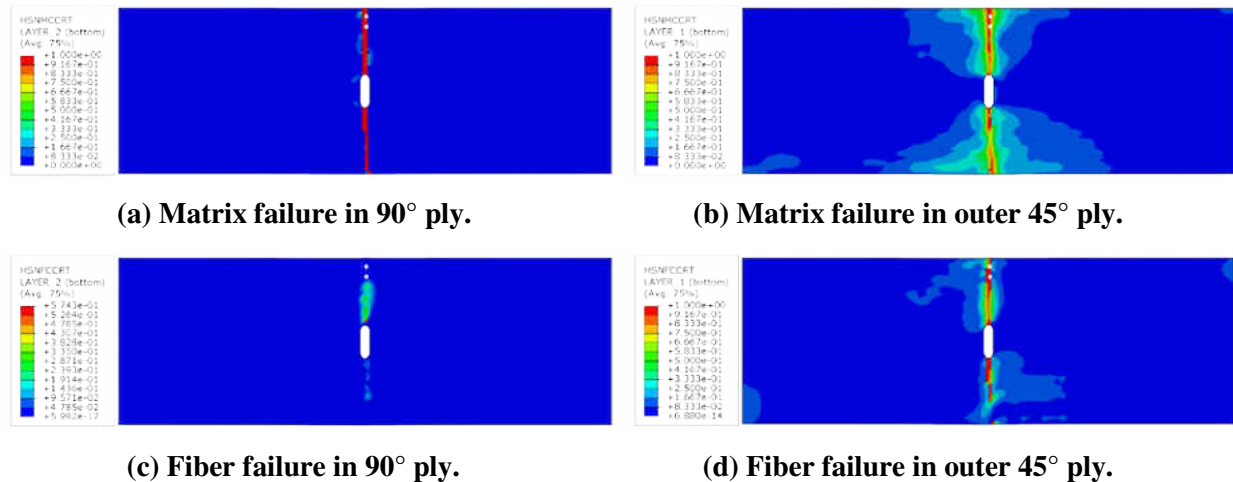


Figure 45. Hashin damage propagation within various plies of the Standard-45C model.

The Hashin matrix failure for the hybrid unidirectional compression laminate within a 90° ply immediately prior to final failure is shown in Figure 46a. There is compressive matrix damage in the transverse direction as well as very minor crack turning on either side of the notch. This is promising again because it shows that the hybrid laminate is possibly able to change failure modes even under compressive loading. The matrix failure in Figure 46b shows a very small amount of the diagonal failure expected in a 45° ply, but the majority of the damage is again along a transverse path. However, since the hybrid laminate is not as likely to have the diagonal failure in the outer ply, indicative of a surface ply peeling, the Standard-45C laminate would likely better reduce fracture energy. The Hashin compressive fiber failure in Figure 46c indicates that there is solely transverse damage, and the 90° ply is likely driving the failure mode of the panel. The final contour plot for the Hybrid-45C laminate, Figure 46d, shows crack progression in the transverse direction with only a small indication of any diagonal failure paths, shown as the light blue contours. Just as in the Standard-45C laminate, the Hybrid-45C laminate exhibits slow and fairly stable crack growth, which is ideal in cases where the design requirements would deem catastrophic failure unacceptable.

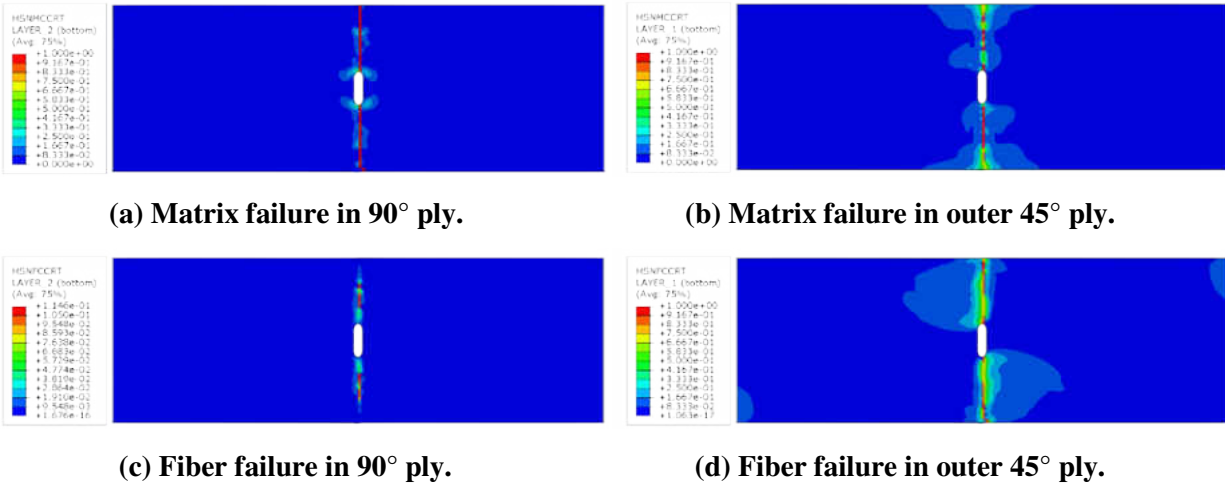


Figure 46. Hashin damage propagation within various plies of the Hybrid-45C model.

The Hashin compressive matrix and fiber failure plots for the 15° and 75° laminates are also shown. The Standard-15C and Hybrid-15C damage propagation images are shown in Figures 47 and 48, respectively, while the Standard-75C and Hybrid-75C contours are shown in Figures 49 and 50, respectively. The comparison between the Standard-15C matrix failure in Figure 47a and the Hybrid-15C matrix failure in Figure 48a shows that the standard laminate has the beginnings of crack turning failure, also seen in Figure 47b in the outer 45° ply, but the hybrid laminate has more longitudinal damage in addition to the transverse damage. All images in Figure 48 show significantly more damage progression within the Hybrid-15C laminate when compared with the Standard-15C models in Figure 47. The standard laminates show that in the next time step there will be a catastrophic failure. This is not as ideal as the more stable growth that is exhibited in the hybrid contours, so for both 15° loading conditions the hybrid laminate has the advantage for this uniaxial loading scenario.

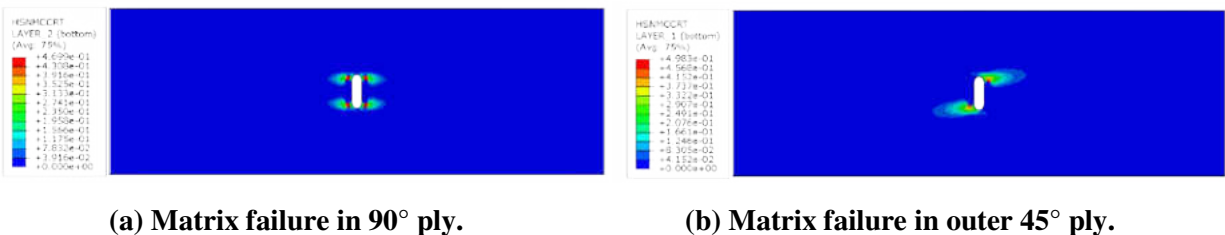
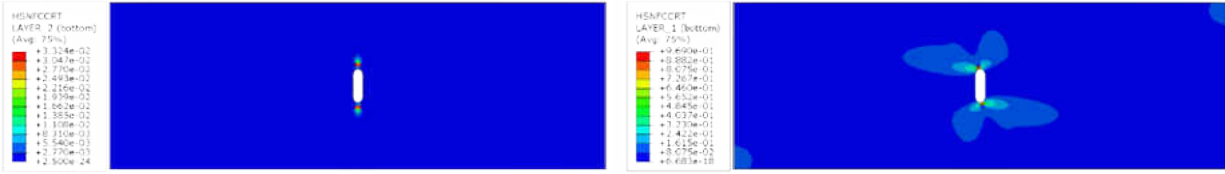
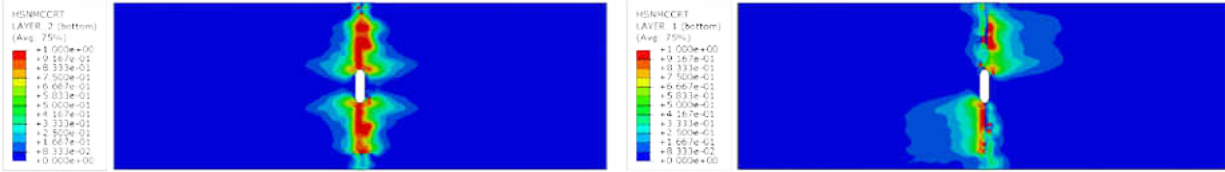


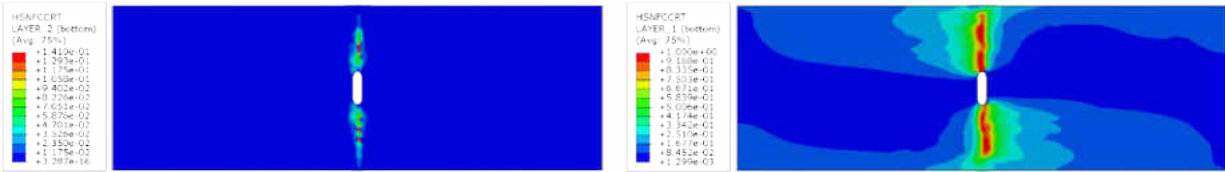
Figure 47. Hashin damage propagation within various plies of the Standard-15C model.



(c) Fiber failure in 90° ply. (d) Fiber failure in outer 45° ply.
Figure 47. Hashin damage propagation within plies of the Standard-15C model (concluded).



(a) Matrix failure in 90° ply. (b) Matrix failure in outer 45° ply.



(c) Fiber failure in 90° ply. (d) Fiber failure in outer 45° ply.

Figure 48. Hashin damage propagation within various plies of the Hybrid-15C model.

The comparison between the Standard-75C matrix failure in Figure 49a and the Hybrid-75C matrix failure in Figure 50a, and even within the 45° ply within Figure 50b, shows that again the hybrid laminate is better able to arrest the damage propagation and start to turn the crack towards the loading direction when subjected to only axial compression. However, as seen in the Hashin 90° ply fiber contours for Figures 49c and Figures 50c, both laminates still exhibit mainly transverse failure. Those same figures also show that there is significant damage growth from the notch tip just before failure, so there is an indication of load redistribution within these laminates as well. Once again, this is important because load redistribution and damage suppression are desirable qualities in certain design scenarios.

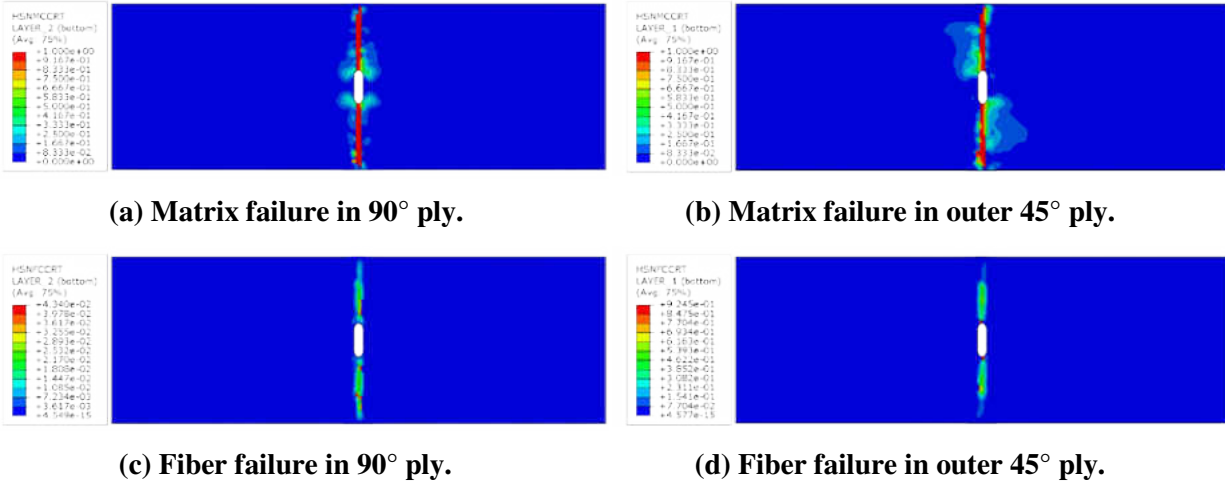


Figure 49. Hashin damage propagation within various plies of the Standard-75C model.

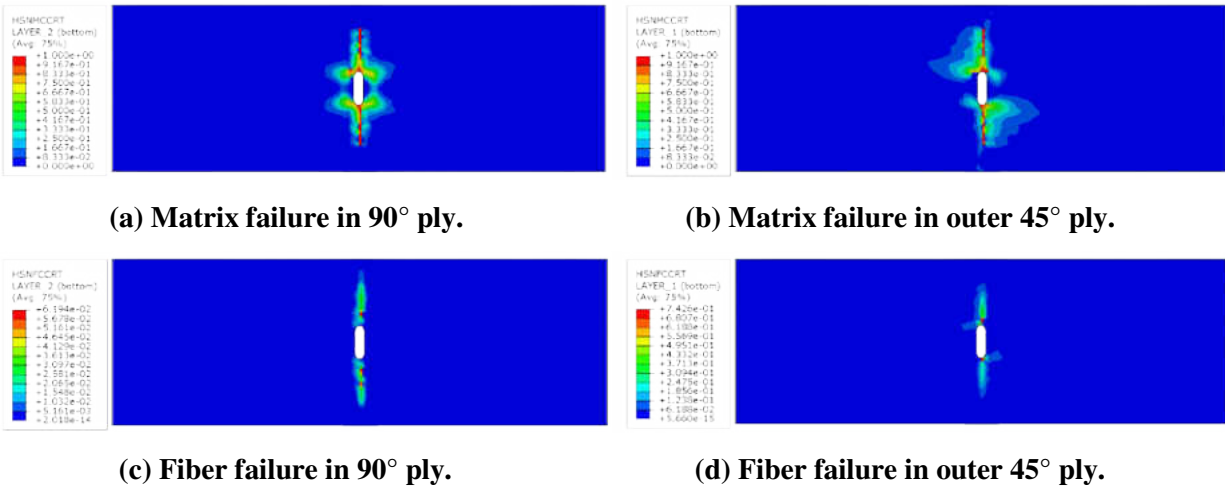


Figure 50. Hashin damage propagation within various plies of the Hybrid-75C model.

Finding the angles to move onward with was more challenging in the compressive cases due to the significantly nonlinear trend of both the standard and hybrid data. The standard tension plot shows significant load advantages when using angles below 30° , with between 20.49-41.13% load advantages over the Standard-45C model. All standard laminates below 45° hold less load with the exception of the 1.30% load increase in Standard-75C previously mentioned. When investigating the hybrid laminates in the same manor, again all laminates below 30° have over a 5% load increase, with Hybrid-10C and Hybrid-40C over 40% better than the Standard-45C. There is also a significant benefit at angles up to 60° , with only Hybrid-70C, Hybrid-75C, and Hybrid-60C failing at less than 20% the Standard-45C comparison model. The comparison plot, shown in Figure 43c, was used again to determine the angles that should be

built into advanced models. Although both high and low angles have advantages for their appropriate standard and hybrid 45° comparisons, there is also what seems to be immediate failure in a few models that would be an interesting investigation with the advanced models. Examples of this catastrophic failure are Standard-15C and Standard-30C, as well as Hybrid-75C and Hybrid-80C, indicated by the overlap of the initiation load and failure load points on the graphs. Using 15° and 75° for the compression cases is also a way to use some of the more conservative load advantages, while still also determining the best possible tension scenarios that can be created. All compression models discussed in this section are also subjected to unidirectional loading only. The more complex loading cases would also need to be investigated to ensure the laminates are superior in all load scenarios. A more thorough design also depends on the advanced models, particularly because the compression models tend to have internal delaminations that are harder to predict with the more simplified models. However, the trends in the simple laminates are good enough to continue the investigation, with the knowledge that a more comprehensive design matrix is needed for a thorough vetting of the laminate advantages.

B. Varying Stacking Sequence and Stiffness Ratios

The previous angle investigation was used to build further knowledge about the effects of stacking sequence on standard and hybrid laminates. In this second investigation, the 15°, 45°, and 75° laminates had plies added in different configurations. To start, the 45° laminates, for both standard and hybrid, were supplemented or changed for a total of five new laminates, as shown in Table 8 below. These five laminates were subjected to both tensile and compressive loading, for a total of twenty new failure predictions. The names on the left of the table are an abbreviated version of the laminate changes, shown in red on the right, with respect to the original laminate. The “_Blocked-0” refers to the grouping together, sometimes called blocking, of all 0° plies in the original laminate. The “_Blocked-90” similarly refers to all 90° plies being blocked or grouped together. The “_Add-0(2)” laminate adds two additional zeros to the laminate, indicated by the solo red zero in the table since the laminate is symmetric. The “_Add-0(4)” laminate not only adds the two red zeros, becoming four in the full laminate again due to symmetry, but the -45° ply moves location within the laminate. The final laminate change, “_Add-0(2)_Sub-90(2)” adds two zeros and removes two nines, so in essence the red 0° replaces the 90° in the original laminate, and then the +45° ply moves location as well. These laminate descriptions are used for all models within this section, for all four combinations of laminate type and loading conditions.

Table 8. Stacking sequence initial laminate changes.

Laminate Name	Stacking Sequence (where θ is 15, 45, or 75)
Original Laminate	[45/90/-45/0 ₂ /45/90/-45/0] _s
Standard-45T_Blocked-0	[45/90/-45/0 ₃ /45/90/-45] _s
Standard-45T_Blocked-90	[45/-45/0 ₂ /45/90 ₂ /-45/0] _s
Standard-45T_Add-0(2)	[45/90/-45/0 ₂ /45/0/90/-45/0] _s
Standard-45T_Add-0(4)	[45/90/0 ₂ /-45/45/0 ₂ /90/-45/0] _s
Standard-45T_Add-0(2)_Sub-90(2)	[45/0/-45/45/0 ₂ /90/-45/0] _s

i. Initial Stacking Sequence Changes

The load-displacement curves for each set of laminate types – tensile standard, tensile hybrid, compressive standard, and compressive hybrid – are shown in Figures 51 and 52. The failure load for the original Standard-45T laminate prediction, shown in Figure 51, was 30.840 kip, and this comparison from the simple model is the baseline for the laminate evaluations. The Standard-45T_Blocked-0 model had a failure load of 29.859 kip and the Standard-45T_Blocked-90 had a failure load of 29.788 kip, which are a lower failure load by 3.18% and 3.41% respectively. The Standard-45T models with additional 0° plies all had higher failure loads than the original laminate, with the Standard-45T_Add-0(2) failing 4.48% higher at 32.221 kip, the Standard-45T_Add-0(4) failed 13.38% higher at 34.965 kip, and the Standard-45T_Add-0(2)_Sub-90(2) failed at the highest failure load at 35.021 kip which is 13.56% higher than the Standard-45T failure load.

For the hybrid tensile cases, the Hybrid-45T failed at 33.185 kip and this is the baseline for the hybrid laminate changes. The Hybrid-45T_Blocked-0 model had a failure load of 29.569 kip, which is 10.90% lower than the baseline, and the Hybrid-45T_Blocked-90 had a failure load of 30.368 kip, which is a lower failure load by 8.49%. These results, along with the standard tension blocked cases, show that, at least for tension loading, blocking plies does not improve the laminate failure loads. There may be internal advantages still, including delamination suppression or other damage redistribution, but those investigations would be better served for the advanced models. The final hybrid laminate changes all fail at higher loads than the original Hybrid-45T model. The Hybrid-45T_Add-0(2) fails at the highest load at 36.068 kip, which is a 8.69% advantage, the Standard-45T_Add-0(4) failed 3.69% higher at 34.409 kip, and the Standard-45T_Add-0(2)_Sub-90(2) failed at a similar load at 34.411 kip which is also rounds to 3.69% higher than the Standard-45T failure load.

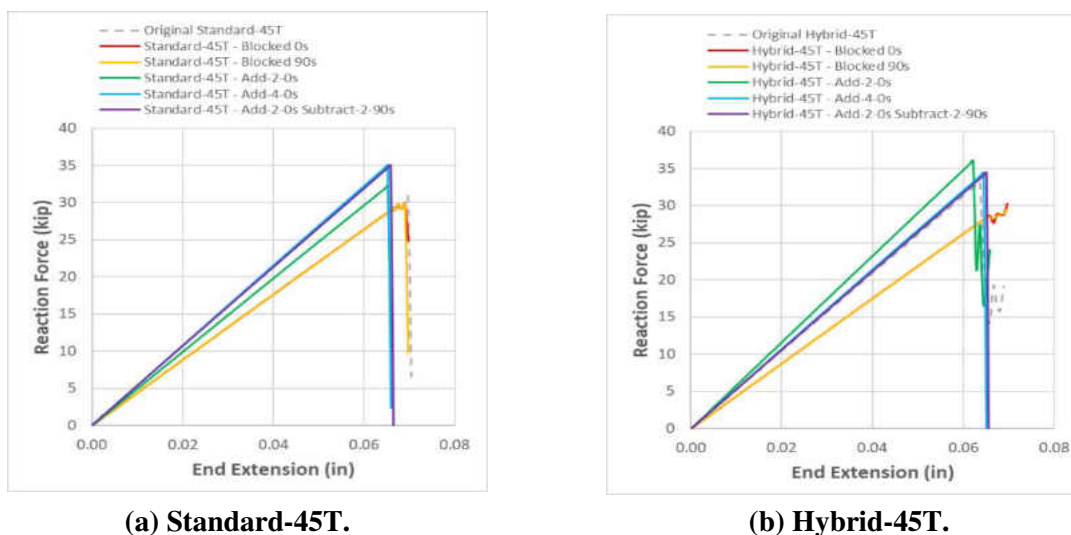


Figure 51. Load vs. displacement curves for tensile 45° laminate changes.

The Standard-45C original laminate and its comparison models are shown in Figure 52a, and the Hybrid-45C set of laminates are shown in Figure 52b. The failure load for the original Standard-45C prediction was 21.165 kip, and this is the baseline for the compressive laminate investigations. The Standard-45C_Blocked-0 model had a failure load of 23.134 kip, which is 9.30% higher than the baseline, and the Standard-45C_Blocked-90 had a failure load of 22.911 kip, which is a higher failure load by 9.67%. The Standard-45C models with added 0° plies also had higher failure loads than the original laminate, with the Standard-45C_Add-0(2) model also failing roughly 9.67% higher at 23.211 kip, the Standard-45C_Add-0(4) failed 17.44% higher at 24.856 kip, and the Standard-45C_Add-0(2)_Sub-90(2) failed at the highest failure load of this group at 25.076 kip which is 18.38% higher than the Standard-45C failure load.

For the hybrid compressive cases, the Hybrid-45C failed at 30.597 kip which is the reference for the hybrid laminate changes. The Hybrid-45C_Blocked-0 model failed at 29.590 kip, which is 3.29% lower than the baseline model, and the Hybrid-45C_Blocked-90 had a failure load of 30.083 kip, which is a lower failure load by 1.68%. These results, unlike the standard compression blocked cases, show that for tension loading and compressive loading of hybrid models, blocking plies does not improve the final failure load. Again, there may be internal advantages not seen with just the failure load number, but the simpler models do not capture everything going on like the advanced models are better equipped for. Finally, the Hybrid-45C_Add-0(2) fails at the highest load at 34.804 kip, which is a 13.75% advantage, the Standard-45C_Add-0(4) failed 4.62% lower at 29.183 kip, and the Standard-45C_Add-0(2)_Sub-90(2) failed at a higher load again at 34.171 kip which is 11.68% higher than the Standard-45C failure load.

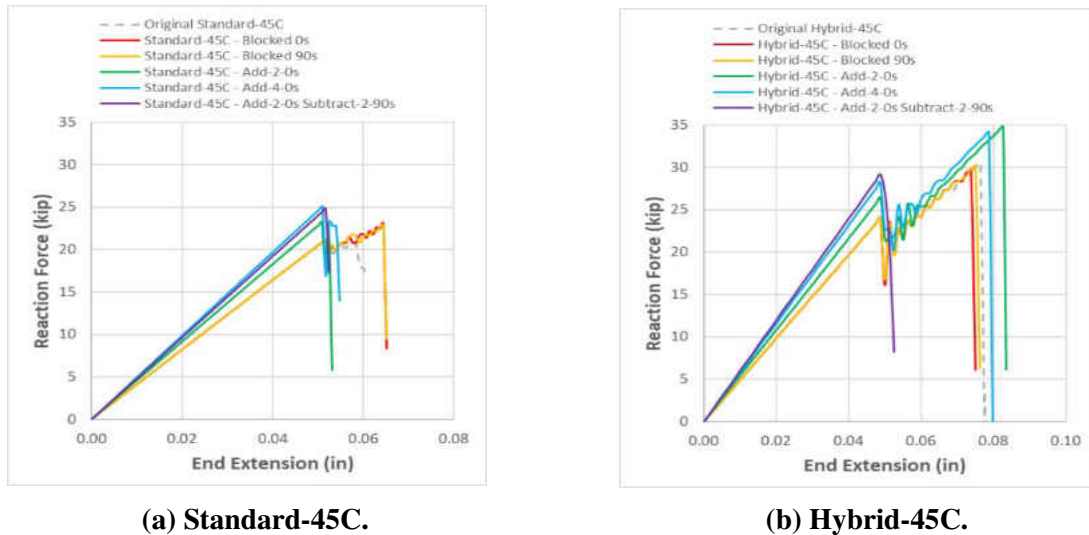


Figure 52. Load vs. displacement curves for compressive 45° laminate changes.

The hybrid compression results are a little more interesting than the other groups, because there is load redistribution in every laminate except the one with the 90° plies removed. In that laminate, the model fails catastrophically and does not continue holding any more load like the 5 others within Figure 52b. The most promising of the tensile laminate changes are the three models that added extra 0° plies. In each analysis, the standard tension laminates with additional zeros fail at loads that are between 5-15% higher, and the hybrid tension laminates with extra zeros fail 3-10% higher than their respective original models. The most favorable of the compressive laminate changes are also the models with added 0° plies, with the exception of the Hybrid-45C_Add-0(2)_Sub-90(2) laminate which had a lower failure load than the baseline Hybrid-45C. The other compression-loaded cases, however, all have around 10-20% higher failure loads than their respective baseline laminates. These three laminate types, “_Add-0(2)”, “_Add-0(4)”, and “_Add-0(2)_Sub-90(2)”, will be used for the secondary investigation into stacking sequence changes. This second investigation uses the 15° and 75° promising angle changes from the ply angle investigation, and adds the extra 0° plies that excelled in this initial stacking sequence study.

ii. Secondary Stacking Sequence Changes

After the twenty models were post-processed, the most promising three laminate types were then rerun for the 15° and 75° angle replacements using the simple modeling style, for an additional twenty-four models. The load versus displacement curves for the Standard-15T and Standard-15C modified laminates, including their comparison with the original Standard-45T or Standard 45C baselines, respectively, are shown in Figure 53. Both graphs show a significant failure load advantage among all three new laminates.

There is also evidence of load redistribution in the model with 2 additional 0° plies, Standard-15T_Add-0(2) in red, and the model with 4 additional 0° plies, Standard-15T_Add-0(4) shown in blue, within the tension graph on the left. The yellow curve without load redistribution has the highest failure load at 41.005 kip, which is 32.96% higher than the original baseline Standard-45T model. For the compression graph on the right, all three curves fail at very similar failure loads, with the yellow curve representing the Standard-15C_Add-0(2)_Sub-90(2) again at the highest failure load. The compressive failure load for this model failed at 29.898 kip, or 41.26% higher than the Standard-45C model. The load-displacement curves for the Standard-75T and Standard-75C laminate changes are shown in Figure 54. The tension curves on the left do not show hardly any tensile load advantage over the Standard-45T model, with only the Standard-75T_Add-0(4) able to fail at more than half a percent higher load than the baseline model. This tension model with 4 additional 0° plies fails at 31.104 kip which is 0.86% higher than the baseline failure load of 30.840. However, although the Standard-15T_Add-0(2) model fails at only 0.35% higher load, this model is able to redistribute the load after some damage occurs around 26 kip. The compressive curves on the right in Figure 54 all show load redistribution after initial damage, with each of them also able to hold between 10-20% more load up to failure.

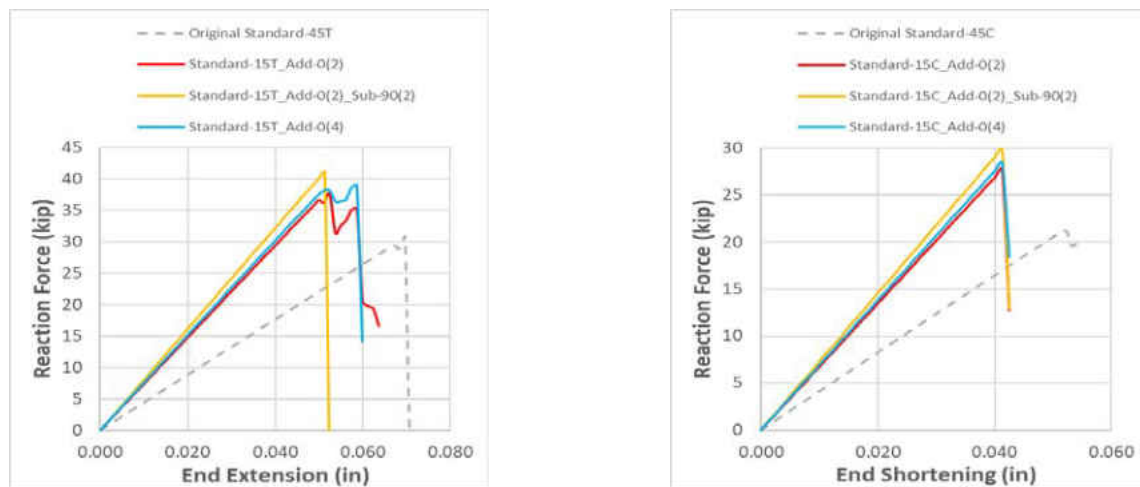


Figure 53. Load-displacement curves for standard tension-loaded (left) and compression-loaded (right) 15° laminate changes and 45° baseline.

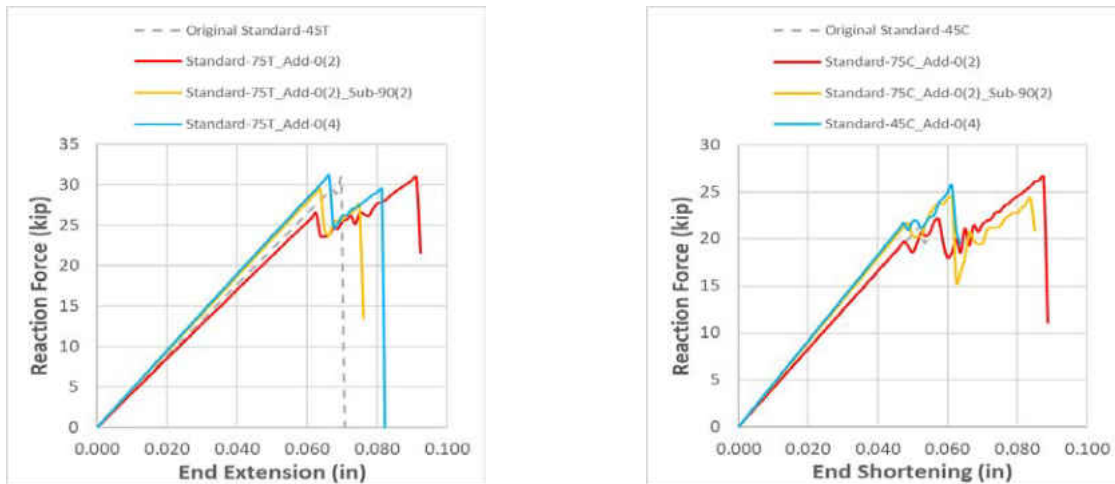


Figure 54. Load-displacement curves for standard tension-loaded (left) and compression-loaded (right) 75° laminate changes and 45° baseline.

The load-displacement curves for the Hybrid-15T and Hybrid-15C modified laminates and their baseline comparison models are shown in Figure 55. The tension graph on the left shows a significant failure load advantage for all three modified laminates. There is also evidence of load redistribution in the Hybrid-15T_Add-0(2) model, plotted in red, and the Hybrid-15T_Add-0(2)_Sub-90(2) laminate, shown in yellow, with the redistribution indicated by the small peaks and valleys within the later portions of the graphs. The yellow curve also has the highest tensile failure load at 51.178 kip, which is 65.95% higher than the original baseline Standard-45T model. The compression graph on the right shows all three curves failing at very similar failure loads, with load distribution evidence again, and all of them failing at over 35% higher loads than the Standard-45C baseline laminate. The load-displacement curves for the Hybrid-75T and Hybrid-75C laminate changes are shown in Figure 56. In this figure, both the tension and compression graphs have evidence of load redistribution again, just like the models with the 15° oriented thin plies. The tension curves show a slight tensile load advantage over the Standard-45T model, with failure loads for these three models between 4-10% higher. The compressive curves on the right side of the figure not only all fail higher than the Standard-45C model, but each of them have a higher damage initiation load than the final failure value of the standard baseline. The model with the largest load advantage is the Hybrid-75C_Add-0(2)_Sub-90(2) laminate, which is predicted to fail at 35.315 kip which is an impressive 66.86% higher than the Standard-45C failure load of 21.165 kip.

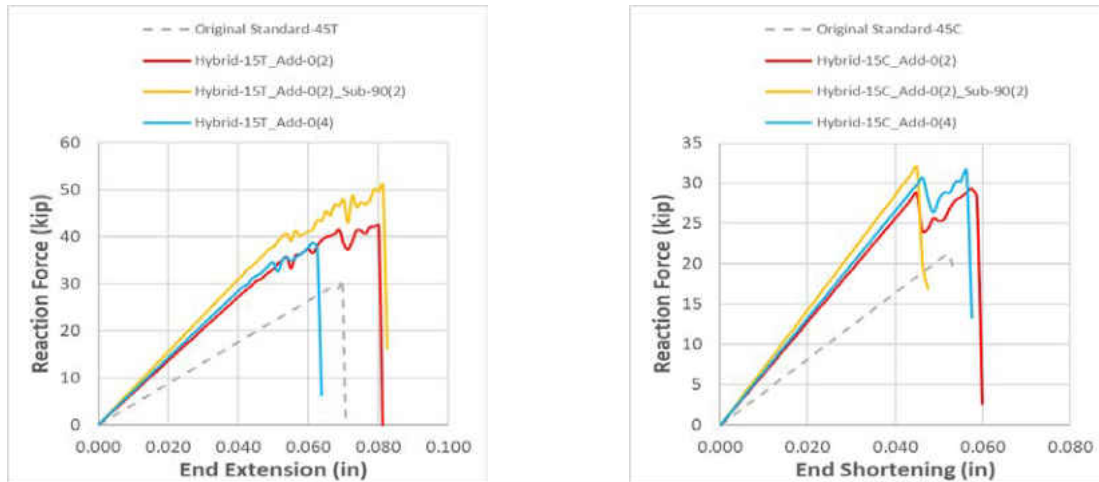


Figure 55. Load-displacement curves for hybrid tension-loaded (left) and compression-loaded (right) 15° laminate changes and standard 45° baseline.

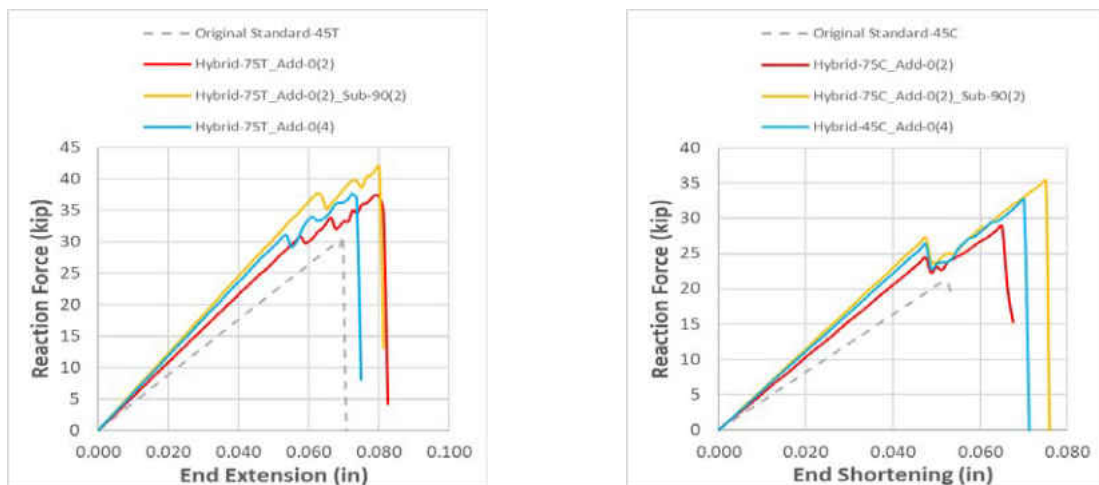


Figure 56. Load-displacement curves for hybrid tension-loaded (left) and compression-loaded (right) 75° laminate changes and standard 45° baseline.

From this final investigation, it is clear that hybrid laminates with more tailored stacking sequences can provide significant load advantages. As seen previously, the hybrid compression-loaded specimens had the most significant advantage over the Standard-45C baseline. It can also be noted that of the three laminates investigated further, any one of them will provide weight savings and strength benefits, as is discussed in the following sections.

IV. Discussion and Results

A. Ply Angle Variation Highs and Lows

The first investigation that was done after the validation process was complete was to replace the commonly used 45° plies with ply angles of various orientations in increments of 10° and 15°. In this exploration, there were failure load advantages seen within many standard-ply laminates, particularly the 15° and 75° orientations that were ultimately selected for both investigations. However, the more advantageous laminates by far were the hybrid laminates that contained both standard-ply and thin-ply composite materials.

The 18-ply hybrid laminates already start with a weight advantage over their 18-ply standard laminate counterparts, with a weight savings of around 25% over the standard-ply specimen. From there, the tensile advantage when looking at the baseline 45° orientations shows that the hybrid model failed at a load of 33.185 kip, which is 7.60% higher than the standard baseline model with 45° plies. The 75° laminates also had a hybrid advantage, with the Hybrid-75T model failing 31.53% higher than the Standard-75T laminate. The only tensile disadvantage occurred when 15° plies were used within the laminates. In that case, the hybrid laminate failed 13.34% lower than the Standard-15T model.

The compression laminates were more consistent than the tension laminates. All three of the ply angle orientations that were in both studies produced hybrid failure load advantages over the standard laminates of the same ply angle orientation. The smallest advantage was the Hybrid-15C which failed 8.81% higher than the Standard-15C model that failed at 26.773 kip. The hybrid laminate with 75° plies failed at 24.704 kip which was 15.22% higher than the equivalent standard laminate, and the greatest advantage was a 44.56% load increase when using the Hybrid-45C rather than the Standard-45C laminate.

In each comparison, the laminate with the 15° plies had the smallest failure load advantage, or did not have one at all. In the final investigation, these 15° orientation laminates were rerun with additional 0° plies and even with fewer 90° plies to determine if there can be a greater advantage when using them. Also in both cases, the greatest load advantage was between the laminates with 75° plies. These were also used to create even greater gains while still taking advantage of the largest weight savings possible.

B. Stacking Sequence Variation Highs and Lows

The stacking sequence investigation started with five additional laminate stacking sequences for each of the hybrid and standard models with the typical 45° plies, run under both tension and compression. Although other published studies have shown that blocked, or grouped, sets of plies can be beneficial for damage suppression, this study did not see large enough advantages to continue their pursuit at this time. Instead, the three other laminates were used to determine benefits of adding extra 0° plies, as well as a case that removed 90° plies along with the extra 0° plies added to the laminate.

The results from the full final investigation are shown in Table 9 and Table 10 as the standard and hybrid modified laminates, respectively. Within both tables, the calculated specimen weight, the predicted failure load, and the comparison of that failure load to the Standard-45T or Standard-45C models are presented. The green background in some cells represents models that have greater than a 20% failure load advantage when compared to the appropriate standard baseline model. In Table 9, there are large advantages for the compression laminates with 75° plies, but the corresponding tension laminates either have a minimal advantage or an actual disadvantage in one case. This points to this ply angle orientation likely not being an ideal candidate for standard-ply only laminates. However, the laminates with 15° plies excel when they are amended with additional 0° plies. All cases have a load advantage greater than 10%, and five of the six explored laminates with 15° plies have greater than 25% higher failure loads when compared with the corresponding baseline models. This yields the conclusion that laminates composed of only standard thickness plies can benefit from stacking sequences that contain 15° off-axis plies, in addition to a large number of 0° plies, when subjected to uniaxial loading. The largest load advantage that still ensures a small weight increase would be for the Standard-15C_Add-0(2)_Sub-90(2) model, which gained an extra 41.26% load while still remaining at the same weight as the Standard-45C model due to the swap of two 0° plies in and two 90° plies out.

Table 9. Weight and strength comparison for standard modified laminate specimens.

Model Name	Weight (lb) (% Difference) [§]	Failure Load (kip)	Standard 45° Comparison*
Standard-15T_Add-0(2)	0.392 (+11.05%)	35.173	+14.05%
Standard-15T_Add-0(2)_Sub-90(2)	0.353 (0%)	41.005	+32.96%
Standard-15T_Add-0(4)	0.431 (+22.10%)	38.988	+26.42%
Standard-15C_Add-0(2)	0.392 (+11.05%)	27.729	+31.01%
Standard-15C_Add-0(2)_Sub-90(2)	0.353 (0%)	29.898	+41.26%
Standard-15C_Add-0(4)	0.431 (+22.10%)	28.370	+34.04%
Standard-45T_Add-0(2)	0.392 (+11.05%)	32.221	+4.48%
Standard-45T_Add-0(2)_Sub-90(2)	0.353 (0%)	34.888	+13.13%
Standard-45T_Add-0(4)	0.431 (+22.10%)	34.981	+13.43%
Standard-45C_Add-0(2)	0.392 (+11.05%)	23.211	+9.67%
Standard-45C_Add-0(2)_Sub-90(2)	0.353 (0%)	24.856	+17.44%
Standard-45C_Add-0(4)	0.431 (+22.10%)	25.076	+18.47%
Standard-75T_Add-0(2)	0.392 (+11.05%)	30.948	+0.35%
Standard-75T_Add-0(2)_Sub-90(2)	0.353 (0%)	29.510	-4.31%
Standard-75T_Add-0(4)	0.431 (+22.10%)	31.104	+0.86%
Standard-75C_Add-0(2)	0.392 (+11.05%)	26.669	+26.01%
Standard-75C_Add-0(2)_Sub-90(2)	0.353 (0%)	24.282	+14.73%
Standard-75C_Add-0(4)	0.431 (+22.10%)	25.692	+21.39%

[§] Weight Comparison: All specimens compared to Standard-45T weight at 0.353 lb.

*Standard 45° Comparison: Tension to Standard-45T failure at 30.840 kip, Compression to Standard-45C failure at 21.165 kip.

In Table 10, there are large advantages for almost all modified laminates, with all but one of the eighteen displayed comparison percentages showing over 10% load increase for the hybrid laminates. The models with 75° plies have large compressive advantages again, but the corresponding tension laminates also provide increased failure loads. This could create a desire for hybrid laminates with 75° plies, especially since in Figure 56 there is evidence of load redistribution which is likely due to damage suppression. Again, the laminates with 15° plies excel with additional 0° plies. All cases have a load advantage greater than 20%, and five of the six 15° off-axis laminates have greater than 35% higher failure loads than the Standard-45T and Standard-45C models, as appropriate. This shows that laminates composed of both standard thickness plies and thin plies can benefit from layups that contain extra 0° plies along with 15° plies. The largest failure load advantage that also ensures a large weight decrease would be for the Hybrid-75C_Add-

0(2)_Sub-90(2) model, which is 25.50% lighter than the standard baseline model, while also failing 66.86% higher. Additionally, the Hybrid-15C_Add-0(2)_Sub-90(2) model, which failed 65.95% higher and is also 25.50% lighter than the Standard-45C model due to the thinner and lighter materials used for the off-axis plies within all of the hybrid laminates.

Table 10. Weight and strength comparison for hybrid modified laminate specimens.

Model Name	Weight (lb) (% Difference) [§]	Failure Load (kip)	Standard 45° Comparison*
Hybrid-15T_Add-0(2)	0.302 (-14.45%)	42.584	+38.08%
Hybrid-15T_Add-0(2)_Sub-90(2)	0.263 (-25.50%)	51.178	+65.95%
Hybrid-15T_Add-0(4)	0.341 (-3.40%)	37.693	+22.22%
Hybrid-15C_Add-0(2)	0.302 (-14.45%)	29.325	+38.55%
Hybrid-15C_Add-0(2)_Sub-90(2)	0.263 (-25.50%)	32.110	+51.17%
Hybrid-15C_Add-0(4)	0.341 (-3.40%)	31.610	+49.35%
Hybrid-45T_Add-0(2)	0.302 (-14.45%)	31.959	+3.63%
Hybrid-45T_Add-0(2)_Sub-90(2)	0.263 (-25.50%)	34.409	+11.57%
Hybrid-45T_Add-0(4)	0.341 (-3.40%)	34.411	+11.58%
Hybrid-45C_Add-0(2)	0.302 (-14.45%)	34.804	+64.44%
Hybrid-45C_Add-0(2)_Sub-90(2)	0.263 (-25.50%)	29.183	+37.88%
Hybrid-45C_Add-0(4)	0.341 (-3.40%)	34.171	+61.45%
Hybrid-75T_Add-0(2)	0.302 (-14.45%)	37.420	+21.34%
Hybrid-75T_Add-0(2)_Sub-90(2)	0.263 (-25.50%)	41.994	+36.17%
Hybrid-75T_Add-0(4)	0.341 (-3.40%)	37.537	+21.72%
Hybrid-75C_Add-0(2)	0.302 (-14.45%)	28.886	+36.48%
Hybrid-75C_Add-0(2)_Sub-90(2)	0.263 (-25.50%)	35.315	+66.86%
Hybrid-75C_Add-0(4)	0.341 (-3.40%)	32.663	+54.33%

[§] Weight Comparison: All specimens compared to Standard-45T weight at 0.353 lb.

*Standard 45° Comparison: Tension to Standard-45T failure at 30.840 kip, Compression to Standard-45C failure at 21.165 kip.

V. Conclusions and Future Work

The most promising laminates that were discovered from the combination of both investigations are those that will be subjected to axial compression loading, but will also still have an axial tensile advantage if that type of loading is desired as well. For the standard laminates, the stacking sequences that contained 15° plies rather than 45° plies were seen to provide the best advantage. However, the standard

compression laminates tended to not have load redistribution, so that would be a disadvantage in scenarios where damage suppression is desired. The hybrid laminates, composed of both standard- and thin-ply materials, were more forgiving and more advantageous. All of the hybrid laminates that were part of the final investigation displayed evidence of load redistribution, as well as higher final failure loads when compared to the standard laminate baselines. This makes the hybrid laminates desirable for a variety of applications and axial loading cases. However, since these simple models were only run with unidirectional loading, more complex load scenarios and the fully advanced models would also need to be investigated to draw full conclusions about the capabilities of the laminates. The simple models are able to predict promising trends, and were deemed enough for this baseline study, but cohesive degradation and biaxial loading are realistic pieces of the design phase that will eventually need to be studied as well.

The future work of this study is to create a test matrix based on a select few of the laminates that were deemed the most beneficial. Those laminates would then be built on the Integrated Structural Assembly for Advanced Composites (ISAAC) Automated Fiber Placement robot and NASA Langley Research Center. After the specimens are built, they would be tested in order to validate the investigation models. For the validation effort, a knockdown factor would be applied between 10-20% for the compression specimens, based on previous validation efforts within this study. This knockdown is not necessary for the laminate investigations due to the self-contained nature of the comparisons.

Once the specimens are tested and the investigation models are validated again, additional laminates can be explored to better tailor the hybrid stacking sequences and further improve weight savings and specimen strength for future use within aerospace applications.

References

- [1] Groupama Image <https://www.topspeed.com/boats/boat-news/groupama-3-establishes-three-new-records-ar40349.html> (Verified 10/19/2020)
- [2] Baley, C., Lan, M., Davies, P., Cartié, D. "Porosity in Ocean Racing Yacht Composites: a Review," *Applied Composite Materials*, Vol. 22, February 2015, pp. 13-28.
- [3] Fuller, J.D. and Wisnom, M.R. "Pseudo-ductility and damage suppression in thin ply CFRP angle-ply laminates," *Composites Part A: Applied Science and Manufacturing*, Vol. 69, February 2015, pp. 64-71.
- [4] Cugnoni, J., Amacher, R., Kohler, S., Brunner, J., Kramer, E., Dransfeld, C., Smith, W., Scobbie, K., Sorensen, L., Botsis, J. "Towards aerospace grade thin-ply composites: Effect of ply thickness, fibre, matrix, and interlayer toughening on strength and damage tolerance," *Composites Science and Technology*, Vol. 168, November 2018, pp. 467-477.
- [5] Arteiro, A., Catalanotti, G., Xavier, J., Linde, P., Camanho, P.P. "Effect of tow thickness on the structural response of aerospace-grade spread-tow fabrics," *Composite Structures*, Vol. 179, November 2017, pp. 208-223.
- [6] Amacher, R., Cugnoni, J., Botsis, J., Sorensen, L., Smith, W., Dransfeld, C. "Thin ply composites: Experimental characterization and modeling of size-effects," *Composites Science and Technology*, Vol. 101, September 2014, pp. 121-132.
- [7] Tsai, S.W., Sihm, S., Kim, R.Y. "Thin Ply Composites" 2005 Structural Dynamics & Materials Conference, Austin, Texas, April 18-21, 2005.
- [8] Moon, J., Kim, M.-G., Kim, C.-G., Bhowmik, S. "Improvement of tensile properties of CFRP composites under LEO space environment by applying MWNTs and thin-ply," *Composites Part A: Applied Science and Manufacturing*, Vol. 42, June 2011, pp. 694-701.
- [9] Furtado, C., Arteiro, A., Catalanotti, G., Xavier, J., Camanho, P.P. "Selective ply-level hybridization for improved notched response of composite laminates," *Composite Structures*, Vol. 145, February 2016, pp. 1-14.
- [10] May, M., Arnold-Keifer, S., Haase, T. "Damage resistance of composite structures with unsymmetrical stacking sequence subjected to high velocity bird strike," *Composites Part C: Open Access*, Vol. 1, August 2020.
- [11] Shi, Q., Zhao, S. "Engineering method to build the composite structure ply database," *Results in Physics*, Vol 6, 2016, pp. 434-439.
- [12] Fotouhi, M., Jalalvand, M., Wisnom, M. "Notch insensitive orientation-dispersed pseudo-ductile thin-ply carbon/glass hybrid laminates," *Composites Part A: Applied Science and Manufacturing*, Vol. 110, July 2018, pp. 29-44.

- [13] <https://www.mscsoftware.com/product/patran> (Verified 11/09/2020)
- [14] <https://www.3ds.com/products-services/simulia/products/abaqus/> (Verified 11/09/2020)
- [15] Turon, Davila, Camanho, Costa “An engineering solution for mesh size effects in the simulation of delamination using cohesive zone models,” *Engineering Fracture Mechanics*, Vol. 74, July 2007, pp. 1665-1682.
- [16] Lovejoy, Andrew E., Scotti, Stephen J., Miller, Sandi G., Heimann, Paula, and Miller, Stephanie S., “Characterization of IM7/8552 Thin-ply and Hybrid Thin-ply Composites,” 2019 Scitech Forum, San Diego, California, January 7-11, 2019.
- [17] ASTM D5766/5766M-11, “Standard Test Method for Open-Hole Tensile Strength of Polymer Matrix Composite Laminates”, ASTM International, 100 Barr Harbor Drive, PO Box C700, West Conshohocken, PA 19428-2959, June, 2019.
- [18] ASTM D6484/6484M-14, “Standard Test Method for Open-Hole Compressive Strength of Polymer Matrix Composite Laminates”, ASTM International, 100 Barr Harbor Drive, PO Box C700, West Conshohocken, PA 19428-2959, June, 2019.
- [19] ASTM D3039/3039M-14, “Standard Test Method for Tensile Properties of Polymer Matrix Composite Materials”, ASTM International, 100 Barr Harbor Drive, PO Box C700, West Conshohocken, PA 19428-2959, August, 2019.
- [20] ASTM D6641/6641M-16, “Standard Test Method for Compressive Properties of Polymer Matrix Composite Materials Using a Combined Loading Compression (CLC) Test Fixture”, ASTM International, 100 Barr Harbor Drive, PO Box C700, West Conshohocken, PA 19428-2959, August, 2019
- [21] Jegley, Dawn C., Waters, William A., and Zahn A. “Testing of Composite Laminate Specimens with Mid-Length Lateral Notches,” NASA TM 2020-5001774, May 2020.
- [22] Lovejoy, Andrew E., Scotti, Stephen J. “Potential Weight Benefits of IM7/8552 Hybrid Thin-ply Composites for Aircraft Structures,” 2019 Scitech Forum, San Diego, California, January 7-11, 2019.
- [23] Zahn, Alana M., Lovejoy, Andrew E. “Test and Analysis Correlation of Standard and Hybrid Standard/Thin-ply Composite Notched Test Specimens” 2020 Scitech Forum, Orlando, Florida, January 6-10, 2020.
- [24] https://www.niar.wichita.edu/coe/NCAMP_Documents/NCAMP_Material_Summaries.pdf (verified 10/23/2018)
- [25] M.J. Laffan, S.T. Pinho, P. Robinson, A.J. McMillian, “Translaminar fracture toughness testing of composites: A review”, *Polymer Testing*, Vol. 31, May 2010, pp. 481-489.

Appendix

A. Sample Material Property Abaqus Input Deck Entries

Standard Ply 190gsm

*MATERIAL, NAME=IM7-190

**

*ELASTIC, TYPE=LAMINA

2.351E+7, 1.30E+6, 0.316, 680000., 680000., 435000.

**

*DAMAGE INITIATION, CRITERION=HASHIN, ALPHA=0.0

371.08E+3, 251.13E+3, 9.29E+3, 41.44E+3, 13.22E+3, 13.22E+3

**

*DAMAGE EVOLUTION, TYPE=ENERGY, SOFTENING=LINEAR

454.09, 146.97, 0.685, 0.685

B. Abaqus Analysis Properties for each Ply Type

	30 gsm	70 gsm	190 gsm
E_{11}^T	21.29 [16]	21.22 [16]	23.51 [24]
E_{11}^C	19.70 [16]	19.50 [16]	20.44 [24]
E_{22}^T	1.49 [16]	1.42 [16]	1.30 [24]
E_{22}^C	1.39 [16]	1.40 [16]	1.41 [24]
ν_{12}^T	0.349 [16]	0.347 [16]	0.316 [24]
ν_{12}^C	0.368 [16]	0.367 [16]	0.356 [24]
G_{12}	0.707 [16]	0.718 [16]	0.680 [24]
G_{13}	0.707*	0.718*	0.680*
G_{23}	0.440**	0.445**	0.435**
X_T	386.10 [16]	362.00 [16]	371.08 [24]
X_C	244.10 [16]	240.22 [16]	251.13 [24]
Y_T	10.22 [16]	11.58 [16]	9.29 [24]
Y_C	38.22 [16]	41.84 [16]	41.44 [24]
S_L	14.46 [16]	15.18 [16]	13.22 [24]
S_T	14.46*	15.18*	13.22*
G_C^{fT} (in-lbf/in ²)	379.77**	303.83**	563.77 [25]
G_C^{fC} (in-lbf/in ²)	416.68**	333.37**	271.32 [25]
G_C^{mT} (in-lbf/in ²)	1.37*	1.37*	1.37 [25]
G_C^{mC} (in-lbf/in ²)	1.37*	1.37*	1.37 [25]

* Assumed

** Calculated

C. Sample Laminate Sequence Abaqus Input Deck Entries

i. Standard Ply Laminate

*SHELL SECTION, COMPOSITE, ELSET=IM7-8552, ORIENTATION=OID1

```

0.0072, 3,IM7-190, 45.
0.0072, 3,IM7-190, 90.
0.0072, 3,IM7-190, -45.
0.0072, 3,IM7-190, 0.
0.0072, 3,IM7-190, 0.
0.0072, 3,IM7-190, 45.
0.0072, 3,IM7-190, 90.
0.0072, 3,IM7-190, -45.
0.0072, 3,IM7-190, 0.
0.0072, 3,IM7-190, 0.
0.0072, 3,IM7-190, -45.
0.0072, 3,IM7-190, 90.
0.0072, 3,IM7-190, 45.
0.0072, 3,IM7-190, 0.
0.0072, 3,IM7-190, 0.
0.0072, 3,IM7-190, -45.
0.0072, 3,IM7-190, 90.
0.0072, 3,IM7-190, 45.

```

ii. Hybrid Ply Laminate

*SHELL SECTION, COMPOSITE, ELSET=IM7-8552, ORIENTATION=OID1

```

0.0028, 3,IM7-70, 45.
0.0072, 3,IM7-190, 90.
0.0028, 3,IM7-70, -45.
0.0072, 3,IM7-190, 0.
0.0072, 3,IM7-190, 0.
0.0028, 3,IM7-70, 45.
0.0072, 3,IM7-190, 90.
0.0028, 3,IM7-70, -45.
0.0072, 3,IM7-190, 0.
0.0072, 3,IM7-190, 0.
0.0028, 3,IM7-70, -45.
0.0072, 3,IM7-190, 90.
0.0028, 3,IM7-70, 45.
0.0072, 3,IM7-190, 0.
0.0072, 3,IM7-190, 0.
0.0028, 3,IM7-70, -45.
0.0072, 3,IM7-190, 90.
0.0028, 3,IM7-70, 45.

```

ZAHN, ALANA

Old Dominion University, Mechanical and Aerospace Engineering Department
238 Kaufman Hall, Norfolk, VA 23529 | 757-683-6363 | azahn002@odu.edu

EDUCATION

Old Dominion University

Master of Science – Aerospace Engineering **2020**

Thesis: “Finite Element Analysis Investigation of Hybrid Thin-Ply Composites for Improved Performance of Aerospace Structures”

State University of New York College at Cortland

Bachelor of Science – Mathematics and Physics Adolescent Education **2010**

ENGINEERING EXPERIENCE

Analytical Mechanics Associates, Inc.

Engineer 3 **November 2018 – Present**

Develop in-house optimization codes to predict structural behavior of tow-steered composite airplane wing panels and composite lunar landing gear struts. Use existing Finite Element Analysis software and to assess strength during all phases of lunar vehicle life, as well as in-flight strength of aircraft after debris impact.

National Institute of Aerospace

Graduate Research Assistant **August 2017 – November 2018**

Studied failure load sensitivity at bond-line interfaces for the Space Launch System and evaluated the damage tolerance of composite aircraft structures using Finite Element Analysis software.

NASA Internships, Fellowships, & Scholarships

Summer Intern **May 2017 – August 2017**

Validated Rapid Design Tools for aircraft structure certification using Finite Element Analysis software.

ADDITIONAL PROFESSIONAL EXPERIENCE

Norfolk Public Schools

Mathematics Teacher **August 2012 – August 2017**

Planned and implemented daily lessons, graded all assignments, and provided comprehensive student and parent feedback to better inform and educate students. As Algebra I Team Lead, created a course roadmap to plan the curriculum for the entire year and collected unit data to plan remediation efforts.

PUBLICATIONS AND AWARDS

NASA Langley Research Center 2020 Group Achievement Award – Advanced Composites Project

Jegley, Dawn C., Waters, W. Allen, Zahn, Alana M., “*Testing of Composite Laminate Specimens with Mid-Length Lateral Notches*”, NASA Technical Memorandum, 2020

Zahn, Alana M., and Lovejoy, Andrew E., “*Test and Analysis Correlation of Standard and Hybrid Standard/Thin-Ply Composite Notched Test Specimens*”, AIAA SciTech Forum Paper and Presentation, 2020

Stapleton, S. et. al., “*Comparison of Design Tools for Stress Analysis of Adhesively Bonded Joints*”, AIAA SciTech Forum Paper and Presentation, 2019

MEMBERSHIPS

AIAA Student Member (2017-Present)